

PREDICTION OF SOUND TRANSMISSION THROUGH ELASTOMERIC BULB
SEALS

A THESIS SUBMITTED TO
THE GRADUATE SCHOOL OF NATURAL AND APPLIED SCIENCES
OF
MIDDLE EAST TECHNICAL UNIVERSITY

BY

SERKAN ATAMER

IN PARTIAL FULFILLMENT OF THE REQUIREMENTS
FOR
THE DEGREE OF MASTER OF SCIENCE
IN
MECHANICAL ENGINEERING

SEPTEMBER 2014

Approval of the thesis:

**PREDICTION OF SOUND TRANSMISSION THROUGH ELASTOMERIC
BULB SEALS**

submitted by **SERKAN ATAMER** in partial fulfillment of the requirements for the degree of **Master of Science in Mechanical Engineering Department, Middle East Technical University** by,

Prof. Dr. Canan Özgen
Dean, Graduate School of **Natural and Applied Sciences** _____

Prof. Dr. Mehmet Çalışkan
Head of Department, **Mechanical Engineering** _____

Prof. Dr. Mehmet Çalışkan
Supervisor, **Mechanical Engineering Dept., METU** _____

Asst. Prof. Gökhan O. Özgen
Co-Supervisor, **Mechanical Engineering Dept, METU** _____

Examining Committee Members:

Prof. Dr. Samim Ünlüsoy
Mechanical Engineering Dept., METU _____

Prof. Dr. Mehmet Çalışkan
Supervisor, Mechanical Engineering Dept, METU _____

Asst. Prof. Gökhan O. Özgen
Co-Supervisor, Mechanical Engineering Dept., METU _____

Asst. Prof. Cüneyt Sert
Mechanical Engineering Dept, METU _____

Prof. Dr. Yusuf Özyörük
Aerospace Engineering Dept, METU _____

Date: 15.09.2014

I hereby declare that all information in this document has been obtained and presented in accordance with academic rules and ethical conduct. I also declare that, as required by these rules and conduct, I have fully cited and referenced all material and results that are not original to this work.

Name, Last Name : Serkan ATAMER

Signature :

ABSTRACT

PREDICTION OF SOUND TRANSMISSION THROUGH ELASTOMERIC BULB SEALS

Atamer, Serkan

M. S. Department of Mechanical Engineering

Supervisor: Prof. Dr. Mehmet Çalışkan

Co-supervisor: Assist. Prof. Gökhan O. Özgen

September 2014, 111 pages

Doors are the weakest parts of the buildings in terms of sound transmission. Examination of sound transmission loss characteristics of doors reveals two separate transmission paths to be considered, namely, transmission through door leaf and leak transmission through bulb seals. Seals are the important parts of the sound transmission loss characteristic of door structure owing to their weakness compared to door leaf. Hence, their insulation capability should be analyzed and optimized to improve sound transmission loss of an acoustical door.

The aim of this research is to predict sound transmission loss of elastomeric bulb seals. This assessment includes two main steps. A static analysis is required to determine the seal shape under compression. Seals are made of elastomers which display nonlinear mechanical behavior. This requires hyperelastic material modeling and nonlinear finite element analysis (FEA). An acoustic analysis to calculate the

sound transmission is then carried on deformed geometry acquired from the first phase of the research.

Different seal geometries, which are already being used in industry, are considered as case studies. Effects of different material characteristics and different seal geometries on sound transmission are investigated. Influences of different hyper elastic material models on sound insulation are studied.

Keywords: Hyperelastic material, sound transmission through door seals, nonlinear FEA

ÖZ

ELASTOMER YAPIDAKİ BALON FİTİLLERİNDE SES GEÇİŞ KAYBI DEĞERLENDİRMESİ

Atamer, Serkan

Yüksek Lisans, Makina Mühendisliği Bölümü

Tez Yöneticisi: Prof. Dr. Mehmet Çalışkan

Ortak Tez Yöneticisi: Assist. Prof. Gökhan O. Özgen

September 2014, 111 sayfa

Kapılar, diğer yapı elemanlarıyla karşılaştırıldığında, ses geçiş kaybı değerlendirmelerinde en zayıf halkayı oluşturur. Kapıların ses geçiş kaybı değerlendirmesi, gövdeden geçerek alıcı ortamına ulaşan ve kapı birleşim noktalarındaki sızıntılardan alıcı ortamına ulaşan gürültü olarak iki ana başlık altında incelenir. Sızıntılar, kapıların ses geçiş kaybı karakteristiklerini önemli ölçüde düşürür. Bu nedenle sızıntıların engellenmesi için uygulanan kapı fitillerinin yalıtım yetkinliklerinin değerlendirilmesi ve geliştirilmesi çok önemlidir.

Bu çalışmada, elastomer yapıdaki balon fitillerin ses geçiş kaybı karakteristiklerinin belirlenmesi amaçlanmıştır. Çalışma, iki ana başlıktan oluşmaktadır. Birinci bölümde, fitillerin belirli bir yük altındaki deforme olmuş geometrilerinin elde edilmesi için yapılan analizler; ikinci bölümde ise bu deforme olmuş geometriler

üzerinden ses geçiş kaybı niteliklerinin belirlenmesi için yapılan akustik çözümler bulunmaktadır. Doğrusal olmayan mekanik davranışlar sergileyen elastomer yapılarından oluşan fitiller hiper elastik malzeme karakteristiklerinin tanımlanabildiği sonlu elemanlar analizleri ile değerlendirilmelidir. Bu analizlerden elde edilen deforme olmuş geometriler, akustik analizlerde başlangıç geometrisi olarak kullanılmak üzere bu bölüme aktarılmıştır.

Endüstride halihazırda kullanılan farklı fitil geometrileri örnek olarak değerlendirilmiştir. Farklı malzeme karakteristiklerinin ve geometrilerinin ses geçiş kaybı üzerine etkisi çalışılmıştır. Farklı hiper elastik malzeme modellerinin sonuçlar üzerine etkisi araştırılmıştır.

Anahtar Kelimeler: Hiperelastik malzeme, kapı fitilleri, ses geçiş kaybı, doğrusal olmayan sonlu eleman analizi

ACKNOWLEDGEMENTS

First of all, I would like to express my deep gratitude to Prof Dr. Mehmet Çalışkan and Assist. Prof. Dr. Gökhan Özgen their endless and invaluable support, understanding, guidance and help throughout the research and writing of this thesis.

I would also like to thank to Zühre Sü Gül and people working in Mezzo Stüdyo for their encouragements and advises on this project. Moreover, I offer my sincere appreciation to Teknokent A.Ş. for their support.

I would also extend my thanks to the companies Bil-Plas Rubber Plastic Industry Trade Ltd. Co. and Standart Profil Co. for supplying seal geometries.

Special thanks should be given to Ferhat Aydoğan and Ersen Arslan for their support and patience during simulations.

Also, completion of this project could not have been accomplished without the support of my family.

At the end I would like to express my gratitude to Pınar, for her support, understanding, patience and inspiration. Without her, I couldn't even imagine to finish my work.

TABLE OF CONTENTS

ABSTRACT	v
ÖZ.....	vii
ACKNOWLEDGEMENTS	ix
TABLE OF CONTENTS	x
LIST OF TABLES	xii
LIST OF FIGURES.....	xiii
LIST OF SYMBOLS	xix
LIST OF ABBREVIATIONS	xx
CHAPTERS	
INTRODUCTION.....	1
1.1. Motivation	1
1.2. Aim and Scope.....	4
1.3. Overview/Outline of the Thesis.....	5
LITERATURE REVIEW.....	7
2.1. Elastomers and Hyperelasticity	7
2.1.1. Elastomers	7
2.1.2. Hyperelasticity	8
2.2. Acoustics	18
2.2.1. Sound Transmission Loss.....	18
2.2.2. Sound Transmission Loss of Elastomeric Bulb Seals.....	21

2.2.3. Fluid Solid Interactions (FSI)	22
HYPERELASTIC FEA MODELS AND SIMULATIONS	27
3.1. Geometry and Mesh Generation.....	27
3.2. Preliminary Decisions and Preprocessing	31
3.3. Materials	34
3.4. Results	37
FEA MODELS OF DEFORMED GEOMETRIES AND ACOUSTIC SIMULATIONS.....	47
4.1. Geometry and Mesh Generation.....	47
4.2. Preliminary Decisions and Preprocessing	48
4.3. Materials	49
4.4. Results	50
SUMMARY AND CONCLUSIONS	77
5.1. Summary	77
5.2. Conclusions	78
5.3. Future work	82
BIBLIOGRAPHY	83
APPENDICES	
APPENDIX A. DEFORMATION RESULTS.....	87

LIST OF TABLES

TABLES

Table 1. Definitions of cases and references.....	36
Table 2. Material constants used in cases*	36
Table 3. Results obtained at different cases for two different geometries	38
Table 4. Standart Profil 2D geometry, solutions with mating body.....	40
Table 5. Case studies defined for acoustic analyses.....	60

LIST OF FIGURES

FIGURES

Figure 1. Effect of the percentage leakage area	2
Figure 2. Adjustable door seals	4
Figure 3. Schematic representation of configuration of elastomer molecules	8
Figure 4. Schematic representation of stress-strain relationship for (a) linear material (b) nonlinear material	9
Figure 5. Schematic representation of stress-strain relationship of hyperelastic material under tension and compression	9
Figure 6. Representation of stretch ratio	10
Figure 7. Example of nonlinearities	16
Figure 8. Solving a non-linear problem with linear solvers.....	17
Figure 9. Newton-Raphson method	17
Figure 10. Divergence and convergence configurations for a nonlinear FEA.....	18
Figure 11. Representation of acoustic FSI.....	24
Figure 12. Model Zero_712 in its application.....	28
Figure 13. 2D model of sealant section.....	28
Figure 14. 3D model created using Zero International model 712	28
Figure 15. Section of seal obtained from Standart Profil Co.	29
Figure 16. 2D model of sealant section.....	29
Figure 17. 3D model and mesh	30
Figure 18. Section of seal obtained from BilPLas	30
Figure 19. 2D model of sealant section.....	31
Figure 20. 3D model and mesh	31
Figure 21. ANSYS WB Project Schematic.....	32

Figure 22. Limitations on Zero_712 geometry	33
Figure 23. Simple study with zero Poisson ratio.....	35
Figure 24. Simple study with Poisson ratio 0.2.....	35
Figure 25. Deformation of Zero International geometry under different compression ratios	42
Figure 26. Deformation of Standart Profil geometry under different compression ratios	43
Figure 27. Deformation of BilPlas geometry under different compression ratios	44
Figure 28. BilPlas sample and its thickness	45
Figure 29. Buckling occurs when the system is under compression.....	45
Figure 30. Storage and loss modulus of a door seal versus frequency.....	50
Figure 31. BilPlas geometry, used in modal analyses, low resolution mesh	51
Figure 32. BilPlas geometry, used in modal analyses, medium resolution mesh	51
Figure 33. BilPlas geometry, used in modal analyses, high resolution mesh	52
Figure 34. Mode numbers and corresponding frequencies	52
Figure 35. Two membrane model approximation.....	53
Figure 36. FE model of two membrane approximation	54
Figure 37. TL obtained from dual membrane model, by transfer matrix method.....	55
Figure 38. TL vs. frequency, obtained from the simple two-membrane FE model ..	55
Figure 39. Rectangular model approximation.....	56
Figure 40. FE model of rectangular model approximation	56
Figure 41. TL obtained from rectangular model, by transfer matrix FEA (Taken from: J. Park et al. Sound Transmission through Elastomeric Bulb Seals.—●—●—: low resolution ;— — —: medium resolution;——: high resolution).....	57
Figure 42. TL vs frequency, obtained from rectangular FE model.....	58
Figure 43. Sound Transmission Loss vs. frequency. BilPlas geometry, with different mesh resolutions.	59
Figure 44 Sound Transmission Loss vs. frequency. BilPlas geometry, with different mesh resolutions. Close-up view at low frequencies.	59

Figure 45. Sound Transmission Loss vs. frequency. BilPlas and Standart Profil geometry, both in Case 1.....	61
Figure 46. Sound Transmission Loss vs. frequency. BilPlas and Standart Profil geometry, both in Case 1.....	61
Figure 47. Sound Transmission Loss vs. frequency. BilPlas and Standart Profil geometry, both in Case 2.....	62
Figure 48. Sound Transmission Loss vs. frequency. BilPlas and Standart Profil geometry, both in Case 2.....	62
Figure 49. Sound Transmission Loss vs. frequency. BilPlas and Standart Profil geometry, both in Case 3.....	63
Figure 50. Sound Transmission Loss vs. frequency. BilPlas and Standart Profil geometry, both in Case 3.....	64
Figure 51. Sound Transmission Loss vs. frequency. BilPlas and Standart Profil geometry, both in Case4.....	64
Figure 52. Sound Transmission Loss vs. frequency. BilPlas and Standart Profil geometry, both in Case 4.....	65
Figure 53. Sound Transmission Loss vs. frequency. BilPlas and Standart Profil geometry, both in Case 5.....	66
Figure 54. Sound Transmission Loss vs. frequency. BilPlas and Standart Profil geometry, both in Case 5.....	66
Figure 55. Sound Transmission Loss vs. frequency. BilPlas and Standart Profil geometry, both in Case 6.....	67
Figure 56. Sound Transmission Loss vs. frequency. BilPlas and Standart Profil geometry, both in Case 6.....	67
Figure 57. Sound Transmission Loss vs. frequency, Standart Profil geometry, Cases 1, 2 and 3.....	68
Figure 58. Sound Transmission Loss vs. frequency, Standart Profil geometry, Cases 1, 2 and 3.....	68
Figure 59. Sound Transmission Loss vs. frequency, Standart Profil geometry, Cases 4, 5 and 6.....	69

Figure 60. Sound Transmission Loss vs. frequency, Standart Profil geometry, Cases 4, 5 and 6	69
Figure 61. Sound Transmission Loss vs. frequency, BilPlas geometry, Cases 1, 2 and 3	70
Figure 62. Sound Transmission Loss vs. frequency, BilPlas geometry, Cases 1, 2 and 3	70
Figure 63. Sound Transmission Loss vs. frequency, BilPlas geometry, Cases 4, 5 and 6	71
Figure 64. Sound Transmission Loss vs. frequency, BilPlas geometry, Cases 4, 5 and 6	72
Figure 65. Effect of resolution in frequency, BilPlas, Case1	72
Figure 66. Effect of resolution in frequency, BilPlas, Case1	73
Figure 67. Effect of model thickness on sound transmission loss.	74
Figure 68. Effect of different boundary conditions, BilPlas, case1	75
Figure 69. Effect of different boundary conditions, BilPlas, case1	75
Figure 70. 3D model of BilPlas geometry. Note the upper flat surface to assign displacement.....	79
Figure 71. 3D model of Standart Profil geometry. Note that displacement cannot be assigned to upper surface	79
Figure 72. Total deformation of sealant, BilPlas, Case1	87
Figure 73. Total deformation of inlet and outlet air structure, BilPlas, Case1.....	88
Figure 74. Total deformation of inside air, BilPlas, Case1	88
Figure 75. Total deformation of sealant, Standart Profil, Case1	89
Figure 76. Total deformation of inlet and outlet air structure, Standart Profil, Case1	89
Figure 77. Total deformation of inside air, Standart Profil, Case1	90
Figure 78. Total deformation of sealant, BilPlas, Case2.....	90
Figure 79. Total deformation of inlet and outlet air structure, BilPlas, Case2.....	91
Figure 80. Total deformation of inside air, BilPlas, Case2	91
Figure 81. Total deformation of sealant, Standart Profil, Case2.....	92

Figure 82. Total deformation of inlet and outlet air structure, Standart Profil, Case2	92
Figure 83. Total deformation of inside air, Standart Profil, Case2.....	93
Figure 84. Total deformation of sealant, BilPlas, Case3.....	93
Figure 85. Total deformation of inlet and outlet air structure, BilPlas, Case3	94
Figure 86. Total deformation of inside air, BilPlas, Case3.....	94
Figure 87. Total deformation of sealant, Standart Profil, Case3.....	95
Figure 88. Total deformation of inlet and outlet air structure, Standart Profil, Case3	95
Figure 89. Total deformation of inside air, Standart Profil, Case3.....	96
Figure 90. Total deformation of sealant, BilPlas, Case4.....	96
Figure 91. Total deformation of inlet and outlet air structure, BilPlas, Case4	97
Figure 92. Total deformation of inside air, BilPlas, Case4.....	97
Figure 93. Total deformation of sealant, Standart Profil, Case4.....	98
Figure 94. Total deformation of inlet and outlet air structure, Standart Profil, Case4	98
Figure 95. Total deformation of inside air, Standart Profil, Case4.....	99
Figure 96. Total deformation of sealant, BilPlas, Case5.....	99
Figure 97. Total deformation of inlet and outlet air structure, BilPlas, Case5	100
Figure 98. Total deformation of inside air, BilPlas, Case5.....	100
Figure 99. Total deformation of sealant, Standart Profil, Case5.....	101
Figure 100. Total deformation of inlet and outlet air structure, Standart Profil, Case5	101
Figure 101. Total deformation of inside air, Standart Profil, Case5	102
Figure 102. Total deformation of sealant, BilPlas, Case6.....	102
Figure 103. Total deformation of inlet and outlet air structure, BilPlas, Case6	103
Figure 104. Total deformation of inside air, BilPlas, Case6.....	103
Figure 105. Total deformation of sealant, Standart Profil, Case6.....	104
Figure 106. Total deformation of inlet and outlet air structure, Standart Profil, Case6	104

Figure 107. Total deformation of inside air, Standart Profil, Case6	105
Figure 108. Total deformation of sealant, BilPlas, Case7.....	105
Figure 109. Total deformation of inlet and outlet air structure, BilPlas, Case7.....	106
Figure 110. Total deformation of inside air, BilPlas, Case7	106
Figure 111. Total deformation of sealant, BilPlas, Case8.....	107
Figure 112. Total deformation of inlet and outlet air structure, BilPlas, Case8.....	107
Figure 113. Total deformation of inside air, BilPlas, Case8.....	108
Figure 114. Total deformation of sealant, BilPlas, Case9.....	108
Figure 115. Total deformation of inlet and outlet air structure, BilPlas, Case9.....	109
Figure 116. Total deformation of inside air, BilPlas, Case9	109
Figure 117. Total deformation of sealant, BilPlas, Case10.....	110
Figure 118. Total deformation of inlet and outlet air structure, BilPlas, Case10.....	110
Figure 119. Total deformation of inside air, BilPlas, Case10	111

LIST OF SYMBOLS

σ	Stress
W	Strain energy
λ_i	Stretch ratio in (i) direction
L_i	Length in (i) direction
ΔL_i	Difference of final and initial length in (i) direction
ε_i	Engineering strain in (i) direction
I_i	Strain invariants in (i) direction
J	Volumetric ratio
p_i	Acoustic pressure
P_i	Acoustic pressure amplitude
j	Imaginary unit
ω	Frequency
k	Wave number
z	Specific acoustic impedance
T	Pressure based transmission coefficient
T_I	Intensity based transmission coefficient
T_{Π}	Power based transmission coefficient
$u_{x,y,z}$	Particle velocity in x,y,z direction
r	Reflection coefficient
ρ_0	Mean fluid density
c	Speed of sound
G	Shear modulus
Q	Mass source in the continuity equation
$\vec{\sigma}(\vec{u}_S)$	Solid stress tensor
\vec{n}	Outward normal unit vector of fluid domain
\vec{u}_S	Displacement in solid

LIST OF ABBREVIATIONS

CR	Compression Ratio
FSI	Fluid Solid Interaction
FEA	Finite Element Analysis
MR	Mooney-Rivlin
ACT	ANSYS Customization Toolkit
APDL	ANSYS Parametric Design Language
NVH	Noise, Vibration and Harshness

CHAPTER 1

INTRODUCTION

1.1. MOTIVATION

Elastomeric rubber seals are frequently used in different industries to prevent water, heat and noise intrusion from one volume to the other. Analysis and improvement of their thermal and noise insulation performance becomes more and more pronounced and important every day.

Bulb seals constitute the weakest link in transmission chain in terms of heat and noise insulation performance. They are important joints in the whole structure. In most of the applications, like the sound transmission loss capacity of a structure having elastomeric bulbs seals, improper sealing applications can reduce effectiveness of the system drastically. Figure 1 shows the effect of the leakage area on sound transmission loss capacity of a wall structure.

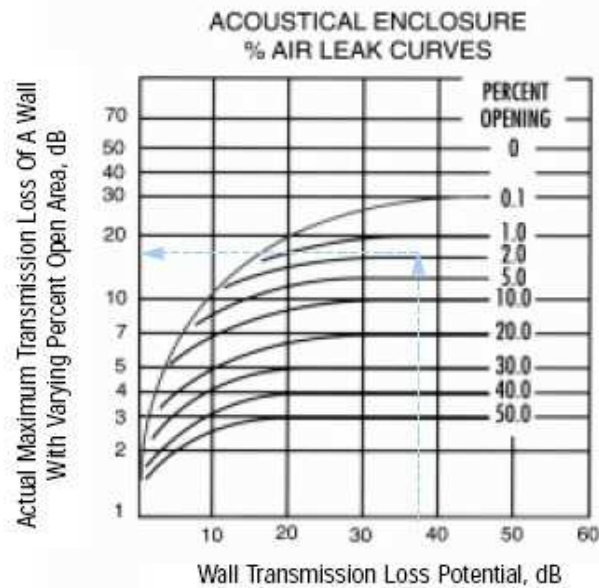


Figure 1. Effect of the percentage leakage area on sound transmission loss characteristics of a wall (Image taken from www.brd-noise.com)

Hence, it is important to analyze physical behavior of the rubber seals for accurate prediction of sound transmission loss characteristics of the whole assembly. However, seals can be considered in full scale models as joints or boundary conditions, which often make the Finite Element Analysis a burden. It is very difficult to include a detailed description of the joint in a full-scale model of the complete structure. Therefore, it is more convenient to analyze the behavior of joints first (elastomeric rubber seals in this case), then to combine the results of the two analyzes. Mainly two applications of the elastomeric rubber bulb seals are the main foci of this thesis.

Firstly, it is very important to consider sound transmission loss characteristic of a door seal in automotive industry. Interior noise levels are becoming more important in new generation cars and acoustic comfort is becoming a baseline consideration. When a vehicle cruising at a speed over 120 km/h, wind noise plays the dominant role for interior noise. Therefore, improvement of the sound transmission loss characteristics of door seals is essential [1]. Two primary noise generation

mechanisms involve the aspiration through small leaks and structural sound transmission due to flow-induced vibrations of the seals. When leaks are present, aspiration noise becomes important. It is crucial to ensure the air-tightness of the sealing system in the car doors.[2]

Secondly, sound insulation requirements for doors have increased due to increased importance of acoustical comfort and the policies enforcing the specifications associated with noise criteria in dwellings, hotels, office areas, hospitals, schools etc. Doors are the weakest links in wall structures, and seals of the doors are the weakest links in door structure from sound isolation standpoint. Besides, doors with improved sound transmission loss capability i.e. acoustical doors, are also very important architecturally, like in multi-purpose auditoria, recording studios, conference rooms as well as hotel room doors and doors to dwellings.

Examination of sound insulation of doors reveals of two separate transmission paths. The former is the structural transmission through the door leaf and the latter is the leakage transmission through the slits [3]. Hence, analysis and improvement of the sound transmission loss characteristics of door seals is crucial.

Both applications require deformed sealant geometry under specified compression ratios and sound transmission loss values of the deformed sealant geometries under consideration. For this reason, analyses conducted in this thesis are composed of two main parts. In the first part, seals are modeled as hyperelastic materials to obtain the deformed geometry under compression. Second part includes the sound transmission loss analysis of the deformed seal geometries

Distance between the mating bodies enclosing the rubber bulb seals is a design parameter. This variable, with the variable of the seal thickness, corresponds to an important design parameter, i.e. **compression ratio** (CR) in the analysis of sound transmission loss of elastomeric bulb seals. Compression ratio determines the effect of sealants and is going to be considered in this study. Figure 2 shows an example of adjustable door sealing systems, in which compression ratio can be modified.

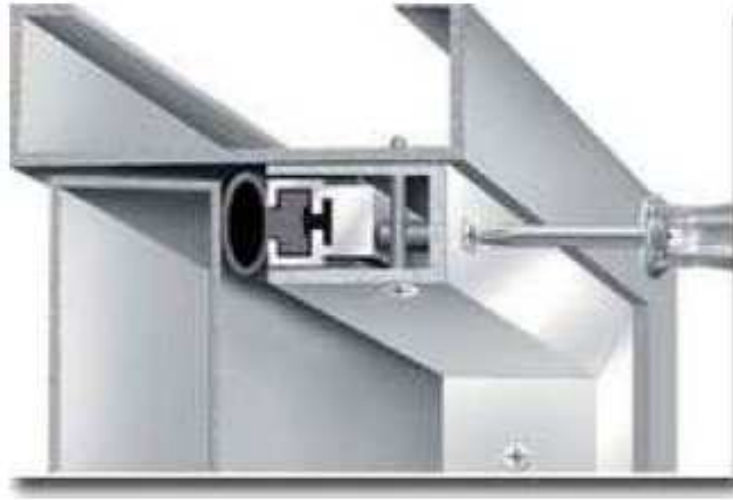


Figure 2. Adjustable door seals (Image taken from www.zerointernational.com)

1.2. AIM AND SCOPE

The analyses will be conducted under two main headings in this thesis. In the first part of the simulations, nonlinear quasi-static analyses will be performed in order to obtain deformed shape of the seal material under different compression ratios. In the second part, sound transmission loss characteristics of sealants in their deformed shapes will be investigated.

In non-linear static analysis, different hyperelastic material models will be implemented on three different sealant geometry. Moreover, different compression ratios will be investigated. As the material constants which will be used to model hyperelastic material behavior are obtained from literature, different material constants will be investigated to determine their effect on the deformed shape of the sealant.

After acquisition of the deformed geometries, these geometries should be carried to a harmonic analysis through which acoustic simulations are going to be made. New

coordinates of the nodes defining sealant geometry will be chased to define new material surfaces. One main limitation in this part is, only the new coordinates (hence deformed geometry) of a sealant is carried to the harmonic analysis. Loading conditions (pre-stress environment) is not in the scope of this work.

In acoustic analysis, acoustic bodies, boundary conditions and excitations will be applied to determine sound pressure levels in determined planes. Acoustic FSI will be considered during acoustic analysis since the geometry includes both fluid and solid media. After solving the acoustic problem, acoustic propagation parameter - sound transmission loss - values will be obtained.

The effect of material characterization on deformation process will be investigated in the first part of the simulations. Possible buckling/wrinkle situations will be studied in different sealant geometries under different compression ratios. Buckling in sealants is not desired since they constitute a weak link in critical path of insulation characteristics. In addition, effect of sealant geometry on sound transmission loss characteristics will be inspected.

1.3. OVERVIEW/OUTLINE OF THE THESIS

This thesis consists of five main chapters. In the first chapter main motivation for the topic of the study is explained. Aim and scope of the thesis is submitted along with expectations from the results and limitations.

In the second chapter, literature review is presented under two main subtitles. In the first part elastomers and hyperelasticity is defined briefly. Hyperelastic material models are also described in this chapter. Second part includes the fundamental acoustical expressions defining sound transmission loss. Head notes of the similar works from the literature related to elastomer sound insulation characteristics are stated. Lastly, mathematical formulation of FSI FE problems indicated with the definitions of boundary conditions and acoustic excitations.

Third chapter consists of the nonlinear static structural analysis of elastomer sealants. Sealant geometries, material characterization, FE models and the results obtained from FEA are given in this part.

In the fourth chapter, full harmonic acoustic analyses are explained. Deformed geometries, carried from the static structural analysis are defined in this chapter. Preliminary decisions of the acoustic FEA are presented. Results obtained from the acoustic analyses for different sealant geometries are provided.

Last chapter includes the discussion about the results and possible improvements for the future studies.

CHAPTER 2

LITERATURE REVIEW

2.1. ELASTOMERS AND HYPERELASTICITY

2.1.1. ELASTOMERS

Elastomers are a class of polymers involving natural and synthetic rubbers with viscoelasticity. They have generally low Young's modulus and high failure strain compared with other materials. They can undergo strain rates up to 700%. Elastomers have long chains of entangled (cross-linked) molecules which strengthen the material. These long molecule chains are randomly oriented within the structure in its undeformed state. When the material is deformed, long chain molecules orient themselves. After releasing, molecules "tangle" themselves back, returning the material in its original shape without permanent deformation. The macromolecular network structure within elastomers enables these materials to undergo very large strain rates, with nonlinear stress-strain relationships. Figure 3 shows schematic representation of configuration of elastomer molecules under deformation [4][5] [6]

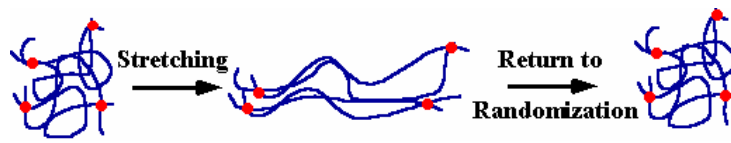


Figure 3. Schematic representation of configuration of elastomer molecules under deformation
[6]

Elastomers are used extensively in many industrial applications because of their wide availability and low cost. Most important aspects of elastomers are their excellent damping and energy absorption characteristics, flexibility, resiliency, incompressibility, long service life, ability to seal against moisture, heat, noise, moldability and variable stiffness. Examples of elastomers can be EPM (ethylene propylene rubber), EPDM(ethylene propylene diene rubber), Butyl Rubber, Nitrile Rubber etc.

Most sealing materials are made of elastomers, differing in compositions. Different compositions give elastomers different strength and hardness values, elasticity, damping characteristics and even conductivity. Hence, elastomers play crucial role in different applications in industry.

Proper analysis of elastomers requires special material modeling and nonlinear finite element analysis tools that are different than those used in metallic parts[7]. As the stress-strain relationship of an elastomer is nonlinear; most elastomeric specimens need to be tested to extract their nonlinear stress-strain behavior to obtain their mathematical characterization of stress-strain relationship. Main goal is to mimic that behavior in the analysis[8].

2.1.2. HYPERELASTICITY

Stress-strain relationship of a hyperelastic material shows nonlinear behavior, different from the linear elastic behavior depicted by Hooke's law. For the linear materials, relation between stress and strain is linear; hence, it can be defined by constant modulus of elasticity. However, the relationship between stress and strain, for hyperelastic materials, is nonlinear. Generic representation of linear and

nonlinear engineering stress-strain relationship is given in Figure 4. Representation of the stress strain relationship of a hyperelastic material, under tension and compression is given in Figure 5.

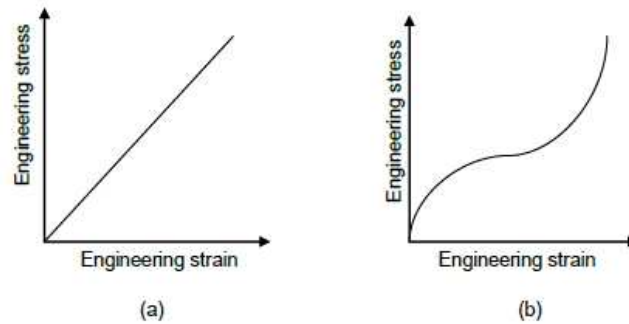


Figure 4. Schematic representation of stress-strain relationship for (a) linear material (b) nonlinear material [5]

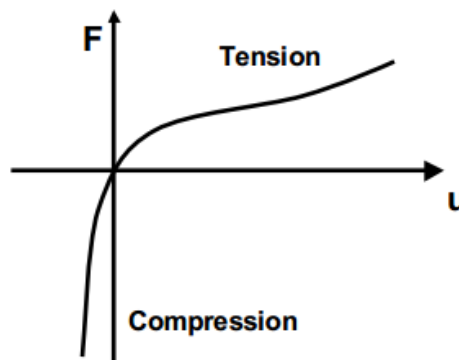


Figure 5. Schematic representation of stress-strain relationship of hyperelastic material under tension and compression [6]

The mathematical theory of small elastic deformations has been developed to high degree of sophistication subjected to certain fundamental assumptions. However, for the materials undergoing large elastic deformations, new mathematical expressions must be derived expressing the stress-strain relationship. Stress - strain relationship of a hyperelastic material can be derived from strain energy density function.

The theory of hyperelasticity is based on the mathematical expression considering the elastic energy stored in a deformed body. Unlike linear elastic behavior, hyperelasticity is not defined as a rate formulation. A **strain energy function** can be defined to characterize the mechanical behavior of hyperelastic materials. Stress component, then, can be calculated using the following equation:

$$\sigma_{ij} = \frac{\partial W}{\partial e_{ij}} \quad (2-1)$$

Strain energy function of a hyperelastic material is defined in terms of stretch instead of strain. The stretch ratio is defined as the deformed length divided by the initial length, given in Equation 2.2 and Figure 6.

$$\lambda_i = \frac{L_i + \Delta L_i}{L_i} = 1 + \varepsilon_i \quad (2-2)$$

$$\varepsilon_i = \frac{\Delta L_i}{L_i} \quad (2-3)$$

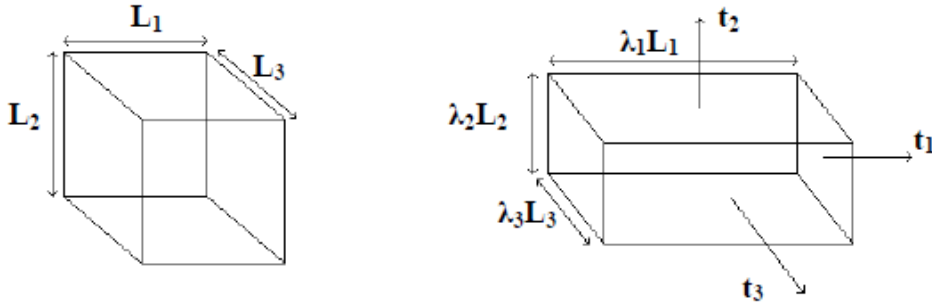


Figure 6. Representation of stretch ratio[9]

The strain energy density functions are in general represented in terms of a weighted summation of strain invariants. The strain invariants I_1 , I_2 and I_3 are functions of the stretch ratios and expressed as: [9]

$$I_1 = \lambda_1^2 + \lambda_2^2 + \lambda_3^2 \quad (2-4)$$

$$I_2 = \lambda_1^2 \lambda_2^2 + \lambda_2^2 \lambda_3^2 + \lambda_1^2 \lambda_3^2 \quad (2-5)$$

$$I_3 = \lambda_1^2 \lambda_2^2 \lambda_3^2 \quad (2-6)$$

Hence volume ratio can be defined as:

$$J = \lambda_1 \lambda_2 \lambda_3 \quad (2-7)$$

If the material is incompressible:

$$J = \lambda_1 \lambda_2 \lambda_3 = 1$$

There are different hyperelastic material models, having different strain energy function definitions. Neo-Hookean, Mooney Rivlin (MR), Yeoh, Arruda-Boyce, Gent and Ogden models are the main hyperelastic material models which will be covered in the next section.

2.1.2.1. HYPERELASTIC MATERIAL MODELS

2.1.2.1.1. NEO-HOOKEAN MODEL

Neo-Hookean model is the simplest model to describe mechanical behavior of hyperelastic materials. Strain energy function is described in terms of the first strain invariant and just one material constant [10]. This model gives good correlation with the experimental data up to 40% strain in uniaxial tension and 90% strain in simple shear. [11]

$$W = C_{10}(I_1 - 3) \quad (2-8)$$

As an example, let's consider a rubber rod, which is stretched uniaxially so that $\lambda_1 = \lambda$ where λ is an arbitrary stretch along the rods length. Assuming the rod material is incompressible, then:

$$\lambda_2 = \lambda_3 = \frac{1}{\sqrt{\lambda}} \quad (2-9)$$

so that

$$\lambda_1^2 \lambda_2^2 \lambda_3^2 = 1 \quad (2-10)$$

With these assumptions, strain energy density function and stress of the rod is found as:

$$\begin{aligned} W &= C_{10}(I_1 - 3) = C_{10}(\lambda_1^2 + \lambda_2^2 + \lambda_3^2 - 3) \\ &= C_{10} \left(\lambda^2 + \frac{2}{\lambda} - 3 \right) \end{aligned} \quad (2-11)$$

$$\sigma = \frac{\partial W}{\partial \lambda} = 2C_{10} \left(\lambda - \frac{1}{\lambda^2} \right) \quad (2-12)$$

2.1.2.1.2. MOONEY-RIVLIN (MR) MODEL

Earliest phenomenological theory of nonlinear elasticity that presented by Mooney and Rivlin have strain energy function definitions expressed in terms of first and second invariants[12] [13][14]

$$W = C_{10}(I_1 - 3) + C_{01}(I_2 - 3) \quad (2-13)$$

Mooney Rivlin model shows good agreement with tensile test data up to 100% strains. However, researches show that it is incapable of describing the compression mode of deformation. [11][14]

Tschoegl's researches imply that, having a third constant in MR model, shows better agreement with the test data. This model is called three term Mooney Rivlin model and has the strain energy function definition as [11]

$$W = C_{10}(I_1 - 3) + C_{01}(I_2 - 3) + C_{11}(I_1 - 3)(I_2 - 3) \quad (2-14)$$

There are different interpretations of MR models, called as Signiorini, Third Order Invariant, Third Order Deformation (James-Green Simpson). Their strain energy function definitions are described below, respectively.

$$W = C_{10}(I_1 - 3) + C_{01}(I_2 - 3) + C_{20}(I_1 - 3)^2 \quad (2-15)$$

$$\begin{aligned} W = & C_{10}(I_1 - 3) + C_{01}(I_2 - 3) \\ & + C_{11}(I_1 - 3)(I_2 - 3) \\ & + C_{20}(I_1 - 3)^2 \end{aligned} \quad (2-16)$$

$$\begin{aligned} W = & C_{10}(I_1 - 3) + C_{01}(I_2 - 3) \\ & + C_{11}(I_1 - 3)(I_2 - 3) \\ & + C_{20}(I_1 - 3)^2 + C_{30}(I_1 - 3)^3 \end{aligned} \quad (2-17)$$

2.1.2.1.3. YEOH MODEL

Yeoh model describes the strain energy function as a function of first strain invariant. This is based on the assumption that the second invariant is constant with stretch.[5]

$$W = C_{10}(I_1 - 3) + C_{20}(I_1 - 3)^2 + C_{30}(I_1 - 3)^3 \quad (2-18)$$

This model is more useful to fit various modes of deformation using the data obtained by the uni-axial testing. This leads reduced requirements on material testing. However, Yeoh states that this model should be used with caution when system undergoes low strain rates. [11]

2.1.2.1.4. ARRUDA-BOYCE MODEL

Arruda-Boyce model, similar to the Yeoh model, is based on first strain invariant. Moreover it claims to mitigate the weakness of the Yeoh model in low strain rate cases.

Arruda-Boyce model, rather than the aforementioned models, is not a phenomenological model. It describes the physics of deformation. The underlying molecular structure of elastomer is represented to simulate the non-Gaussian behavior of individual chains in the network thus representing the physics of network deformation[4][11]

Arruda-Boyce model shows agreement with the cases up to 300% strains.[14]

As well as first strain invariant I_1 , Arruda boyce model depends on the chain density n , Boltz-mann constant k , number of the rigid links composing a single chain N , and temperature θ [5]

$$\begin{aligned} W = nk\theta & \left[\frac{1}{2}(I_1 - 3) + \frac{1}{20N}(I_1^2 - 9) \right. \\ & + \frac{11}{1050N^2}(I_1^3 - 27) \\ & + \frac{19}{7000N^3}(I_1^4 - 81) \\ & \left. + \frac{519}{673750N^4}(I_1^5 - 243) \right] \end{aligned} \quad (2-19)$$

2.1.2.1.5. GENT MODEL

Like Arruda-Boyce model, Gent model also depends on the physics of deformation. The strain energy function is defined as the function of first strain invariant I_1 , shear modulus G and a limiting factor I_m which is $I_1 - 3$, taking into account limiting polymeric chain extensibility.[11][5]

$$W = \frac{-G}{2} I_m \ln \left[1 - \frac{I_1 - 3}{I_m} \right] \quad (2-20)$$

2.1.2.2. HYPERELASTIC ANALYSIS: NONLINEARITIES

Unlike metals, rubber requires many more properties to characterize its behavior. The behavior of rubber is nonlinear in terms of both material and geometrical aspects. Hence, it can be further complicated in terms of temperature, loading rate, strain history and so on.

There are lots of theoretical models in attempts to characterize rubber mechanical behavior. However, most of them have expressions including simplest geometries and loading cases.

Fortunately, FEA programs can simulate elastomeric material behavior to understand and optimize the rubber in the engineering field [15]. However, simulation of a rubber material in finite element formulation is highly nonlinear. There are three main reasons to a rubber deformation process be nonlinear [6]

1. Structure itself experiences large deformations. Its geometric configuration can cause nonlinear behavior
2. A nonlinear stress-strain relationship is another source of nonlinearities
3. Contact is a changing status nonlinearity. In case of sealants, contact is very crucial to understand

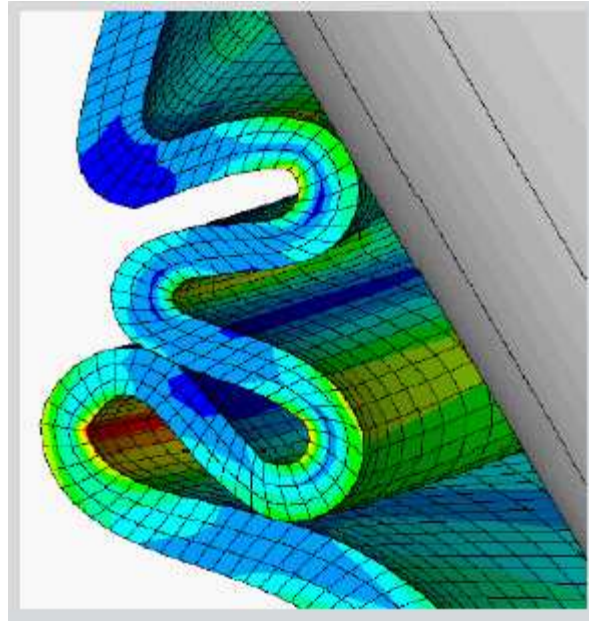


Figure 7. Example of nonlinearities: large deformation, nonlinear material characterization and contact [6]

FEA programs often use linear solvers. But it is possible to overcome a nonlinear problem with linear solvers. In a linear analysis, a problem can be solved directly with a set of linear equations. However, for a nonlinear problem, can be analyzed using an iterative series of linear approximations.

In this work *ANSYS Mechanical* will be used to simulate nonlinear rubber deformation process. *Mechanical* uses an Newton-Raphson iteration procedure.

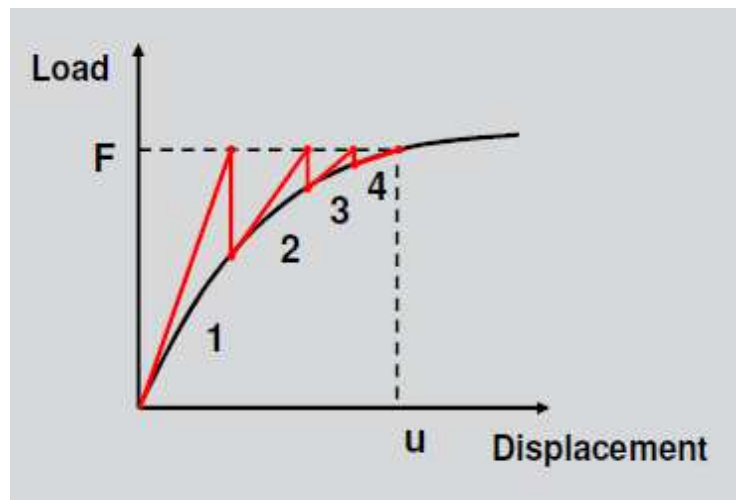


Figure 8. Solving a non-linear problem with linear solvers [6]

In the Newton-Raphson method, the total load is applied to the system to obtain resulting displacement. With the resulting displacement, internal forces are calculated. If the initial applied force and internal force are not equal, a new stiffness matrix is calculated based on the current conditions. This process is repeated until the initial and internal forces are equal. Figure 9 shows the representative explanation of the Newton-Raphson method.

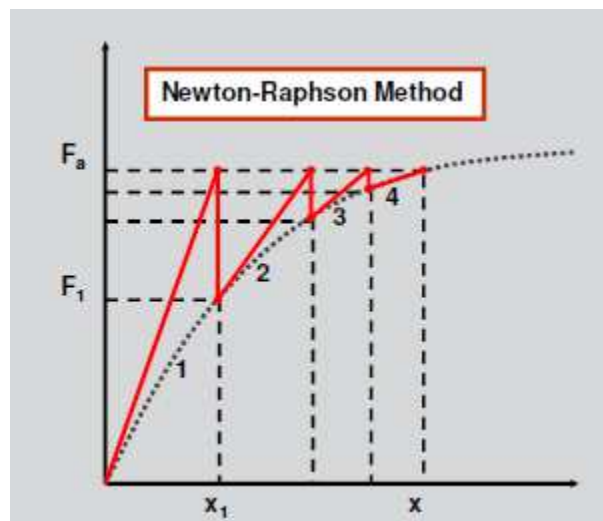


Figure 9. Newton-Raphson method [6]

However, Newton Raphson method does not guarantee to converge in all cases. Starting configuration should be inside the *radius of convergence*. Figure 10 shows the possible divergence and convergence configurations for a nonlinear FEA using Newton Raphson method.

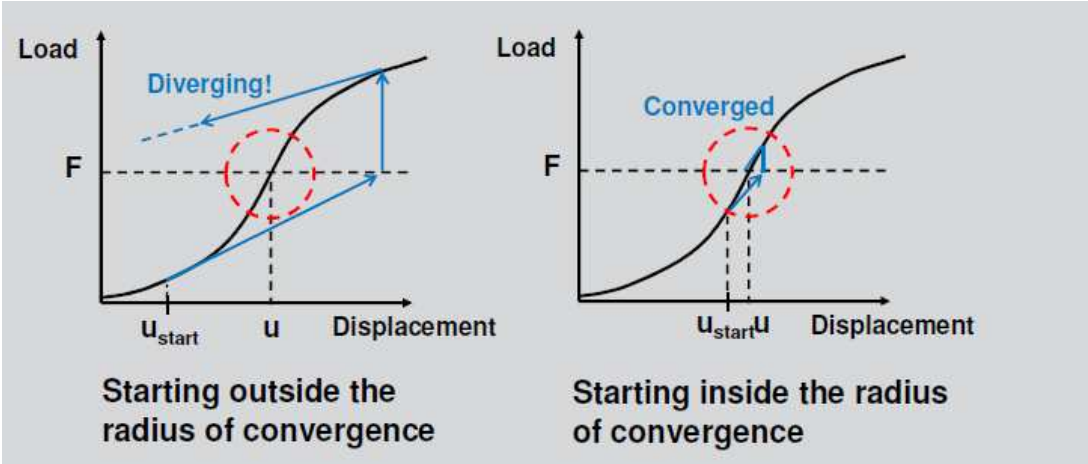


Figure 10. Divergence and convergence configurations for a nonlinear FEA [6]

For this reason, nonlinear FEA requires different preliminary decisions to be made. Introducing *load steps*, dividing the loading case in *substeps*, and using a *trial-and-error* method are sample methods to overcome divergence issues related to the nonlinear FEA analysis.

2.2. ACOUSTICS

2.2.1. SOUND TRANSMISSION LOSS

When acoustic wave encounters the boundary of a second medium, reflected and transmitted waves are generated. The mathematical expressions can easily be obtained for the transmission phenomenon when both incident wave and the plane between the two media are assumed to be planar.[16]

When the two media are fluids, one can obtain the mathematical expression for the transmission as below. Let the incident and reflected waves travel in a fluid that has specific acoustic impedance $r_1 = \rho_1 c_1$. ρ_1 is the equilibrium density of the fluid and

c_1 is the speed of sound in Medium 1. The second medium where the transmitted wave propagates is assumed to have specific acoustic impedance of $r_2 = \rho_2 c_2$.

Incident wave travelling in the +x direction is:

$$p_i = P_i e^{j(\omega t - k_1 x)} \quad (2-21)$$

which, when striking the boundary, generates a reflected wave

$$p_r = P_r e^{j(\omega t + k_1 x)} \quad (2-22)$$

and a transmitted wave

$$p_t = P_t e^{j(\omega t - k_2 x)} \quad (2-23)$$

Where k_1 and k_2 are wave numbers in medium 1 and medium 2, respectively. Transmission coefficients based on pressure, intensity and power, then, can be defined as:

*Pressure
Transmission
Coefficient*

$$T = \frac{P_t}{P_i} \quad (2-24)$$

*Intensity
Transmission
Coefficient*

$$T_I = \frac{I_t}{I_i} = \left(\frac{r_1}{r_2}\right) |T|^2 \quad (2-25)$$

*Power
Transmission
Coefficient*

$$T_{\Pi} = \left(\frac{A_t}{A_i}\right) T_I = \left(\frac{A_t}{A_i}\right) \left(\frac{r_1}{r_2}\right) |T|^2 \quad (2-26)$$

There are two boundary conditions to be satisfied:

(1) The acoustic pressures on both sides of the boundary must be equal (*continuity of the pressure*)

(2) The normal components of the particle velocities on both sides of the boundary must be equal (*continuity of the normal component of velocity*)

$$p_i + p_r = p_t \quad (2-27)$$

$$u_i + u_r = u_t \quad (2-28)$$

Division of these two equations yield:

$$\frac{p_i + p_r}{u_i + u_r} = \frac{p_t}{u_t} \quad (2-29)$$

since a plane wave has $\frac{p}{u} = \mp z$ the sign depending on the direction of propagation becomes

$$z_1 \frac{p_i + p_r}{u_i + u_r} = z_2 \quad (2-30)$$

which leads to the reflection coefficient

$$r = \frac{z_2 - z_1}{z_2 + z_1} \quad (2-31)$$

Since, in the absence of boundary losses, $1 + r = \tau$

$$\tau = \frac{2z_2}{z_2 + z_1} \quad (2-32)$$

And the intensity transmission coefficient is

$$T_I = \frac{4z_2z_1}{(z_2 + z_1)^2} \quad (2-33)$$

However, for a fluid solid interaction acoustic problem, the mathematical expressions are much more complex. The governing equations for an acoustical FSI problem will be given in the following sections.

2.2.2. SOUND TRANSMISSION LOSS OF ELASTOMERIC BULB SEALS

In the literature different studies about sound transmission loss characterization of elastomeric bulb seals are present. Park et al. studied sound transmission loss of elastomeric bulb seals by forming different simple mathematical models and compared the results obtained from FEA. For the acoustical models with exact shape of the seal, FE results are compared with experimental results performed in reverberation chamber. He also examined the seal surface velocity during transmission by a laser vibrometer. Effects of material properties and different compression ratios were investigated[2]. Gür and Norman considered effects of different material properties on sound transmission characteristics of a sealant. They also developed a FE based acoustic FSI analysis tool to determine transmission loss. From a simple, single layer FE model up to complex automotive door seal systems, they performed FEA for different aspects of seals, namely, boundary conditions, layer numbers, entrance length, material density, seal constitutive model and seal prestress [17]. Li, also used reverberation chambers to measure transmission loss of a sealant rather than just calculating it with analytical and numerical methods. He also mentioned that, for the low frequencies, dual membrane model is a good approximation, while for the mid and high frequency range, FEA with the exact shape of the seal will yield more reasonable results[1]. Andro et al. also considered this case as a two step analysis - static and acoustic. They performed uni-axial tests for hyperelastic material characterization and ACTRAN for acoustic analyses. Analyses were performed in 2D in their work. Lastly, they performed a sensitivity analyses in order to evaluate the influence of the parameters used in study such as compression ratio, material properties of the seal and seal geometry [18]. Stenti et al. consider the car door and door sealant as a combined structure. They studied the structure-borne vibration transmission of a door seal and its effect on full-vehicle NVH analysis. The effect of seal on door dynamic response was obtained, and the results were used to extract an equivalent linearized seal model in the form of mass-spring-dashpot system to be used in full vehicle NVH analyses [9]. Also there is an US Patent numbered 5,940,788 defining a method and system for designing vehicle

door seals based on sound transmission characteristics. Steps were defined to obtain deformation and transmission loss[19].

Hongisto also studied sound insulation of doors into two chapters, structural and leak transmission. In the first part of his work, he concluded that the total sound reduction index of a door is equally dependent on both transmission paths. Acoustical tests were performed on tape-sealed doors and doors have opened seals. By comparing these two results, he obtained the noise contributions of two paths into sound transmission. Transmission from leaks was predicted using the theories for slit and aperture prediction. In the second part of his study, obtained results are also compared to the experimental results carried on different metal or timber doors. For the doors with and without seals, he concluded that different mathematical models were useful regarding the slit and aperture transmission [3], [20],[21].

Herrera and Recuero experimented different seal type application on specified doors. Experimental results, then, compared with a combination of sound insulation models. He concluded that, for the doors with different sound transmission coefficient, Hongisto's research shows errors and needs to be corrected. Also he pointed out that, leakages on seal structures can create errors in measurements [22].

Also door closure sound is an important phenomenon considering seals. Petniunas et al. examined the relationship between closure sound quality and door system design. They observed that door closing sound quality is primary related to its loudness and sharpness [23]. Mahale et al. describes a methodology for interior noise source identification and its analysis for benchmarking. Car door seals constitute an important part of the interior noise source within the car bodies [24].

2.2.3. FLUID SOLID INTERACTIONS (FSI)

In acoustic FSI problem, structural dynamics equations must be considered together with the fluid momentum equations and the flow continuity equations. Fluid momentum and continuity equations are simplified to obtain acoustic wave equations by the following assumptions [25]

- The fluid is compressible (density changes due to pressure fluctuations)
- There is no mean flow of fluid.

Acoustic wave equation is given as:

$$\nabla \left(\frac{1}{\rho_0} \nabla p \right) - \frac{1}{\rho_0 c^2} \frac{\partial^2 p}{\partial t^2} + \nabla \left[\frac{4\mu}{3\rho_0} \nabla \left(\frac{1}{\rho_0 c^2} \frac{\partial p}{\partial t} \right) \right] = - \frac{\partial}{\partial t} \left(\frac{Q}{\rho_0} \right) + \nabla \left[\frac{4\mu}{3\rho_0} \nabla \left(\frac{Q}{\rho_0} \right) \right] \quad (2-34)$$

where

c: speed of sound

ρ_0 : mean fluid density

μ : dynamic viscosity

p: acoustic pressure

Q: mass source in the continuity equation

t: time

The discretized structural equation and the lossy wave equation must be considered simultaneously in acoustic FSI problems. The wave equation will be discretized in the next pages, followed by the derivation of the damping matrix to account for the dissipation at the FSI interface. Assuming a harmonically varying pressure is given by

$$p(\vec{r}, t) = Re[p(\vec{r})e^{j\omega t}] \quad (2-35)$$

where

p: amplitude of the pressure fluctuation

j: imaginary constant(square root of -1)

ω : frequency (rad/s)

t: time

Equation 2-34 will reduce to the inhomogeneous Helmholtz equation:

$$\begin{aligned} \nabla \left(\frac{1}{\rho_0} \nabla p \right) - \frac{\omega^2}{\rho_0 c^2} p + j\omega \nabla \left[\frac{4\mu}{3\rho_0} \nabla \left(\frac{1}{\rho_0 c^2} p \right) \right] = -j\omega \left(\frac{Q}{\rho_0} \right) + \\ \nabla \left[\frac{4\mu}{3\rho_0} \nabla \left(\frac{Q}{\rho_0} \right) \right] \end{aligned} \quad (2-36)$$

Figure 11 shows the schematic representation of a acoustic fluid-solid coupling in 2D analyses. In this figure, structural elements and acoustic elements are separated with the special acoustic elements with Key Option(2)=0. That defines the acoustical coupling option **open** for these elements.

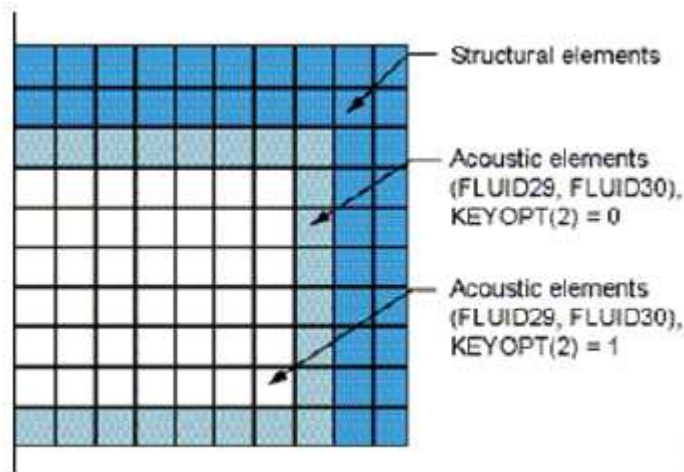


Figure 11. Representation of acoustic FSI [25]

The coupling conditions on the interface between the acoustic fluid and the structure are given by

$$\vec{\sigma}(\vec{u}_S)\vec{n} + p\vec{n} = 0 \quad \text{on } \Gamma_1 \quad (2-37)$$

$$\vec{n} \cdot \vec{u}_S - \vec{n} \cdot \vec{u}_F = 0 \quad \text{on } \Gamma_1 \quad (2-38)$$

where

$\vec{\sigma}(\vec{u}_S)$: solid stress tensor

p: acoustic pressure

\vec{u}_S : displacement in solid

\vec{u}_F : displacement in acoustic fluid

\vec{n} : outward normal unit vector of fluid domain

Equation 2-37 is a kinetic condition relating the solid stress to the pressure imposed on the interface by sound. Equation 2-38 is a kinematic condition that assumes that there is no friction between the solid and acoustic fluid on the interface.

CHAPTER 3

HYPERELASTIC FEA MODELS AND SIMULATIONS

In this chapter, geometry forming, meshing techniques, material characterization, boundary conditions and excitation definitions are presented along with results obtained from FEA. Analyzes reported in this chapter are twofold. Firstly, effects of material constants and different hyperelastic material modeling on total deformation results are explained. Secondly, phenomena of buckling or wrinkle in bulb seals are analyzed. Calculated deformed geometries in 3D are carried to the acoustic analyses. Lengths of the 3D models are arbitrarily chosen.

3.1. GEOMETRY AND MESH GENERATION

Three main different sealant geometries are used in this research. These three geometries are taken from three important companies working on the rubber industry for years. The first one is taken from the "Zero International". Zero International is a company specialized on door and window sealing and gasketing systems. They have high-performance acoustic gaskets as well as antibacterial, RFI protected, finger protected and radioactive dust protected sealants. Figure 12 shows the model used in door gasketing system. Figure 13 and 14 shows the 2D model of the sealant used in buckling analyses and 3D model that is used for full analysis to be carried within acoustic analyses.

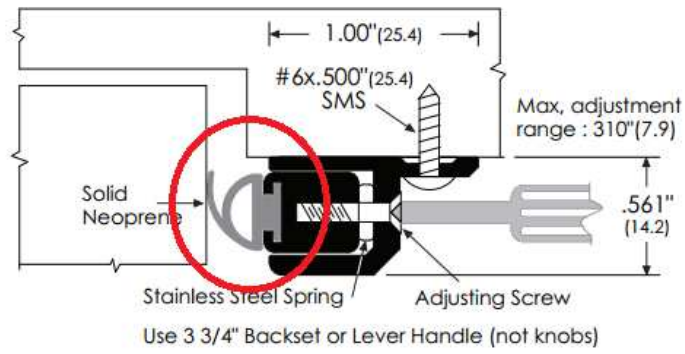


Figure 12. Model Zero_712 in its application

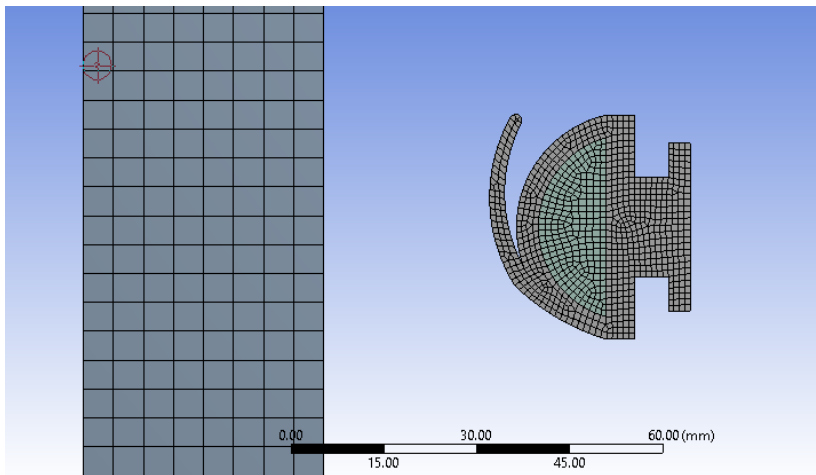


Figure 13. 2D model of sealant section and potential mating surface used in buckling analyses

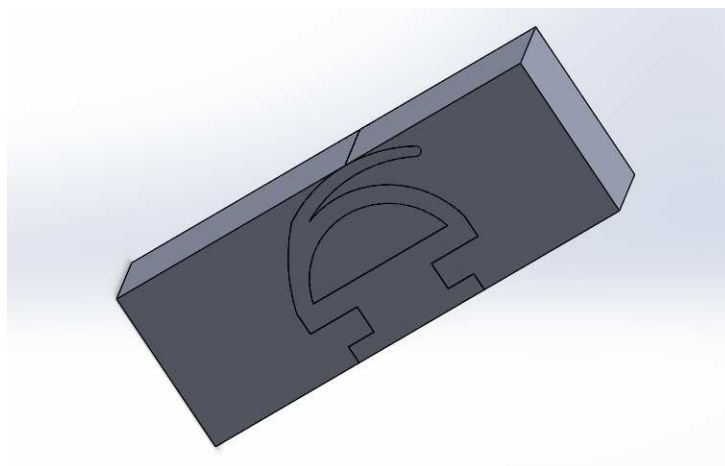


Figure 14. 3D model created using Zero International model 712

The second sealant geometry is taken from the "Standart Profil" company which is also specialized in automotive gasketing systems. The geometry used in this research is a hood seal designed to act as a barrier between the car body and cowl to prevent water and dust leakage in difficult working and environmental conditions. Figure 15 shows the CAD of the hood seal taken from the Standart Profil Company. Figure 16 shows the 2D model of the sealant and mating body to be used in buckling analyses. Full 3D model is used in deformation analysis is presented in Figure 17.



Figure 15. Section of seal obtained from Standart Profil Co.

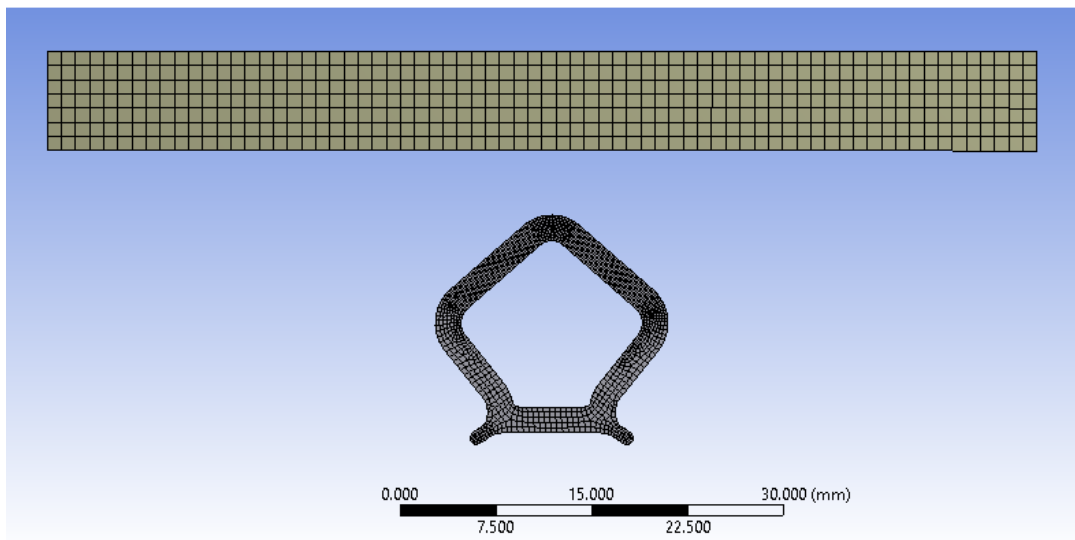


Figure 16. 2D model of sealant section and potential mating surface used in buckling analyses

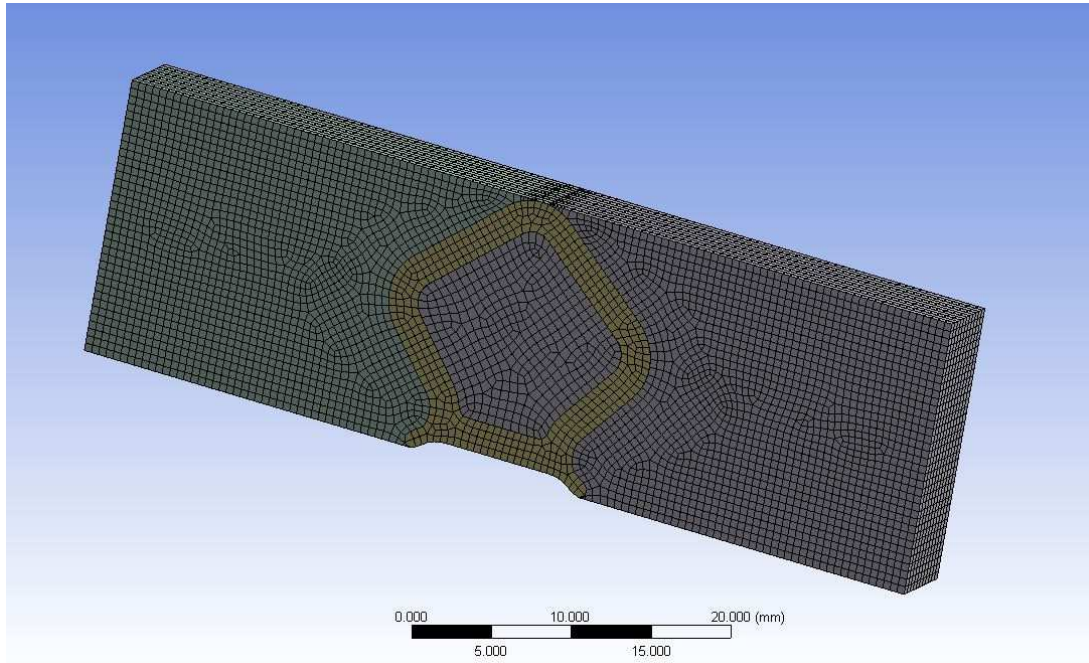


Figure 17. 3D model and mesh created using geometry obtained from Standart Profil

The last sealant geometry taken from the BilPlas, serves as plastic-rubber production in industry. Having horizontal top surface, this geometry is a little bit different from other sections. Figure 18 shows the geometry obtained from BilPlas Company and Figure 19 shows the 2D meshed model used in buckling analyses. 3D model used in full analyses is given in Figure20.

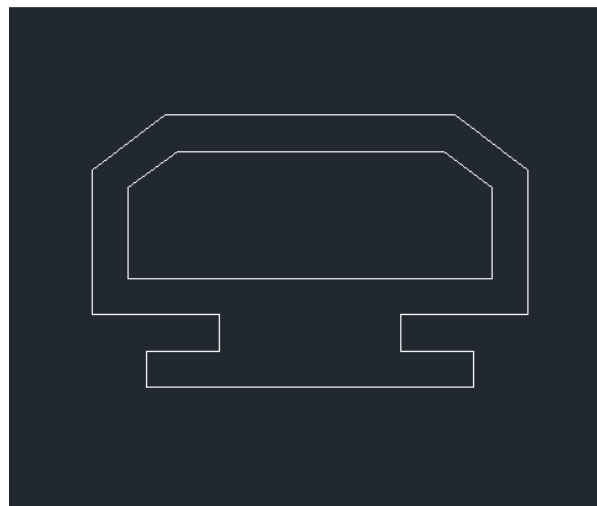


Figure 18. Section of seal obtained from BilPLas

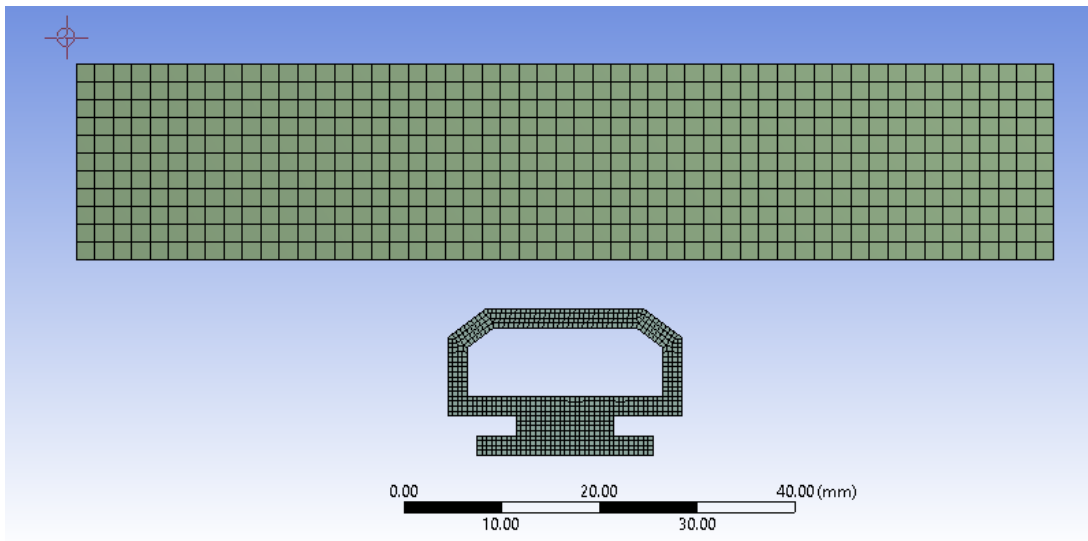


Figure 19. 2D model of sealant section and potential mating surface used in buckling analyses

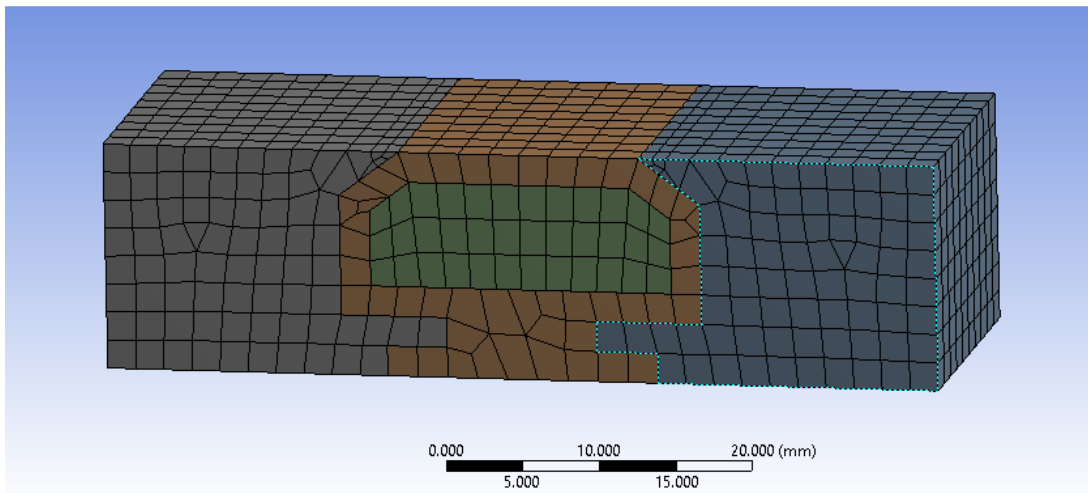


Figure 20. 3D model and mesh created using geometry obtained from BilPlas

3.2. PRELIMINARY DECISIONS AND PREPROCESSING

Two different objectives are specified before the analyses. First one is to obtain deformed geometries of sealants and the other is to observe any possible buckling that may occur under contact.

For the deformation analysis, 3D models are used, since they will be carried to the harmonic analyses in which acoustic analyses are performed. Acoustic analyses are carried in 3D and the initial geometry for the acoustic analyses is obtained from the deformed geometries. Creation and manipulation of deformed geometries is a burden in ANSYS environment and has some limitations. Nodal coordinates of the deformed geometry is tracked after deformation and new geometry is formed upon deformation using updated coordinates. However, it is not possible to add or subtract geometry afterwards; hence total geometry should be created intuitively beginning from the first analyses. Inlet, outlet and internal air parts are modeled at the static analyses, even though they don't have any effect on the deformation process. Figure 21 shows the project schematic used in ANSYS workbench environment to obtain the deformed geometry. Inside static structural analysis, parts are tracked using named selections and with the command UPCOORD, new coordinates of the nodes are transferred to the finite element modeler.

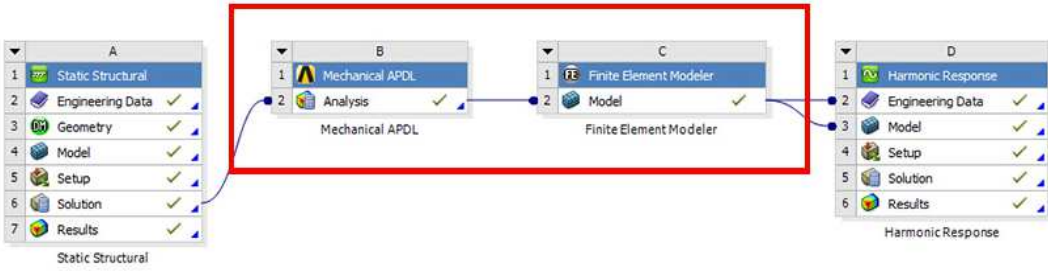


Figure 21. ANSYS WB Project Schematic. Boxed parts are used to obtain deformed geometries

Nevertheless, only two of three geometries can be used in full 3D deformation analyses. The section obtained from Zero International Co. has gaps between its surfaces and modeled air mesh elements disappears under compression. That causes problems in 3D deformation analyses. Figure 22 shows the meshed 3D mode of Zero_712 geometry, direction of deformation (red) and elements that are going to disappear under compression (green).

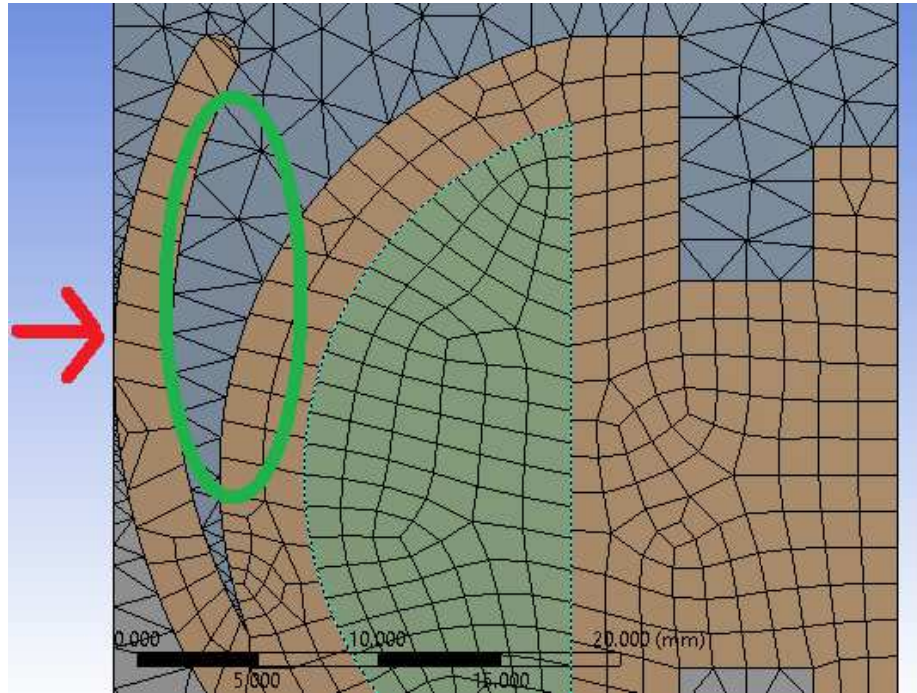


Figure 22. Limitations on Zero_712 geometry

Ten different material constants were taken from the literature to characterize rubber behavior. Even though the mechanical behavior of rubber material is closely connected to the composition, the studies where material constants are obtained are related to the incompressible elastomeric bulb seals, and mostly having the same hardness values. These ten different cases with ten set of material constants are compared with each other to comprehend if any differences or inconsistencies occur. Moreover, since the geometries are not very complex and extensive, a reasoning was applied to understand if the different material constant sets taken from the literature are acceptable to define material behavior.

For the buckling analyses, 2D models are used with mating bodies, since the geometries in this particular case are not used in acoustic analyses. 2D models are easy to simulate and save time. An example of buckling, if it is observed in FEA, is given in specific figures with the sealants compressed in clamp.

3.3. MATERIALS

For three different geometries, two main materials, air and elastomer, are defined for the simulations.

The air parts within the 3D models are hard to model in static structural analyses. Yet, they shouldn't interfere with the simulation of the deformation process of elastomeric seals. For the static structural analysis, then, these air parts are modeled with dummy material characterization with zero Poisson's ratio and nearly zero elastic modulus so that they have no effect on the deformation simulations. Hence, their geometry is not corrupted so that no side effect is transferred to the harmonic analyses. This is because, when positive Poisson's ratio is implemented, expanding of the air part in the lateral direction when the system is under compression. This would spoil the geometry of air part which would, in turn, cause problems in acoustic analysis. For the logical reasoning, a simple study was realized in a 2D square material with zero and positive Poisson's ratio adopted. In Figure 23, model is stretched upwards where the model has zero Poisson's ratio defined, so that no lateral deformation is observed. However, Figure 24 shows the same situation, with Poisson's ratio 0.2, that the lateral deformation is observed. Hence, zero Poisson's ratio is rational to use in air parts for static structural analysis, since the only important and expected result is the deformed shape of the sealant geometry.

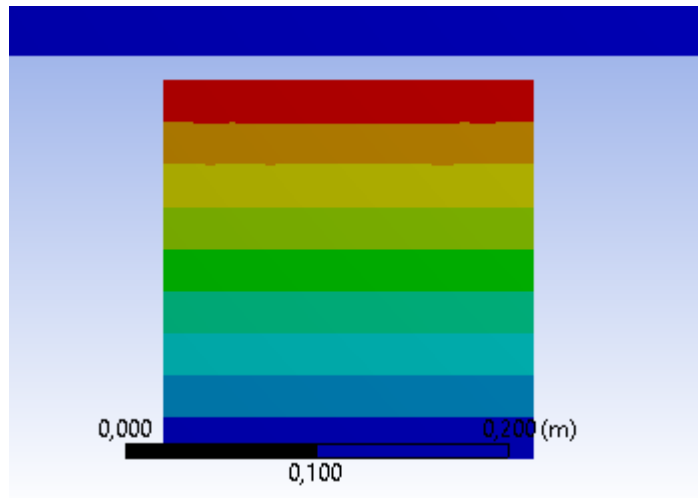


Figure 23. Simple study with zero Poisson ratio

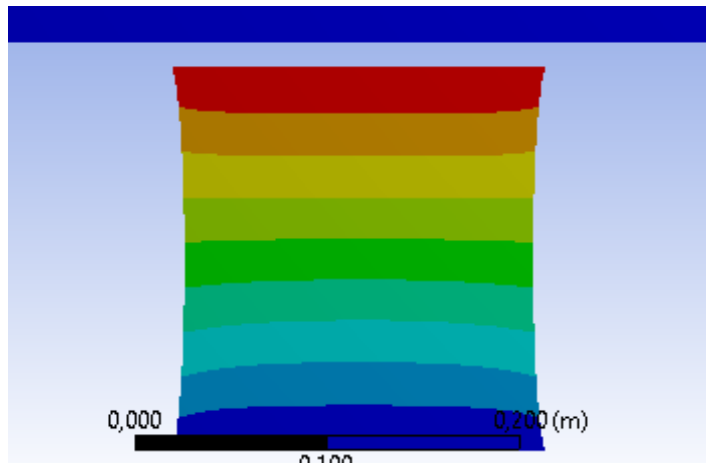


Figure 24. Simple study with Poisson ratio 0.2

For the sealant geometry, 10 different material constants are taken from the literature, having different hyperelastic material models. Material constants, and the related hyperelastic material models are tabulated in Table 1 and 2.

Table 1. Definitions of cases and references

Case Number	Reference	Material Model
1	MSC Software Technical Paper_Whitepaper [11]	Neo-Hookean
2	Charlton D.J & Yang J. [15]	2 term MR - 1
3	Charlton D.J & Yang J.[15]	2 term MR - 2
4	Charlton D.J & Yang J.[15]	5 term MR - 1
5	Charlton D.J & Yang J.[15]	5 term MR - 2
6	MSC Software Technical Paper_Nonlinear FEA of Elastomers[11]	3rd order Ogden
7	Stenti A., Moens D., Desmet W.[9]	5 term MR
8	Comsol Technical Paper[26]	2 term MR
9	Dikmen E., Başdoğan I.,[14]	2 term MR
10	Dikmen E., Başdoğan I.,[14]	Arruda Boyce

Table 2. Material constants used in cases*

Case Number	Material Model	Material Constants
1	Neo-Hookean	$\mu = 1.1 \text{ MPa}$ $D_1 = 0$ $\rho = 1200 \text{ kg/m}^3$
2	2 term MR - 1	$c_{10} = 0.4789 \text{ MPa}$ $c_{01} = 0.4447 \text{ MPa}$ $D_1 = 0$
3	2 term MR - 2	$c_{10} = 0.7497 \text{ MPa}$ $c_{01} = 0.05112 \text{ MPa}$ $D_1 = 0$
4	5 term MR - 1	$c_{10} = -7.958 \text{ MPa}$ $c_{01} = 9.821 \text{ MPa}$ $c_{11} = -9.9337 \text{ MPa}$ $c_{20} = 2.544 \text{ MPa}$ $c_{02} = 11.73 \text{ MPa}$ $D_1 = 0$
5	5 term MR - 2	$c_{10} = 0.6822 \text{ MPa}$ $c_{01} = 0.1796 \text{ MPa}$ $c_{11} = -0.03119 \text{ MPa}$ $c_{20} = 0.002114 \text{ MPa}$ $c_{02} = 0.004673 \text{ MPa}$ $D_1 = 0$

Table 2. Material constants used in cases * (Continued)

6	3 rd order Ogden	$\mu_1 = 0.63 \text{ MPa}$ $\mu_2 = 0.0012 \text{ MPa}$ $\mu_3 = -0.01 \text{ MPa}$ $\alpha_1 = 1.3 \alpha_2 = 5.0 \alpha_3 = -2.0$ $D_1 = 0 \ D_2 = 0 \ D_3 = 0$
7	5 term MR	$c_{10} = 0.0932811 \text{ MPa}$ $c_{01} = 0.0902353 \text{ MPa}$ $c_{11} = 0.0062266 \text{ MPa}$ $c_{20} = 0.0063716 \text{ MPa}$ $c_{02} = 0.0003311 \text{ MPa}$ $D_1 = 0$
8	2 term MR	$c_{10} = 0.37 \text{ MPa}$ $c_{01} = 0.11 \text{ MPa}$ $D_1 = 0$
9	2 term MR	$c_{10} = 0.1220719 \text{ MPa}$ $c_{01} = -0.029116 \text{ MPa}$ $D_1 = 0$
10	Arruda Boyce	$\mu = 0.033379 \text{ MPa}$ $\lambda_L = 0.9736532$ $D_1 = 0$

* Detailed information about material constants is given in Section 2.1.2.1 "Hyperelastic Material Models". These are the constants defining strain energy density functions for each hyperelastic material model.

3.4. RESULTS

For different cases, the same loading and boundary conditions are applied. Total deformation results for different geometries in different cases are illustrated in the following figures.

In BilPlas geometry, the system has a deformation of 2mm downwards. Other boundary conditions are kept the same. Also, the same mesh configurations are employed in ten different cases.

Standart Profil's geometry is different than BilPlas's geometry since its top surface is not flat. Hence, displacement condition cannot be applied directly to the system. Instead the following procedure is applied:

- The forcing (2N, downwards) is applied to the sealant geometry and inner air structure to get deformed shape in specified time steps. The magnitude of the forcing taken arbitrarily in this study to obtain proper deformation for the acoustic analyses. However, in real applications, this forcing describes another important parameter which is the door closure force. Examination of door closure force is not in the scope of this study. Yet, the same methodology can be applied for the situations where the door and sealant mating conditions, namely, the door closure force, are specified.
- From the deformed shape, deformation information is obtained through the time steps
- The same deformation and time step information is given as the deformation boundary condition to the inlet and outlet air surfaces to obtain a flat surface on the top of the whole model

Maximum values on total deformation results are displayed in Table 3 for two geometries and ten cases. Detailed information about analyses is presented in the Appendix.

Table 3. Results obtained at different cases for two different geometries

Case	Maximum values on total deformation of sealant - BilPlas (mm)	Maximum values on total deformation of sealant - Standart Profil (mm)
1	2,01	3,37
2	2,01	1,84
3	2,01	2,19
4	2,01	0,82

Table 3. Results obtained at different cases for two different geometries (Continued)

5	2,01	1,99
6	2,02	1.93
7	2,01	Did not converge
8	2,01	Did not converge
9	2,01	Did not converge
10	2,01	Did not converge

As can be seen from table 3, total deformation results are nearly the same for BilPlas geometry, while the results are not consistent for Standart Profil geometry. Difference in loading conditions due to the limitations of the 3D geometries used should yield these results. Yet, for the 2D conditions of Standart Profil geometry, no such discrepancies occur. Table 4 shows the results of Standart Profil geometry, when it is under compression by a mating body, for 10 cases. Detailed information related to the results is given in Results and Discussions chapter.

Table 4. Standart Profil 2D geometry, solutions with mating body

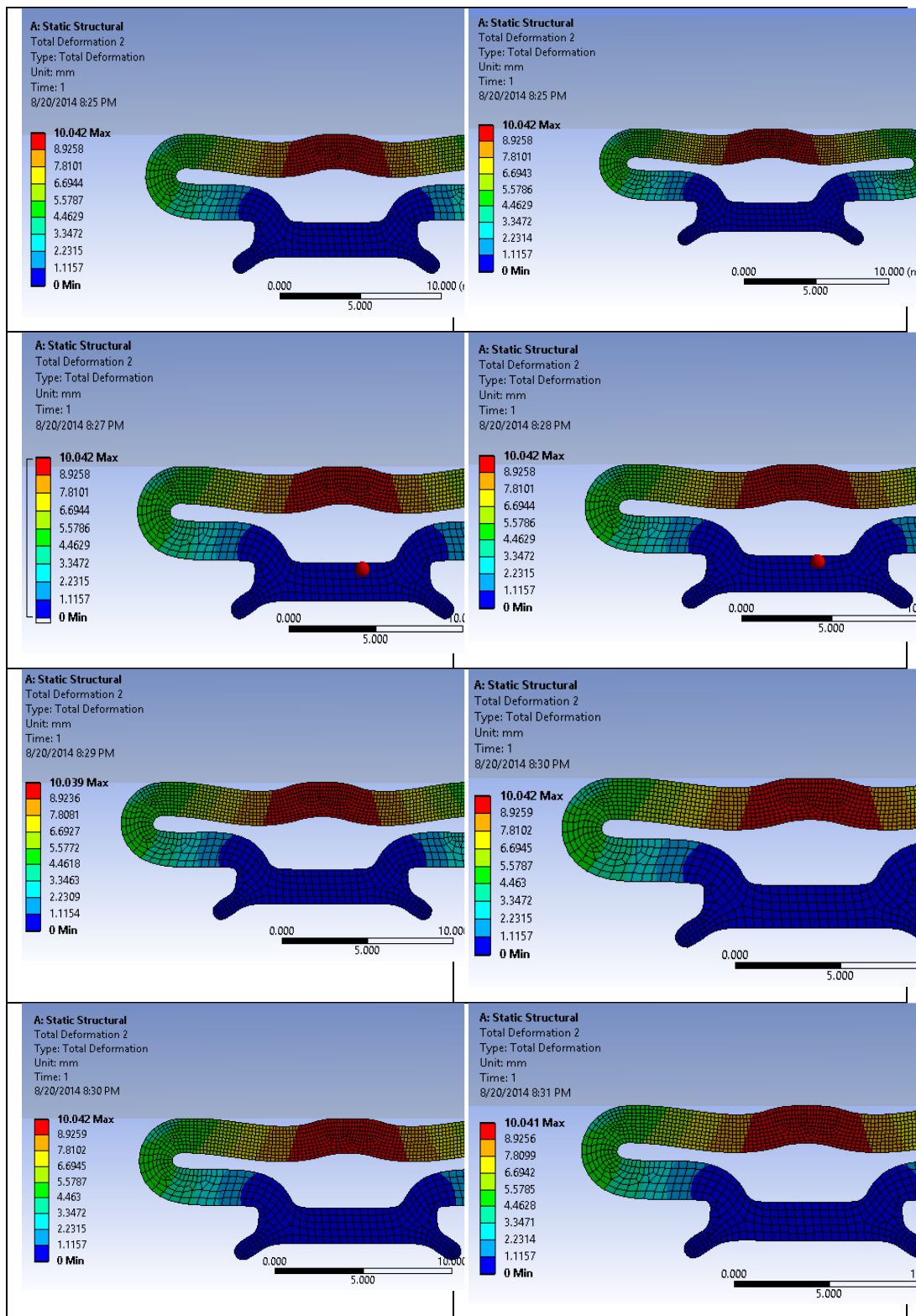
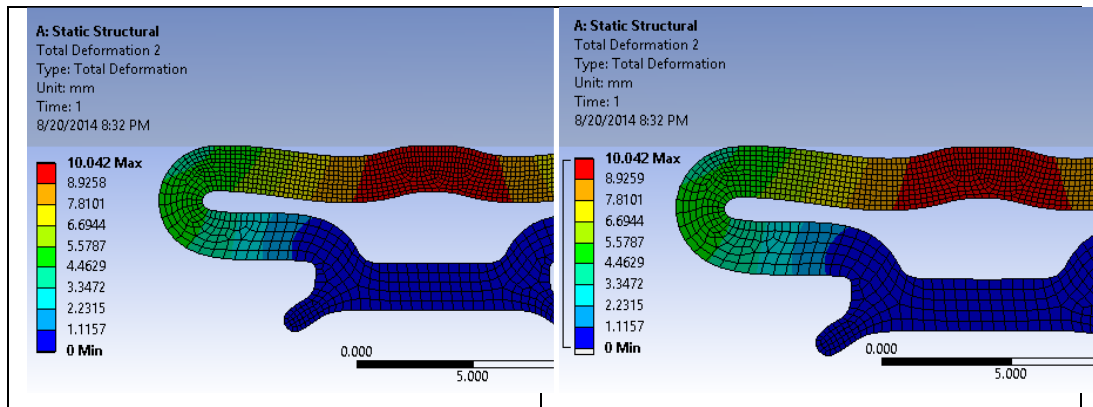
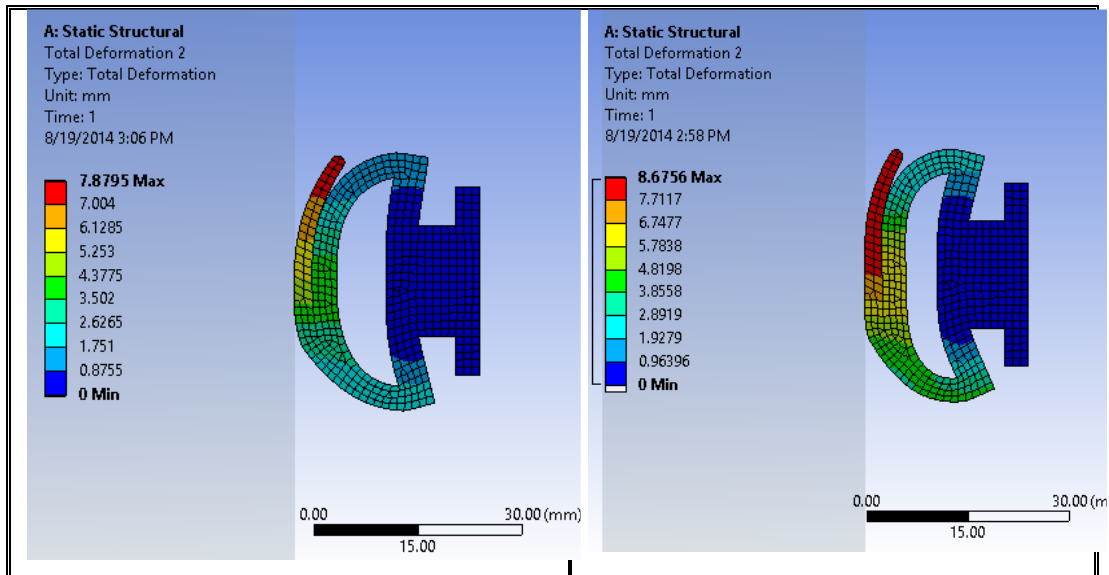


Table 4. Standart Profil 2D geometry, solutions with mating body (Continued)



Buckling or wrinkle is an important phenomenon in sealants since it can drastically decrease a sealant’s thermal and noise insulation capability. All of the sealant geometries, in 2D, having material constants defined in case 2 are subjected to different compression ratios and results are given in the following figures:



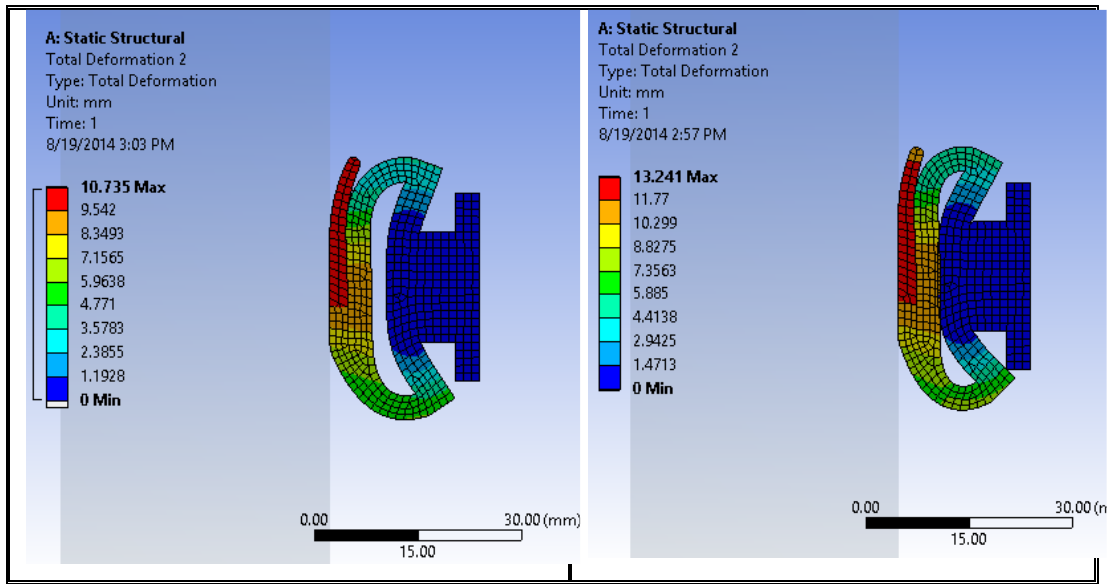
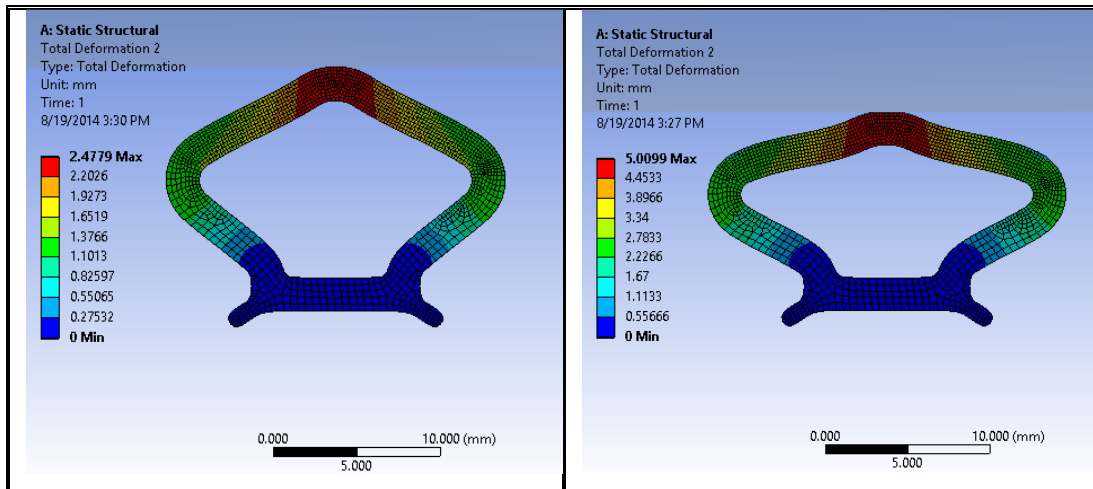


Figure 25. Deformation of Zero International geometry under different compression ratios



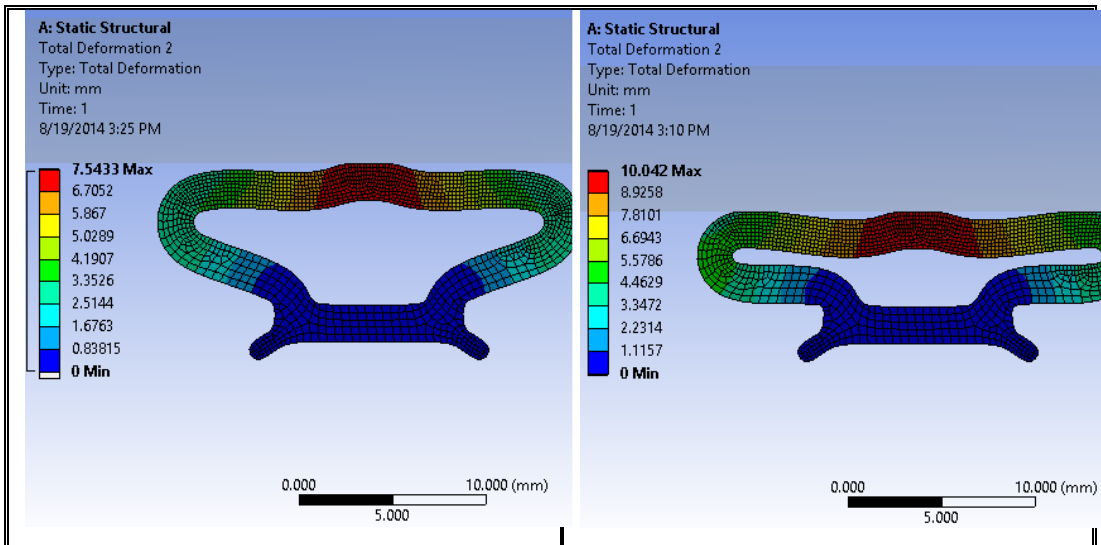
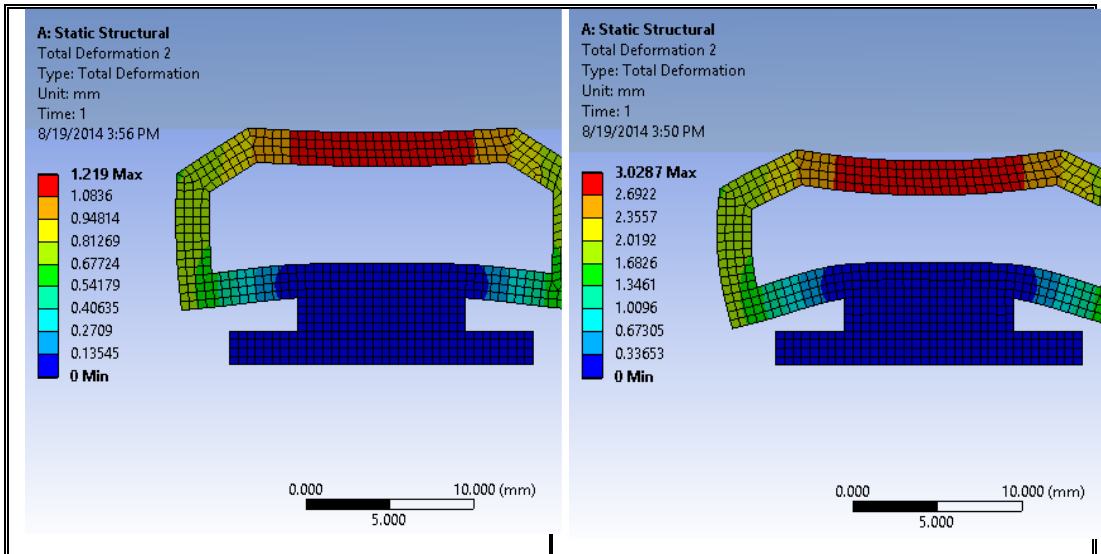


Figure 26. Deformation of Standart Profil geometry under different compression ratios



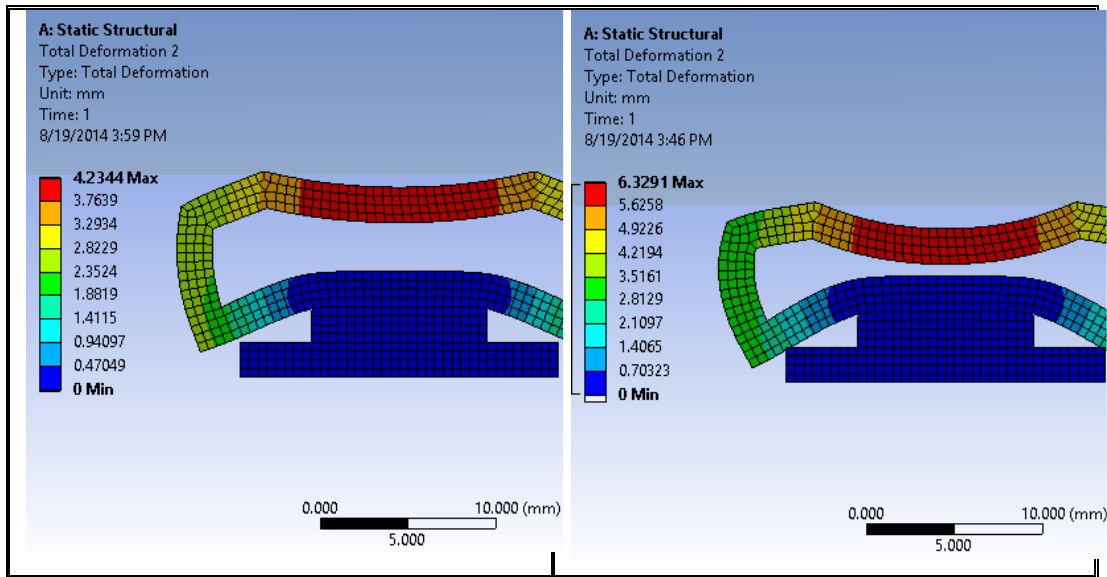


Figure 27. Deformation of BilPlas geometry under different compression ratios

As can be seen in Figures 25-27, BilPlas Geometry and Standart Profil geometry buckle under high compression ratios. However, Zero International geometry does not buckle since it has a one-end-free extra surface preventing buckling.

In order to verify results obtained from buckling analyses, BilPlas sealant sample is compressed in a clamp to see if any buckling occurs. Figure 28 shows the non deformed BilPlas sample. In its compressed form, it buckles and this situation is illustrated in Figure 29. Buckling can easily be observed; although the deformed geometry obtained from FEA results are not the same with the situation demonstrated in Figure 29. This is because the difference in boundary conditions at the bottom surface of the sealant, where it is not exactly simulated in the clamp.



Figure 28. BilPlas sample and its thickness



Figure 29. Buckling occurs when the system is under compression

CHAPTER 4

FEA MODELS OF DEFORMED GEOMETRIES AND ACOUSTIC SIMULATIONS

4.1. GEOMETRY AND MESH GENERATION

BilPlas and Standart Profil geometries are used in acoustic FEA. Sectional geometries are obtained from the first part of analyses. For the BilPlas geometry, since total deformation is the same for all the situations, sound transmission loss value has been determined for different compression ratios. However, for the Standart Profil geometry, geometry determination was not clear in 3D analyses, hence, one of the solutions having similar total deformation value with the BilPlas geometry is used.

Mesh resolution is fine enough to solve high frequency excitations. BilPlas geometry has mesh size of 1.5 mm and Standart Profil geometry has mesh size of 1mm. Minimum 6 elements are needed for the shortest wavelength considered in an acoustical FEA.

Highest frequency considered in this study is 4000 Hz. Wave speed of air is considered as 340 m/s, while for the seal layers, speed of sound can be obtained by using following equation: [2]

$$c_L = \sqrt{\frac{E(1-\nu)}{\rho_s(1+\nu)(1-2\nu)}} \quad (4-0-1)$$

The speed of sound in elastomer is lower than air, hence the critical value can be obtained by considering elastomer properties. Speed of sound in elastomer is around 97.4 m/s, changing with the Young's modulus value. For this sound speed, wavelength at 4000 Hz is found to be 24.3mm, which is longer than six times of element size, both for BilPlas and Standart Profil geometry.

High order, 3D, 20-node elements (FLUID220) are used in air medium. This element has some restrictions [25]

- The element must not have a zero volume.
- The element may not be twisted such that it has two separate volumes. This occurs usually when the element nodes are not in the correct sequence.
- All elements must have 20 nodes. A prism-shaped element may be formed by defining duplicate L and S and duplicate P and W nodes. A tetrahedron or pyramid shape is also available.
- The fluid is compressible (density changes due to pressure variations).
- There is no mean flow of the fluid.
- Note that the acoustic pressure is the excess pressure from the mean pressure.
- Analyses are limited to relatively small acoustic pressures so that the changes in density are small compared with the mean density

4.2. PRELIMINARY DECISIONS AND PREPROCESSING

For the acoustic FEA, 4 parts are modeled for both cases. Three air parts and sealant body. Detailed material description is given in the following section.

For the acoustic analyses, ANSYS Acoustics Customization Toolkit (ACT_Acoustics) is used. ACT_Acoustics can solve 3D acoustic problems and this capability eliminates the need for APDL in analyses. In this toolkit, acoustic bodies, boundary conditions and loads can be

defined in ANSYS Workbench environment. Moreover, it is possible to post process acoustical analyses results such as transmission loss based on power definition.

ANSYS ACT_Acoustics takes the fluid solid interaction into account. FSI surfaces can be defined in ANSYS Mechanical after installing ACT_Acoustics extension. Lastly, acoustic radiation boundary conditions can be applied at the inlet and outlet section of the model to characterize non-reflective boundary conditions.

Fixed and frictionless boundary conditions are applied to the elastomer structure to define its mounting structure and symmetry condition, respectively.

Acoustic fluid elements considered in acoustic bodies have pressure and particle velocity as variables. From these two quantities it is possible to determine the acoustic intensity over a surface. Acoustic power, hence, can be calculated using the intensity and area of the surfaces. ACT_Acoustics is able to define "ports" on surfaces in which acoustic power based quantities are calculated. Considering the first port of the system is the inlet and the second port of the system as the outlet, ANSYS can evaluate power result plots between two ports and obtain sound transmission loss graphs as a function of frequency.

4.3. MATERIALS

Air and elastomer parts are modeled in acoustic analyses. Air is defined as an acoustic body in which Helmholtz equation is considered. The fluid is assumed to be compressible and without any mean flow. Viscous effects and temperature dependent parameters are also neglected. Mass density of the air is taken as 1.2041 kg/m³ and speed of sound is defined as 343.24 m/s

Elastomers have frequency dependent modulus and damping characteristics. However, frequency dependency is overlooked in the assignment of these parameters in this study. Storage and loss modulus of a similar seal structure were measured in the study of Ando et. al. Figure 30 shows the storage and loss modulus of the elastomer versus frequency.

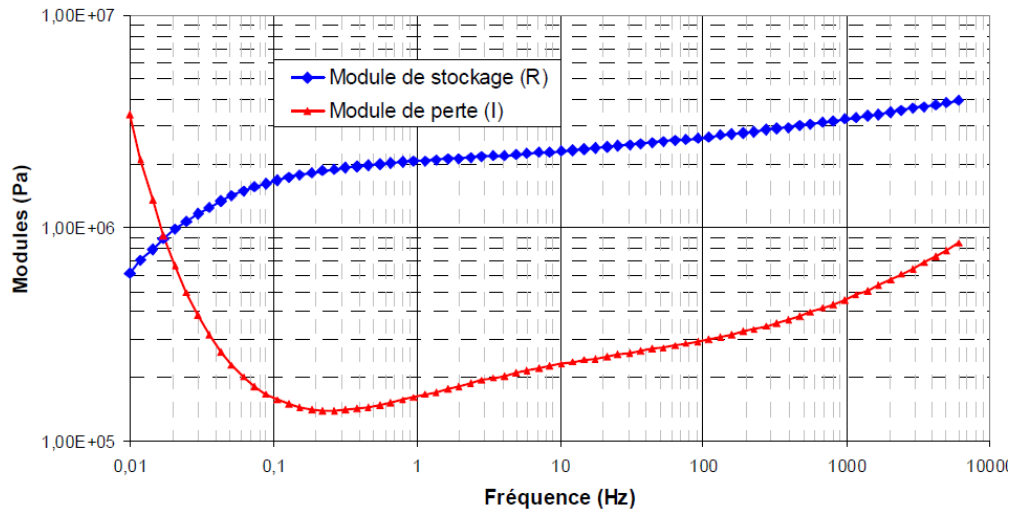


Figure 30. Storage and loss modulus of a door seal versus frequency (Taken from B. Andro et al., Prediction of Sound Transmission through Automotive Door Seal Systems)

Figure 30 shows that (in blue line), storage modulus of sealants can differ from 0.6 MPa to 4 MPa. In order to consider the effect of Young's modulus, different Young's moduli values are assigned to the elastomer structure and transmission loss values are compared.

Similarly, different loss factor values are assigned to elastomer structure in acoustic analyses to observe the effect of damping on sound transmission loss.

4.4. RESULTS

Before any harmonic analyses are performed, a convergence study is performed in modal analyses using seal geometries with different mesh resolutions. BilPlas geometry is used in this convergence study. Figures 31-33 shows different mesh resolutions. This convergence study is performed to observe resonance frequencies of seal in different mesh resolutions.

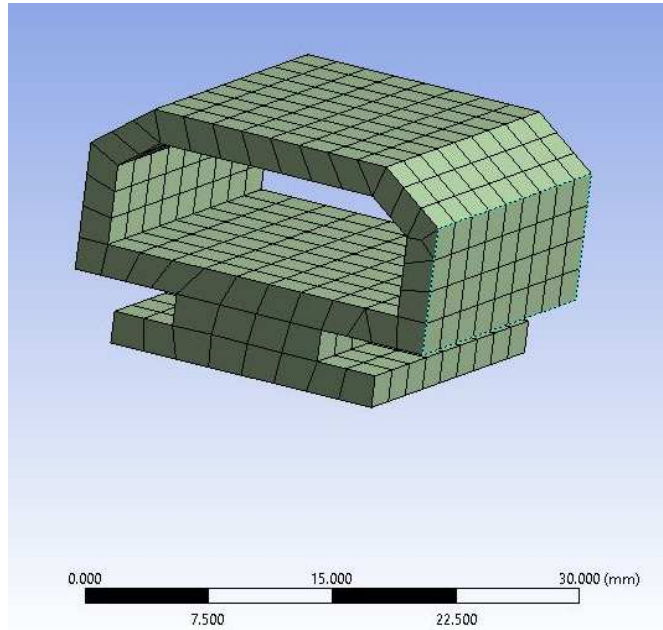


Figure 31. BilPlas geometry, used in modal analyses, low resolution mesh

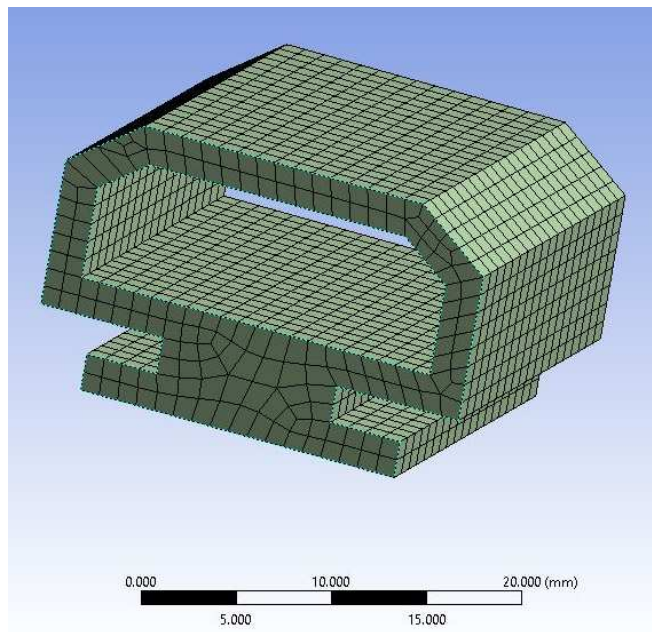


Figure 32. BilPlas geometry, used in modal analyses, medium resolution mesh

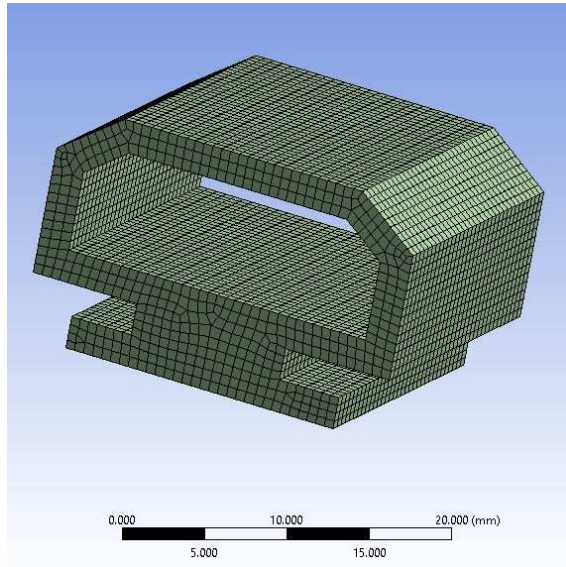


Figure 33. BilPlas geometry, used in modal analyses, high resolution mesh

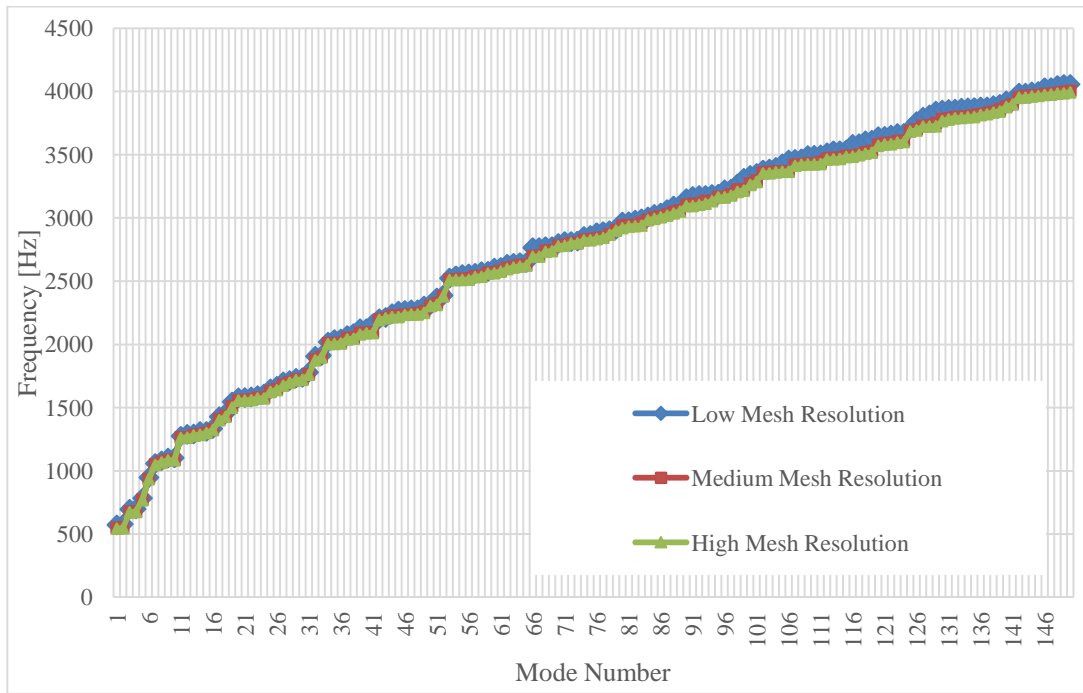


Figure 34. Mode numbers and corresponding frequencies with three different mesh resolutions

Modal analyses results show that, for all three mesh resolutions, model is capable of determining mode shapes of the seal geometry. All three models have showed nearly

same resonance frequencies up to 4000 Hz. Seal has been found to have nearly 150 modes within the range of study.

In order to verify the acoustic FEA results, two simplified seal models are considered. These models are:

- Two membrane model
- Simple rectangular model

Two-membrane model is an approximation of sealant structure such that two structurally independent membranes separated by an air gap as Park et al. considered.[2] Figure 31 shows the mathematical model of two-membrane model.

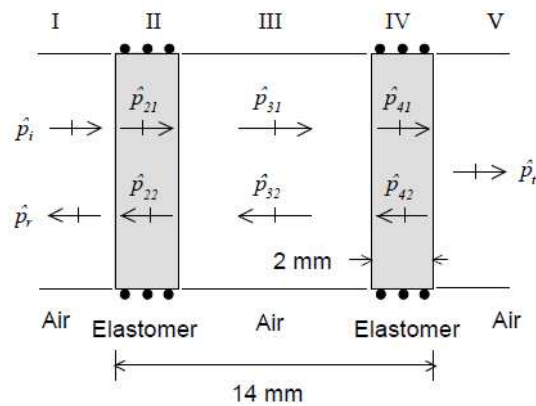


Figure 35. Two membrane model approximation (Taken from: J. Park et al. Sound Transmission through Elastomeric Bulb Seals)

The seal membranes are free to move along the direction of wave propagation. Friction forces on the upper and lower boundaries are neglected. Within the air cavity, sound field is assumed to be formed of planar incident and reflected waves. Elastomer thickness is 2mm and the distance between elastomer layers is 10mm. EPDM used in this simple two-membrane model has material density of $\rho_s = 370 \text{ kg/m}^3$ and Poisson's ratio $\nu = 0.4$. The dissipation due to material damping was neglected in this simple study. Nominal stiffness of the seal material is taken as 2.3 MPa.

Simple FE model of two membrane model is formed to compare results obtained from transfer matrix method. Figure 36 shows the simple two-membrane FE model.

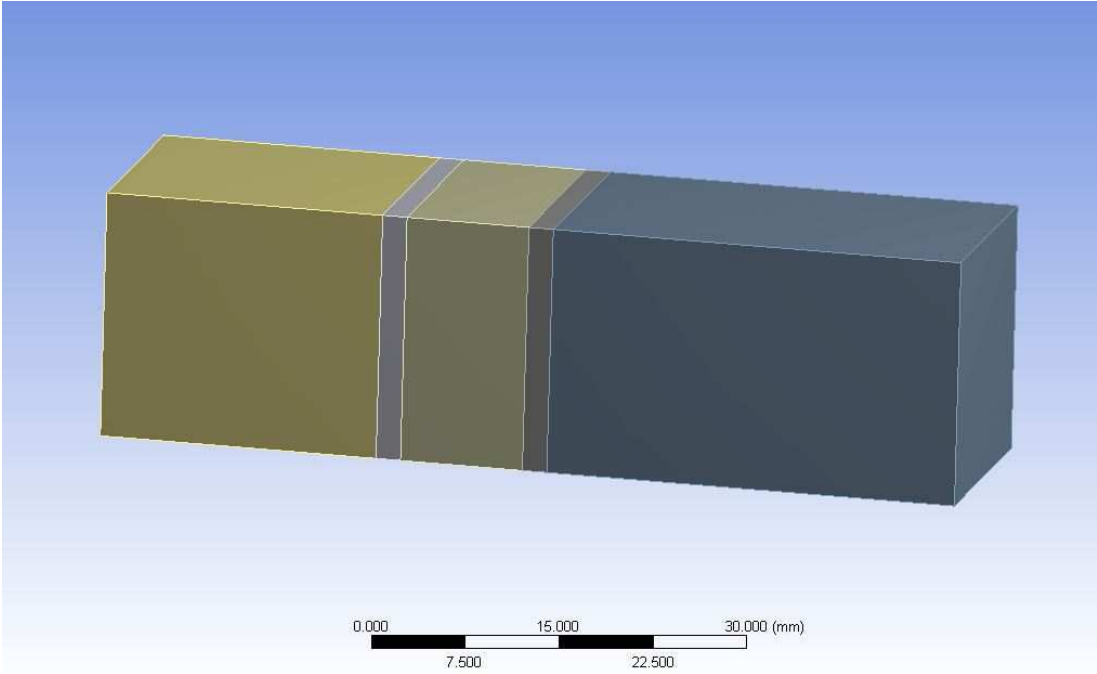


Figure 36. FE model of two membrane approximation

Park et al. used transfer matrix method to calculate sound transmission loss. Imposition of pressure and velocity continuity at the boundaries is considered. Hence the results obtained from transfer matrix method are given in Figure 37.

Same acoustic body definitions, boundary conditions and excitations are used in simple FE model with the full acoustic model. Results obtained from FE model of two membrane model shows the similar trend with the results obtained from transfer matrix model. Figure 38 shows the results obtained from simple FE model.

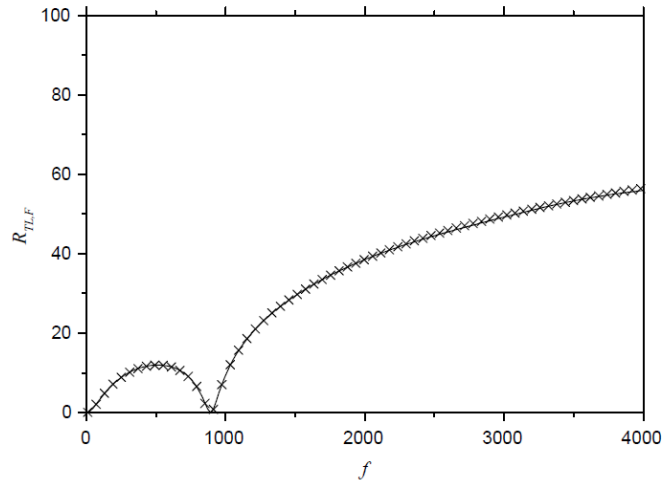


Figure 37. TL obtained from dual membrane model, by transfer matrix method (Taken from: J. Park et al. Sound Transmission through Elastomeric Bulb Seals)

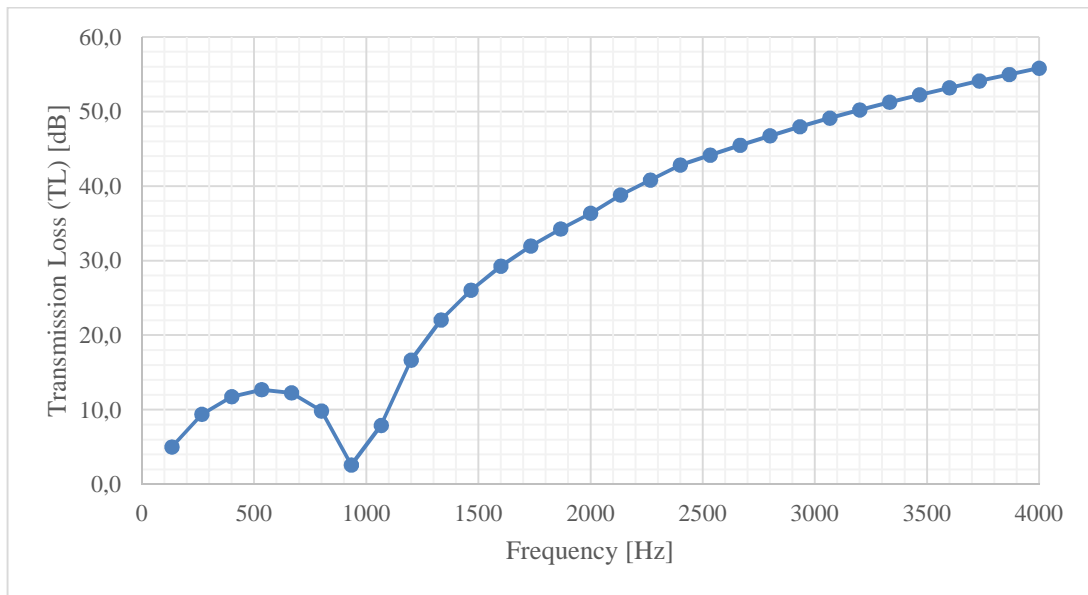


Figure 38. TL vs. frequency, obtained from the simple two-membrane FE model

It can be concluded from comparison of the two results shown in Figure 37 and Figure 38 that, acoustic applied boundary conditions, excitations, FSI surface and acoustic body definitions are correct and meaningful.

Another model of the sealant is the rectangular model illustrated in Figure 39. Rectangular model is slightly more complex than the two membrane model. Figure 39 shows the dimensions and the boundary conditions of rectangular model.

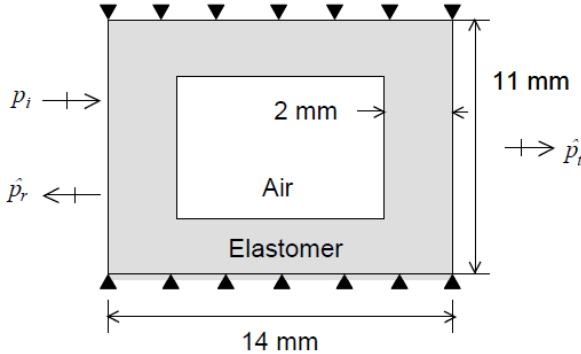


Figure 39. Rectangular model approximation (Taken from: J. Park et al. Sound Transmission through Elastomeric Bulb Seals)

The seal membranes are fixed in this case, in the direction of wave propagation. The same material characterization is used with the two-membrane model.

Simple FE model of rectangular model is formed to compare results obtained from transfer matrix method. Figure 33 shows the simple two membrane FE model.

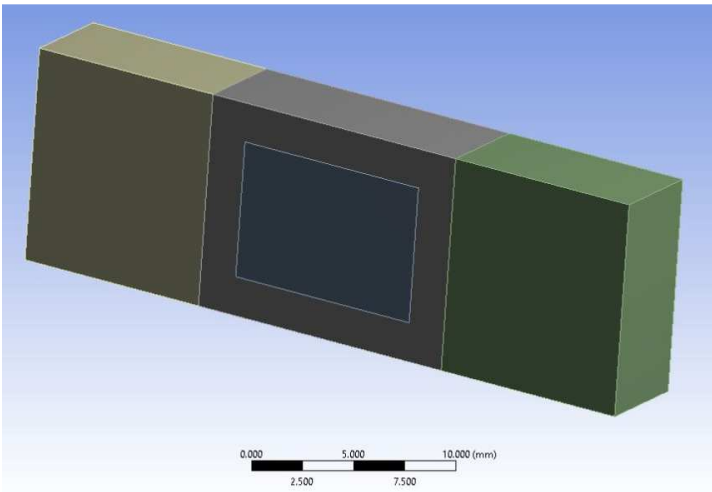


Figure 40. FE model of rectangular model approximation

Park et al performed a convergence study in rectangular model with different element sizes. Similar study is performed with FEA of rectangular model in ANSYS. Similar boundary conditions are applied. Figure 41 shows the results obtained from Park's work, while the results obtained from ANSYS is given in Figure 42. In this figure, results with different element size are given. For the lowest mesh resolution, transmission loss values show discrepancies at high frequencies.

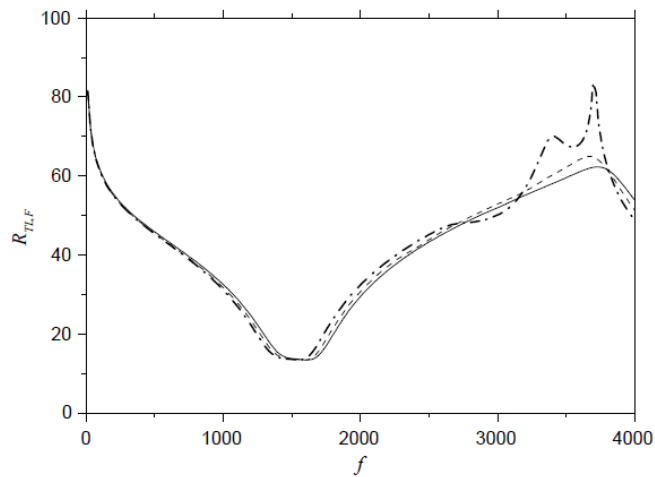


Figure 41. TL obtained from rectangular model, by transfer matrix FEA (Taken from: J. Park et al. Sound Transmission through Elastomeric Bulb Seals. -●-●-: low resolution ; - - -: medium resolution; —: high resolution)

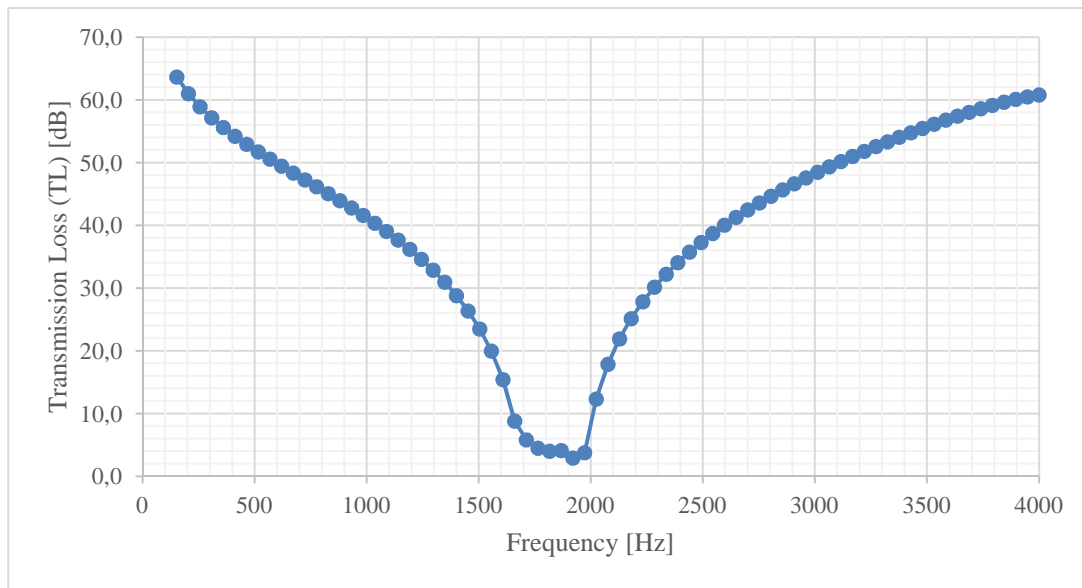


Figure 42. TL vs. frequency, obtained from rectangular FE model

Similar trends are observed between two results shown in Figures 41 and 42. However, minimum transmission loss values can differ 6-7 dB between two models. Frequencies where dip occurs slightly differ in both cases. FE model exhibits higher dip frequency than the transfer matrix model.

A convergence study was performed using Bil Plas geometry with different mesh resolutions. Three different mesh resolutions are used, keeping all the other analyses' parameters similar. Results obtained from this convergence study are given in Figure 43. Low mesh resolution has the mesh size lower than the size applied for other cases. Medium mesh resolution has exactly same mesh size with the analyses performed in other cases. Lastly, high mesh resolution has smaller elements. Figure 43 shows that, for medium and high resolution analyses, similar results are obtained. For low mesh resolution, differences occur in the high frequency range, as it is the case in results obtained from rectangular model in Park's work.

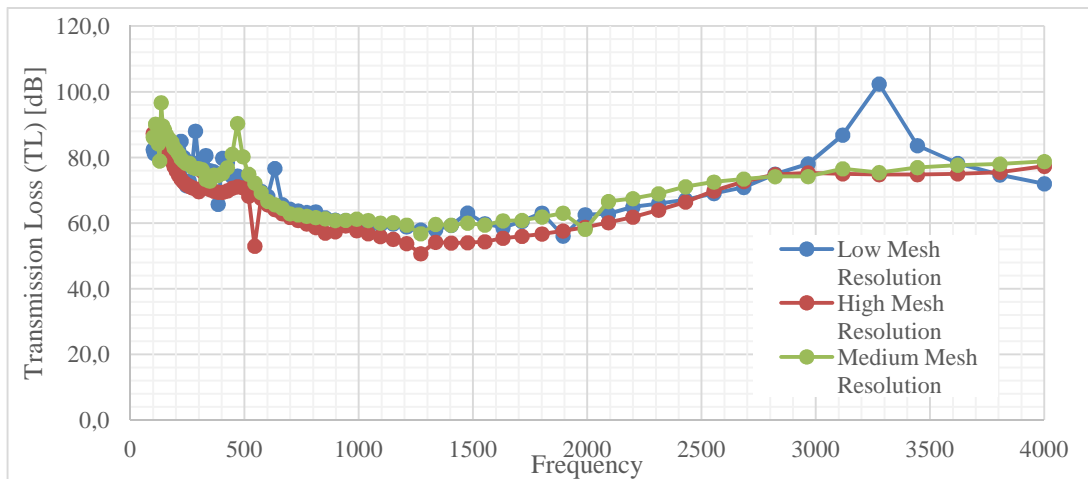


Figure 43. Sound Transmission Loss vs. frequency. BilPlas geometry, with different mesh resolutions.

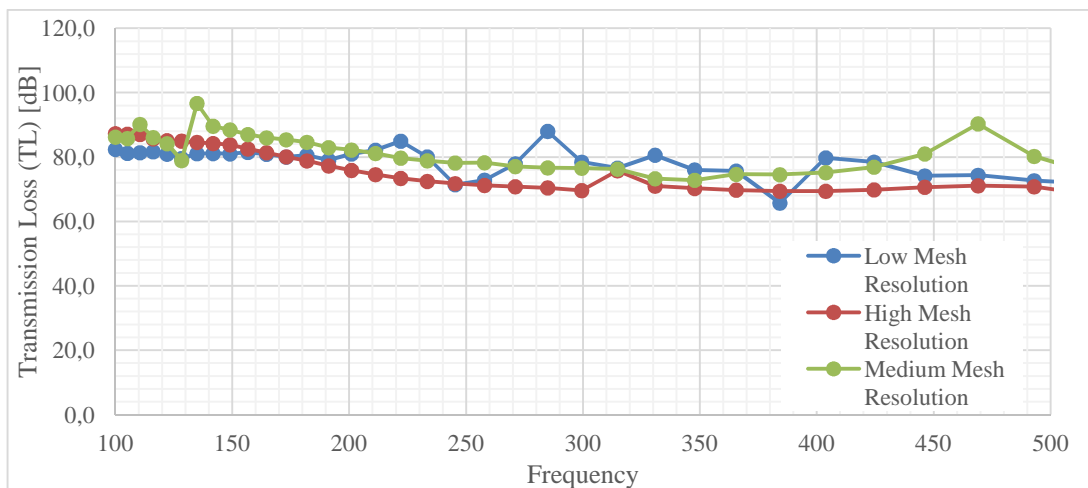


Figure 44 Sound Transmission Loss vs. frequency. BilPlas geometry, with different mesh resolutions. Close-up view at low frequencies.

For the full model acoustic analyses, different case studies are defined. Table 5 shows the case studies and their definitions used in acoustic analyses. Results obtained from these analyses are displayed in the corresponding figures, below.

Table 5. Case studies defined for acoustic analyses

Case Number	Definition
Case 1	Elastomer Young's modulus : 3MPa Elastomer Poisson's ratio: 0.45 Elastomer loss factor: 0.15
Case2	Elastomer Young's modulus : 1.8MPa Elastomer Poisson's ratio: 0.45 Elastomer loss factor: 0.15
Case3	Elastomer Young's modulus : 0.6MPa Elastomer Poisson's ratio: 0.45 Elastomer loss factor: 0.15
Case4	Elastomer Young's modulus : 1.8MPa Elastomer Poisson's ratio: 0.45 Elastomer loss factor: 0.05
Case5	Elastomer Young's modulus : 1.8MPa Elastomer Poisson's ratio: 0.45 Elastomer loss factor: 0.15
Case6	Elastomer Young's modulus : 1.8MPa Elastomer Poisson's ratio: 0.45 Elastomer loss factor: 1

Figures 45-56 show that, for all the cases, BilPlas geometry has more transmission loss capacity than Standart Profil at low frequencies, while the working frequencies for Standart Profil geometry are found to be medium and high frequencies.

It can be observed from results that, both geometries show different behavior for different frequencies and different cases. Hence, it is important to compare the frequency content of the noise source for deciding the application of seal geometries.

Figure 45 and 46 shows BilPlas and Standart Profil geometries, both in Case 1. After 1000 Hz, Standart Profil geometry has more sound transmission loss capacity. However, for low frequencies, sound insulation capability of BilPlas is higher.

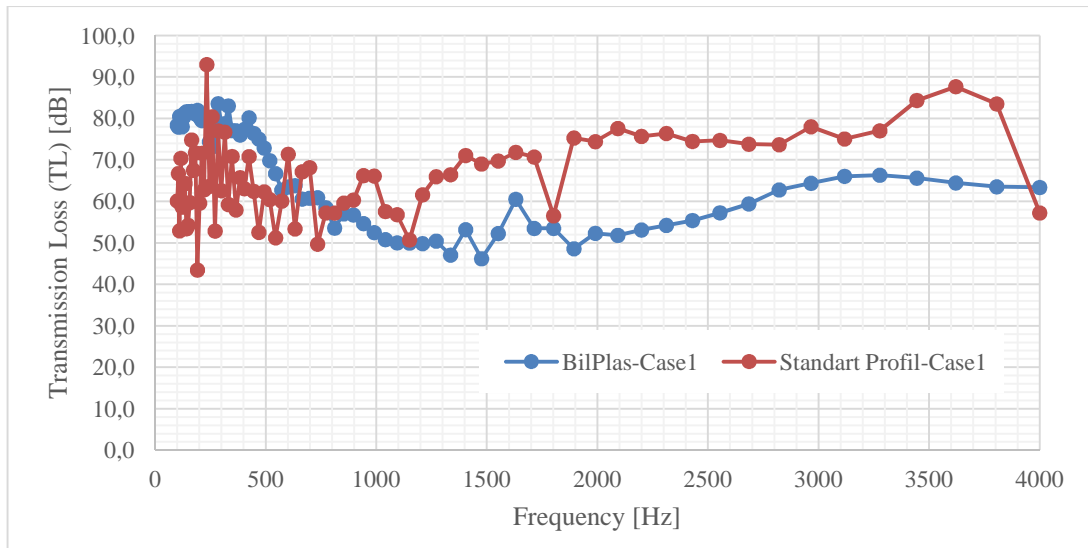


Figure 45. Sound Transmission Loss vs. frequency. BilPlas and Standart Profil geometry, both in Case 1 (Young's Modulus: 3MPa, loss factor:0.15)

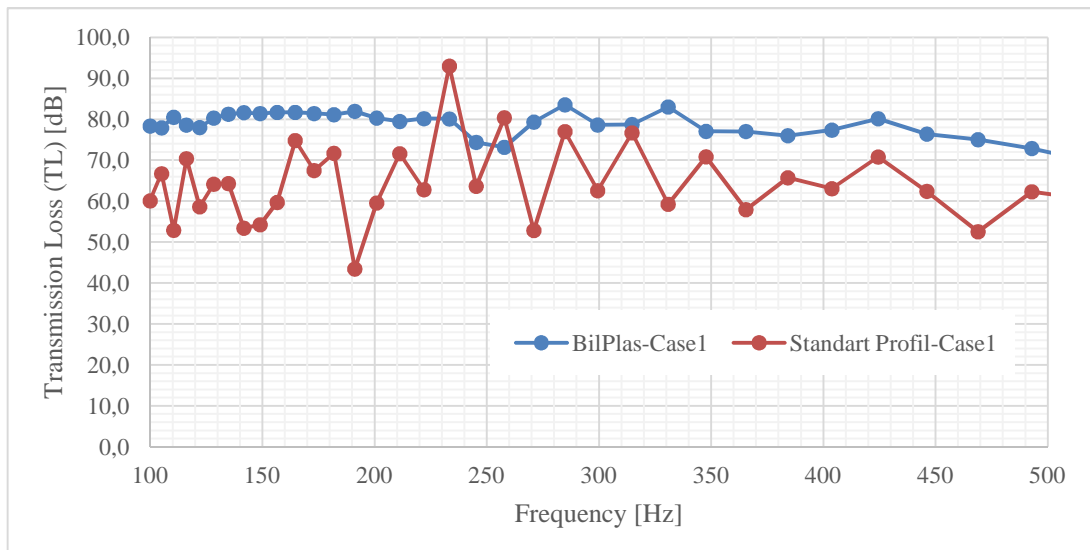


Figure 46. Sound Transmission Loss vs. frequency. BilPlas and Standart Profil geometry, both in Case 1 (Young's Modulus: 3MPa, loss factor:0.15. Close-up view at low frequencies)

Figures 47 and 48 show both geometries in Case 2. Similar trends are obtained with the case 1. Between 1000 - 3000 Hz, superiority of Standart Profil geometry is clear. However, after 3000 Hz, both geometries show similar behavior. For low frequencies, on the other hand, BilPlas geometry has more insulation capability.

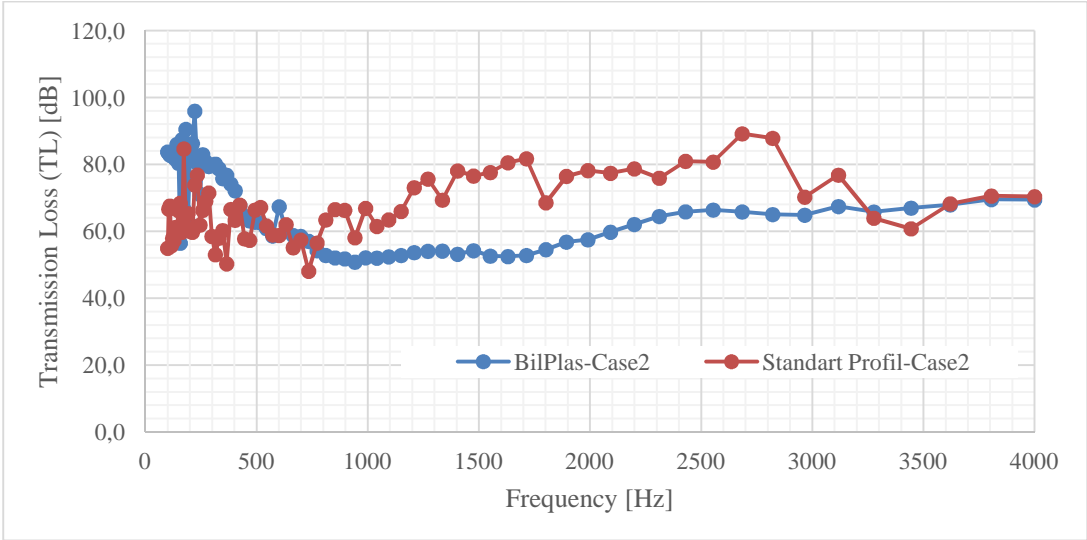


Figure 47. Sound Transmission Loss vs. frequency. BilPlas and Standart Profil geometry, both in Case 2 (Young's Modulus: 1.8MPa, loss factor:0.15)

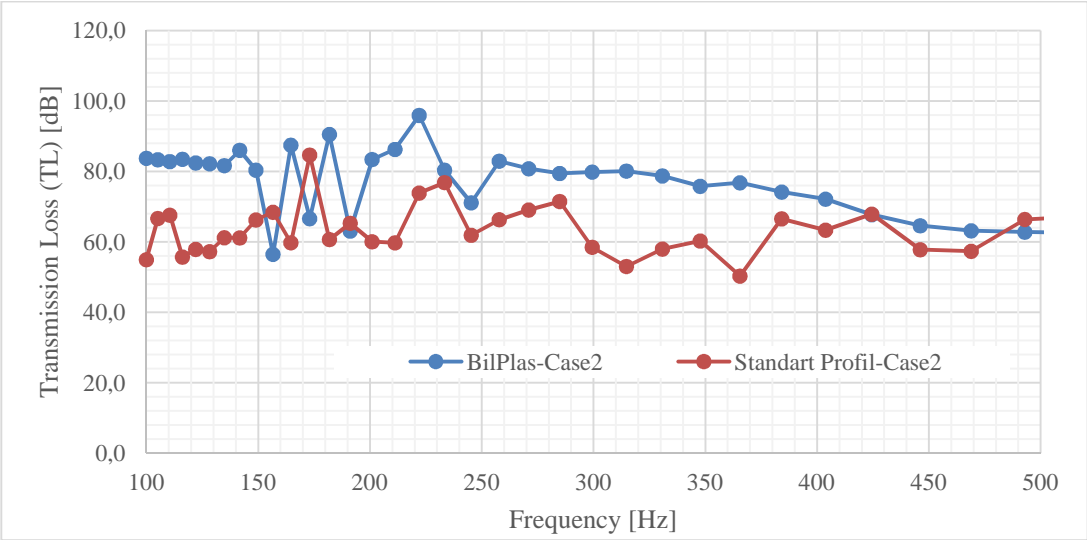


Figure 48. Sound Transmission Loss vs. frequency. BilPlas and Standart Profil geometry, both in Case 2 (Young's Modulus: 1.8MPa, loss factor:0.15. Close-up view at low frequencies)

Similar trends obtained in Case 3 as shown in Figure 49 and 50. Between 500 - 2000 Hz and 2500 - 4000 Hz, Standart Profil has more sound transmission loss capacity. Between 2000 Hz and 2500 Hz, although, both geometries have similar characteristics. At low frequencies, around 400 Hz, Standart Profil is more effective. However, the trend in sound transmission loss vs frequency graph is fluctuating. Even though BilPlas geometry has lower transmission loss values at low frequencies, it is more stable and preferable.

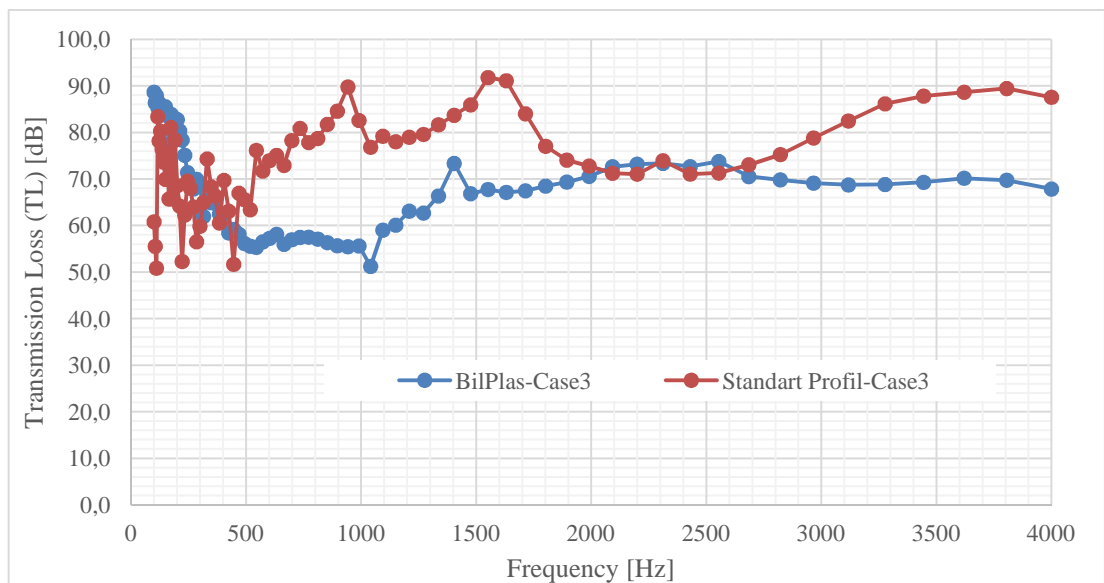


Figure 49. Sound Transmission Loss vs. frequency. BilPlas and Standart Profil geometry, both in Case 3 (Young's Modulus: 0.6MPa, loss factor:0.15)

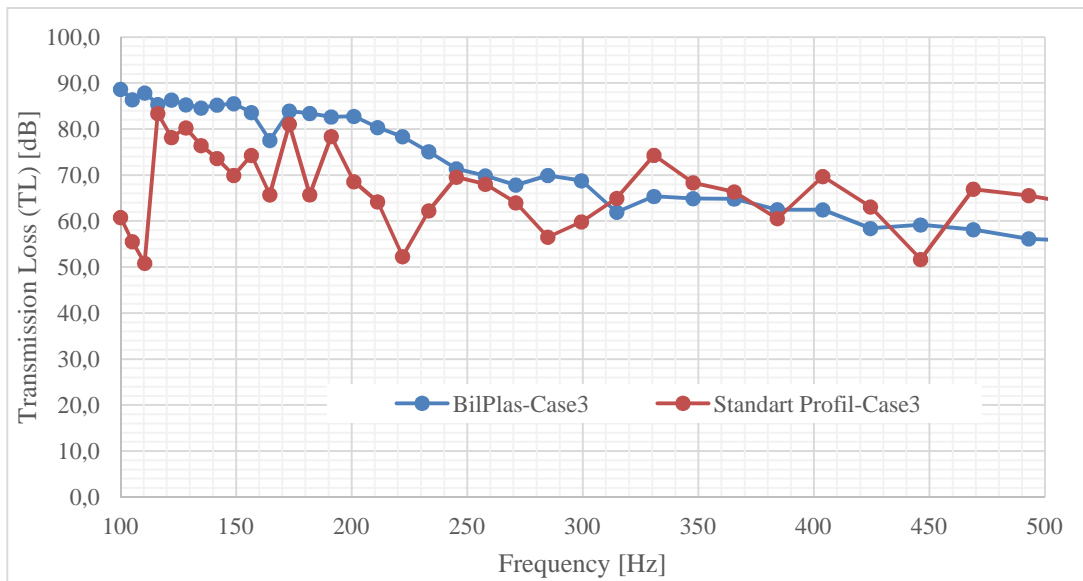


Figure 50. Sound Transmission Loss vs. frequency. BilPlas and Standart Profil geometry, both in Case 3 (Young's Modulus: 0.6MPa, loss factor:0.15. Close-up view at low frequencies)

Similar results are obtained for Case 4. Tendencies are similar with the former cases, as shown in Figures 51 and 52.

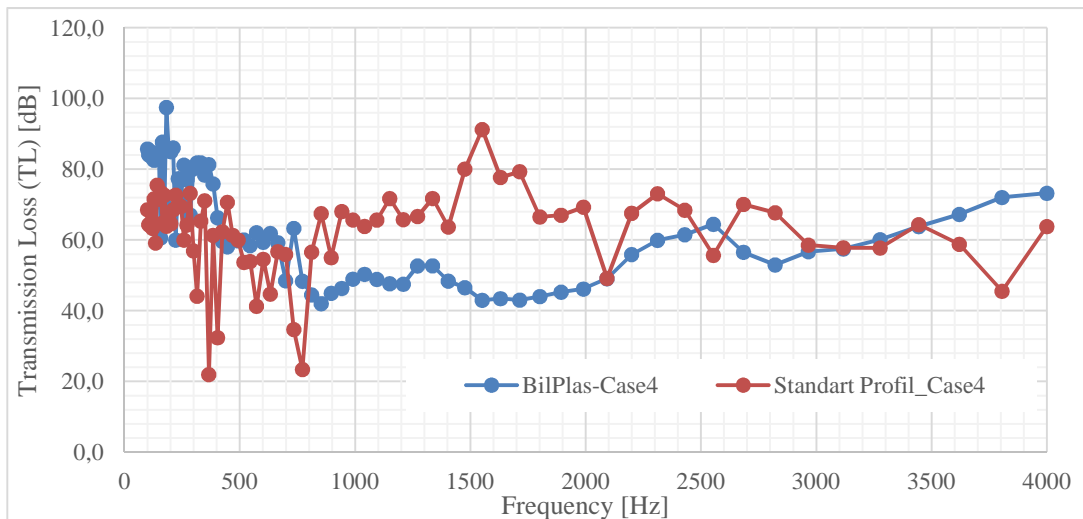


Figure 51. Sound Transmission Loss vs. frequency. BilPlas and Standart Profil geometry, both in Case4(Young's Modulus: 1.8MPa, loss factor:0.05)

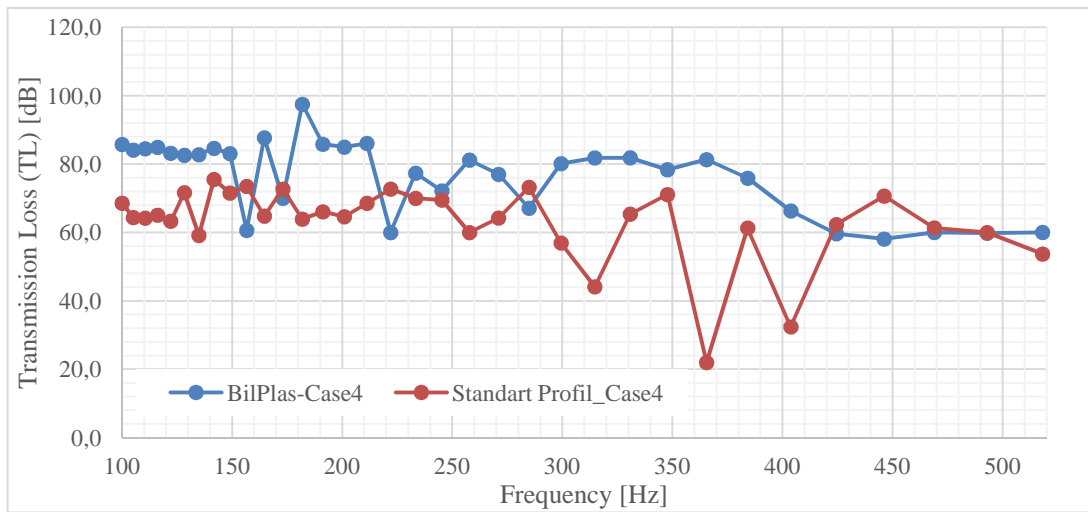


Figure 52. Sound Transmission Loss vs. frequency. BilPlas and Standart Profil geometry, both in Case 4 (Young's Modulus: 1.8MPa, loss factor:0.05. Close-up view at low frequencies)

Mid and high frequency behavior for two geometries are similar with the former cases. Again for case 5, low frequency estimations show that BilPlas geometry has highersound insulation capacity. Results shown in Figures 53 and 54.

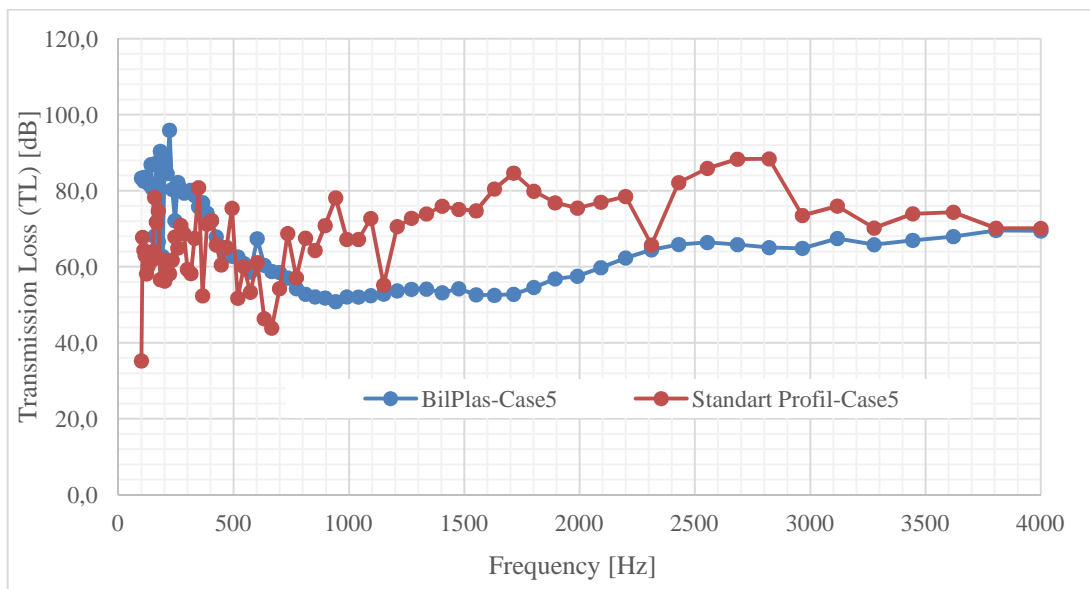


Figure 53. Sound Transmission Loss vs. frequency. BilPlas and Standart Profil geometry, both in Case 5 (Young's Modulus: 1.8MPa, loss factor:0.15)

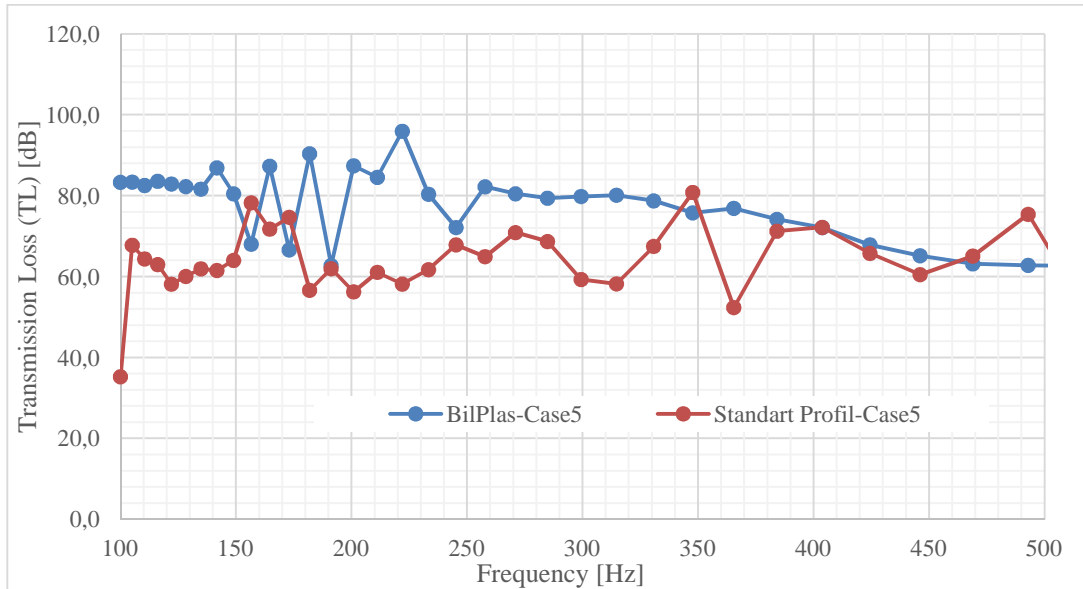


Figure 54. Sound Transmission Loss vs. frequency. BilPlas and Standart Profil geometry, both in Case 5 (Young's Modulus: 1.8MPa, loss factor:0.15. Close-up view at low frequencies)

Geometries show nearly same transmission loss capacity for mid and high frequencies. At the low frequencies, BilPlas show both higher and stable performance. Results are displayed in Figures 55 and 56.

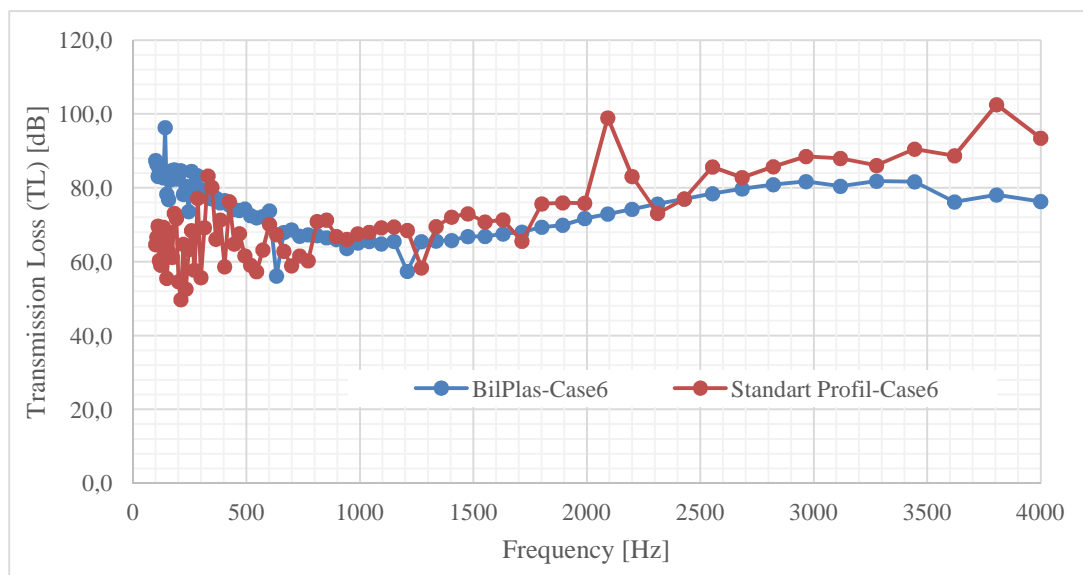


Figure 55. Sound Transmission Loss vs. frequency. BilPlas and Standart Profil geometry, both in Case 6 (Young's Modulus: 1.8MPa, loss factor:1)

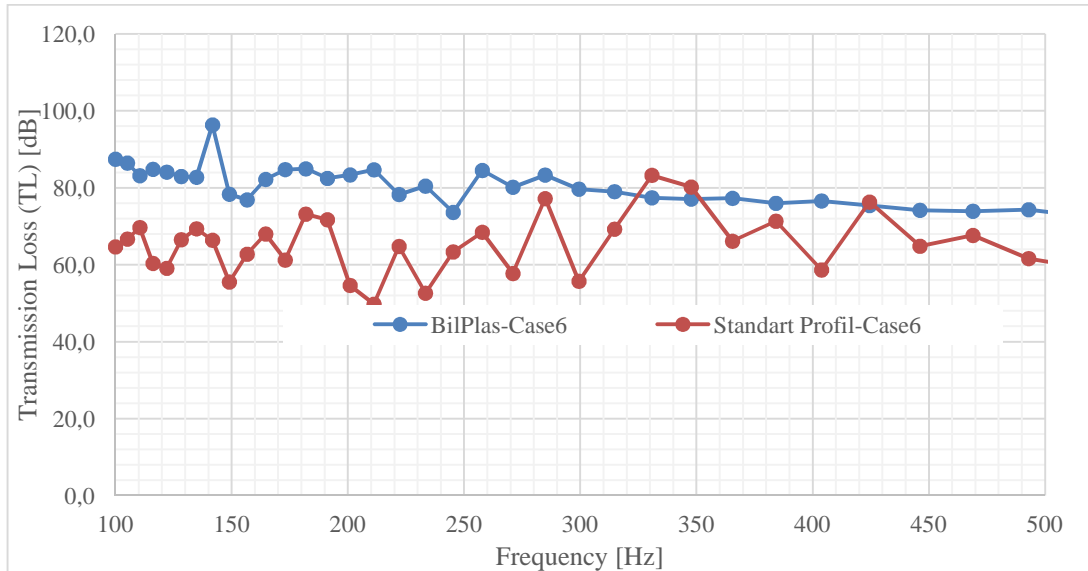


Figure 56. Sound Transmission Loss vs. frequency. BilPlas and Standart Profil geometry, both in Case 6 (Young's Modulus: 1.8MPa, loss factor:1. Close-up view at low frequencies)

Figures 57 and 58 show Standart Profil results in Cases 1, 2 and 3. These 3 cases have different modulus values while keeping the loss factor constant. It can be observed that, between 500 Hz and 1750 Hz, case 3 has the highest sound transmission loss values. Decreasing the modulus values increases the sound transmission loss value of the sealant system within that frequency range. However, between 2000- 3000 Hz case 2 shows marginally better performance. For noise sources having different frequency contents, different cases can be adopted.

For low frequencies, it is hard to obtain the most suitable cases. Results show fluctuating behavior. However, even though it has some exceptions, case 3 displays the highest transmission loss characteristics.

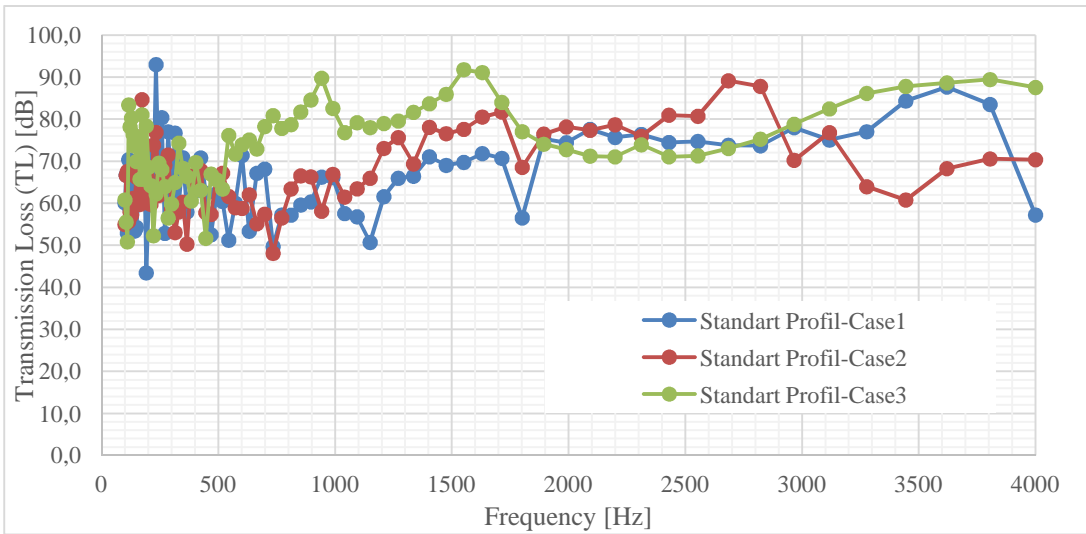


Figure 57. Sound Transmission Loss vs. frequency, Standart Profil geometry, Cases 1, 2 and 3 (Young's modulus: case1:3MPa, case2:1.8MPa, case3:0.6MPa; loss factor:0.15 for all cases)

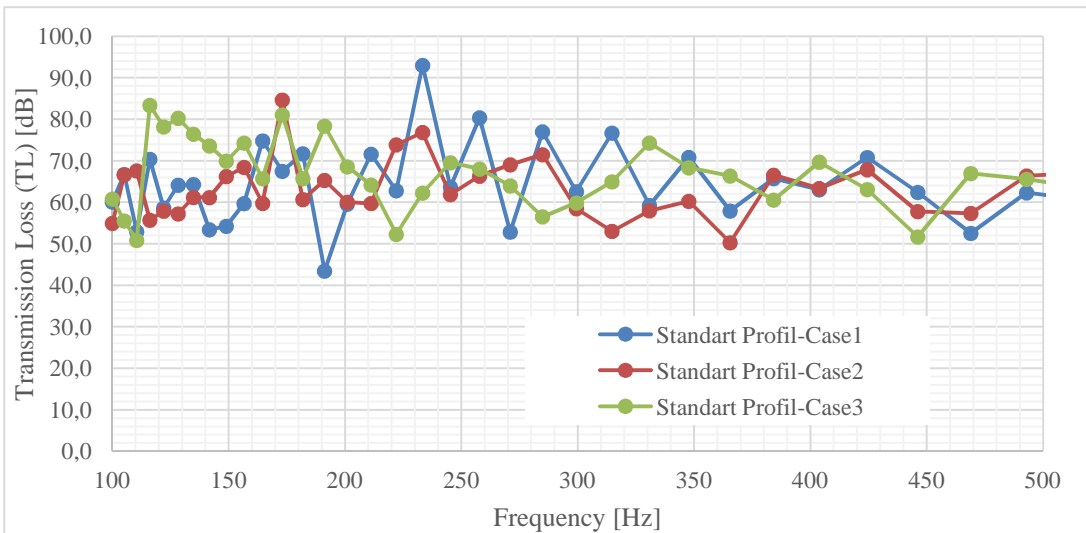


Figure 58. Sound Transmission Loss vs. frequency, Standart Profil geometry, Cases 1, 2 and 3 (Young's modulus: case1:3MPa, case2:1.8MPa, case3:0.6MPa; loss factor:0.15 for all cases. Close-up view at low frequencies)

Standart Profil geometry results in Cases 4, 5 and 6 are shown in Figures 59 and 60. After 2500 Hz, case 5 has the most isolation capability. This result shows that, increasing the loss factor may yield increased results in mid and high frequency ranges. For the low frequency range, increasing the loss factor flattens the dips and improves the system total isolation performance.

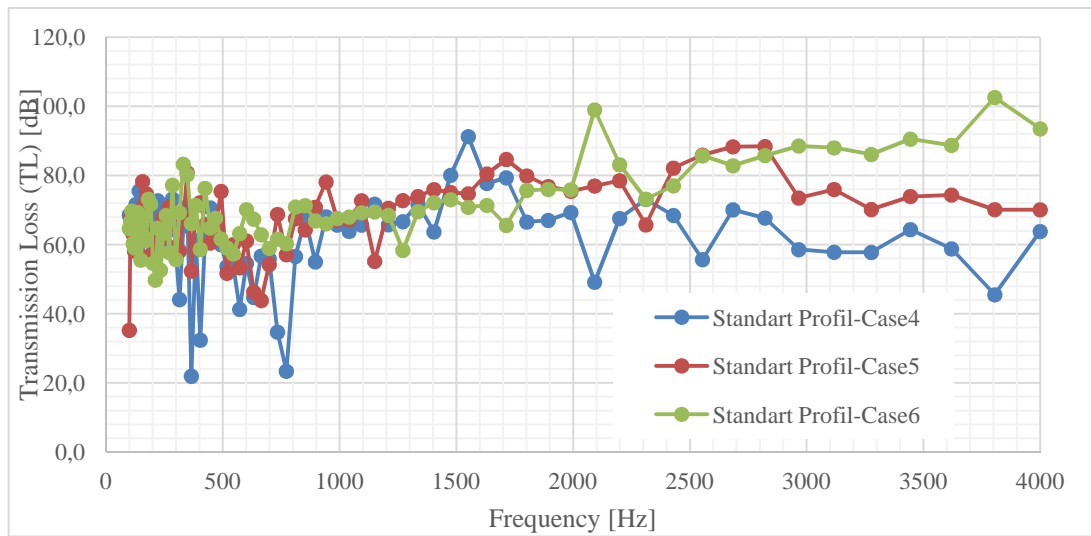


Figure 59. Sound Transmission Loss vs. frequency, Standart Profil geometry, Cases 4, 5 and 6 (Loss factor: case4:0.05, case5:0.15, case6:1; Young's modulus:1.8 for all cases)

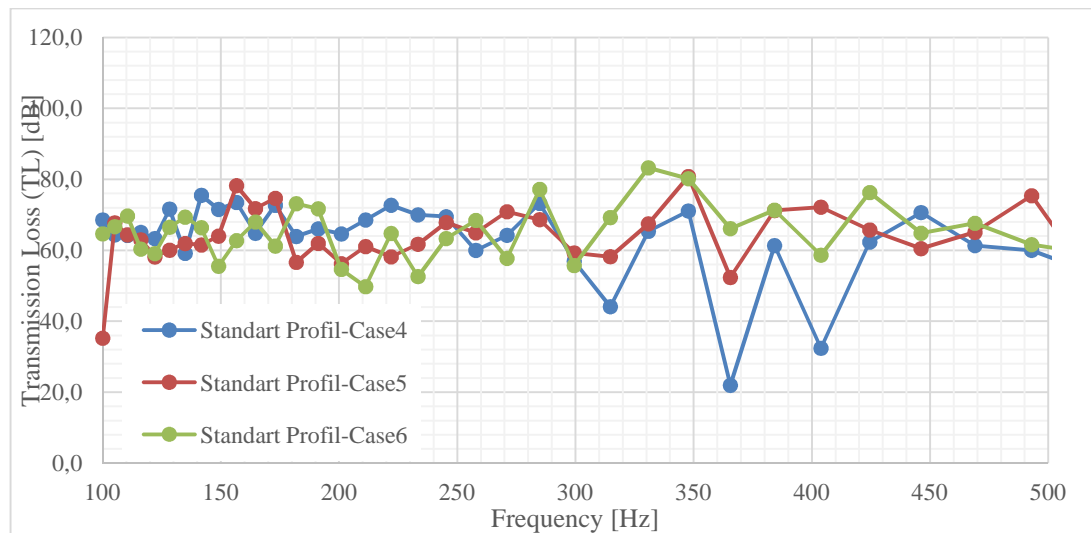


Figure 60. Sound Transmission Loss vs. frequency, Standart Profil geometry, Cases 4, 5 and 6 (Loss factor: case4:0.05, case5:0.15, case6:1; Young's modulus:1.8 for all cases. Close-up view at low frequencies)

Figure 61 and 62 shows BilPlas geometry in Cases 1,2 and 3. Between 1000 Hz - 3000 Hz, case 3 has the most insulation capacity. After 3000 Hz, it is found out that transmission loss is not a function of system modulus anymore. Decreasing the modulus value increases the transmission loss of the system after 1000 Hz. For the

low frequency range, on the other hand, case 1 shows both stable and high transmission loss performance.

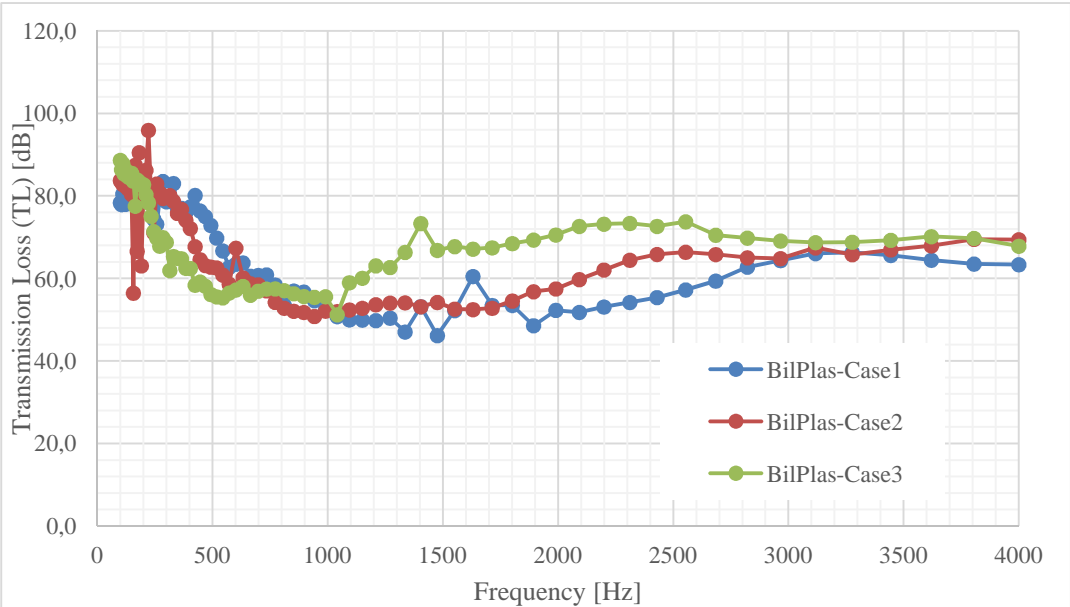


Figure 61. Sound Transmission Loss vs. frequency, BilPlas geometry, Cases 1, 2 and 3 (Young's modulus: case1:3MPa, case2:1.8MPa, case3:0.6MPa; loss factor:0.15 for all cases)

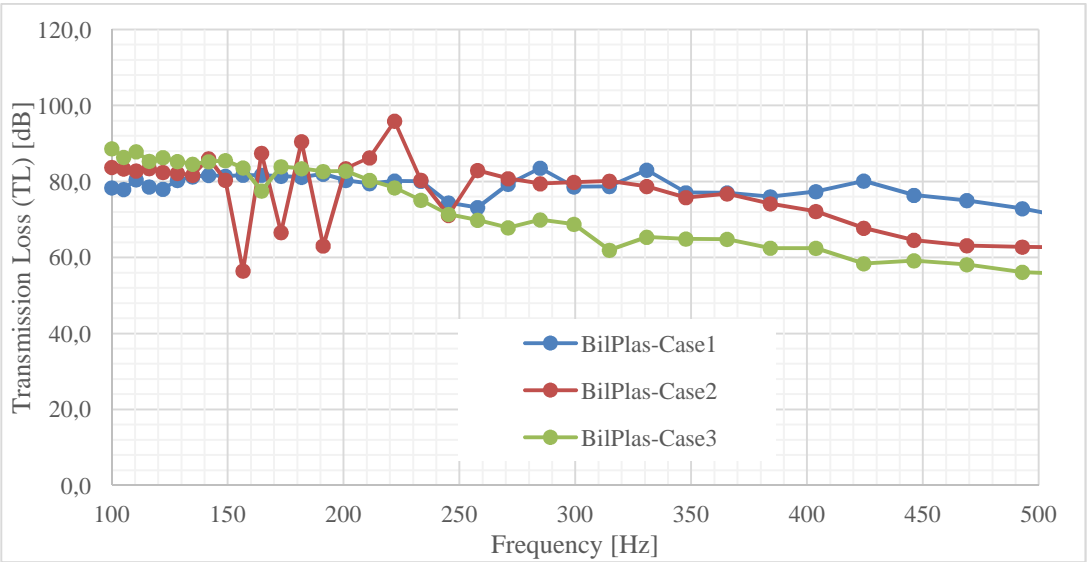


Figure 62. Sound Transmission Loss vs. frequency, BilPlas geometry, Cases 1, 2 and 3 (Young's modulus: case1:3MPa, case2:1.8MPa, case3:0.6MPa; loss factor:0.15 for all cases. Close-up view at low frequencies)

Lastly, cases 4,5 and 6 for BilPlas geometry are demonstrated in Figures 63 and 64. Figure 63 shows that increasing the loss factor of the system increases the transmission loss values significantly. Moreover, it flattens the curves such that the system shows more stable behavior over a wide frequency range. The same interpretation can be applied for the low frequency range. Increasing the loss factor will significantly increase the transmission loss of the system between 400 and 500 Hz and flattens the dips occurred at the low frequency range.

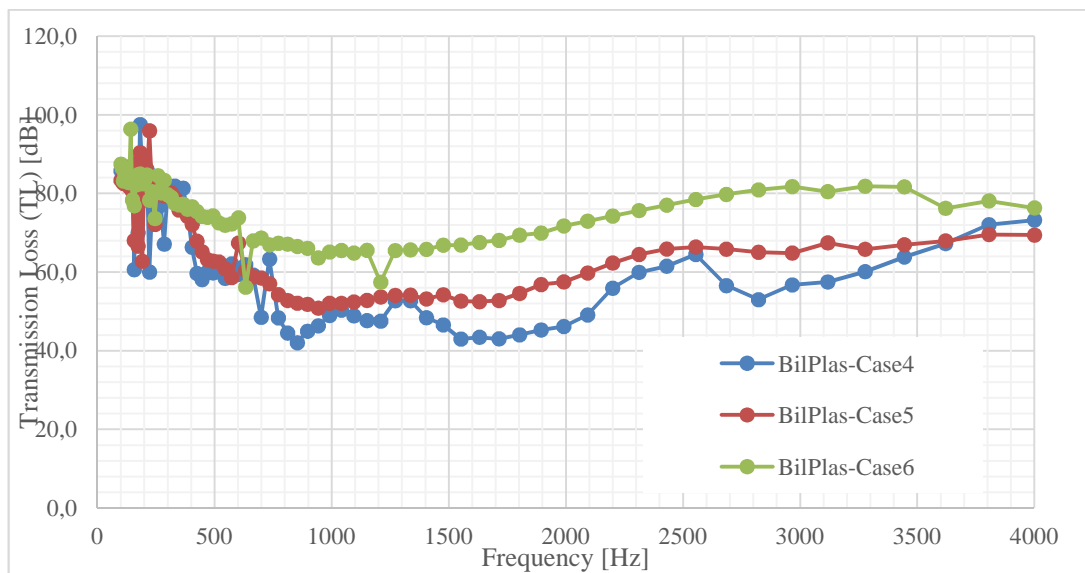


Figure 63. Sound Transmission Loss vs. frequency, BilPlas geometry, Cases 4, 5 and 6 (Loss factor: case4:0.05, case5:0.15, case6:1; Young's modulus:1.8 for all cases)

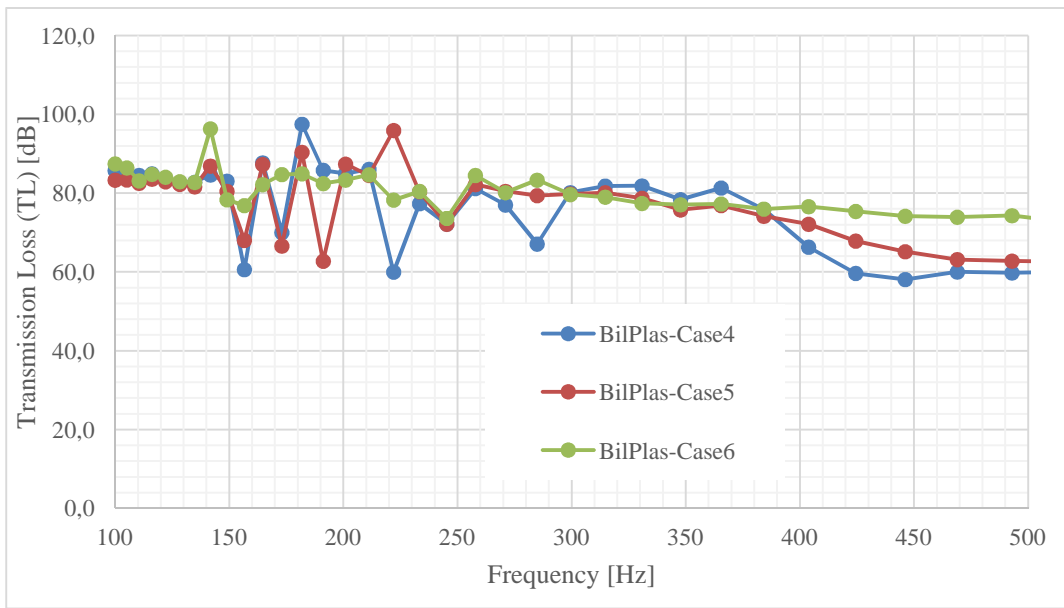


Figure 64. Sound Transmission Loss vs. frequency, BilPlas geometry, Cases 4, 5 and 6 (Loss factor: case4:0.05, case5:0.15, case6:1; Young's modulus:1.8 for all cases. Close-up view at low frequencies)

In order to determine the effect of resolution in frequency (frequency increments), different results are obtained with different resolutions in frequency and results are given in Figure 55 and 56.

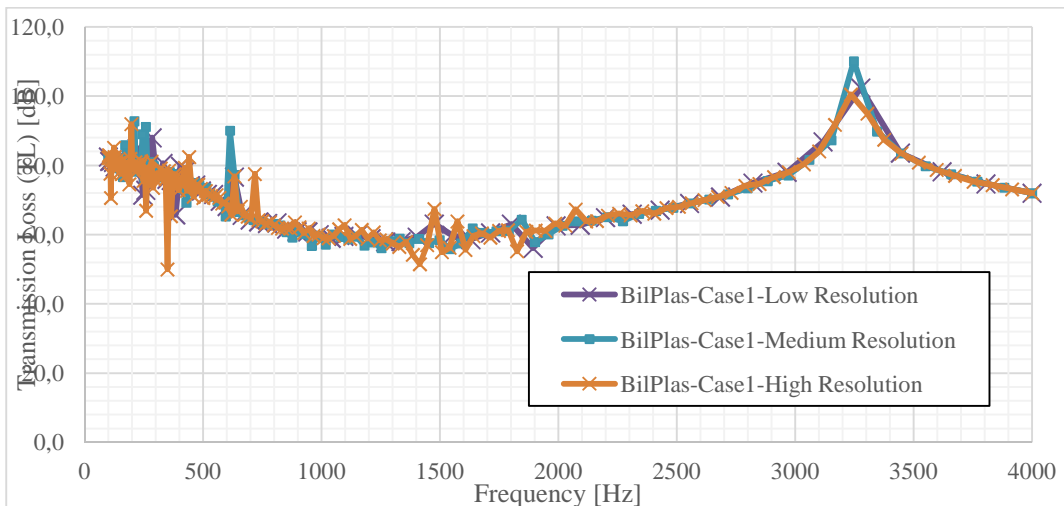


Figure 65. Effect of resolution in frequency, BilPlas, Case1

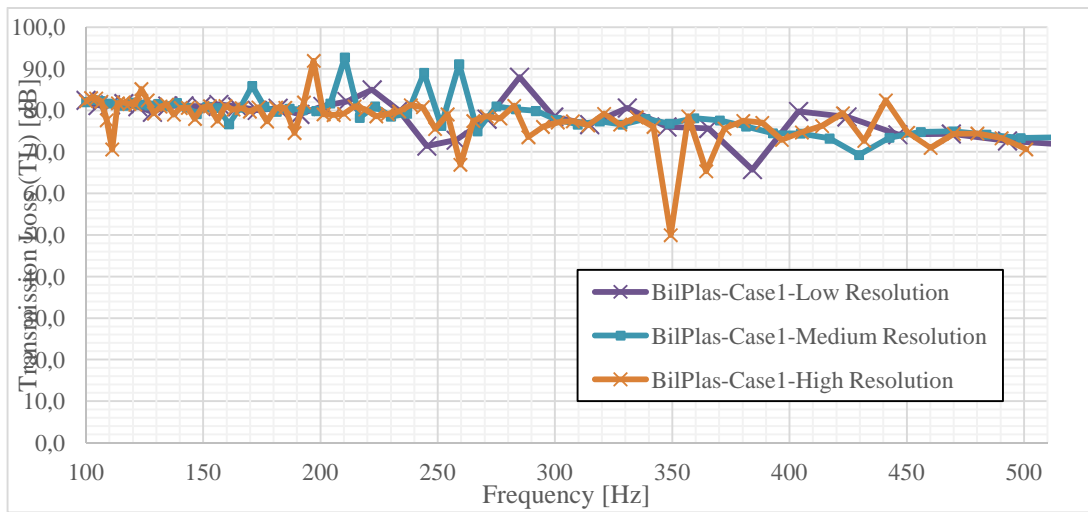


Figure 66. Effect of resolution in frequency, BilPlas, Case1 (Close-up view for low frequencies)

Model thickness is not taken as a design parameter. It is identified only for the acoustical analyses to be performed. To determine the effect of model thickness on the sound transmission loss, model thickness is doubled for BilPlas - Case1 and two results are compared with each other in Figure 57. It should be noted that the outcomes are exactly same for two different model thicknesses.

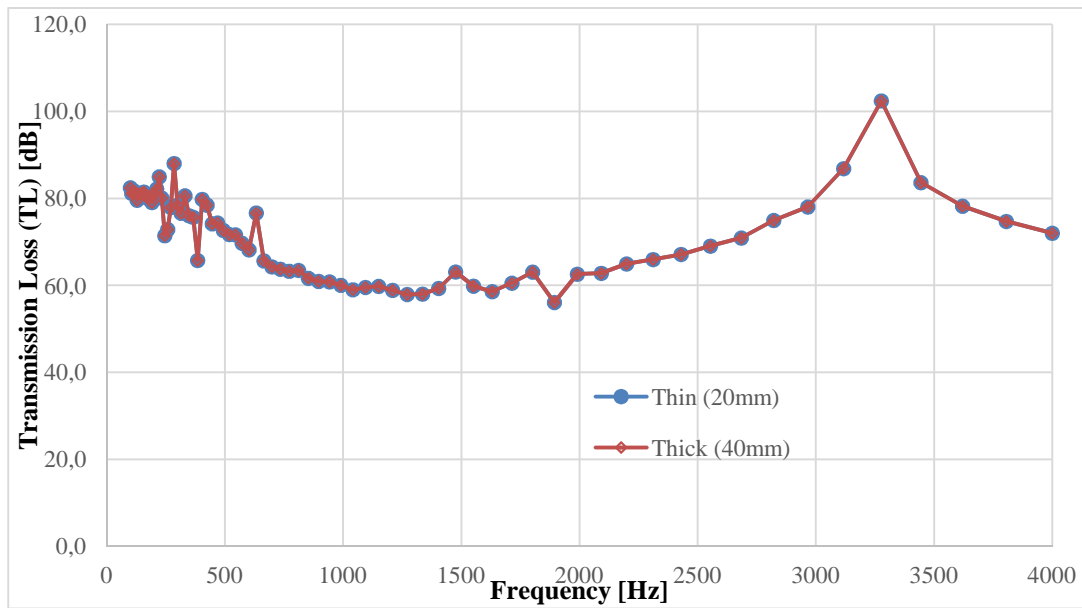


Figure 67. Effect of model thickness on sound transmission loss. Both results are the same.

Lastly, two different boundary conditions specified on outlet sides are compared. In the first part, only the outlet surface in the direction of wave propagation is assumed to have radiation boundary condition. This situation is described in Figures 58 and 59 as "old" boundary condition. In the latter case, all of the boundaries on outlet side air part are modeled to have radiation boundary condition. This situation is also described as "new" boundary condition in the same figures.

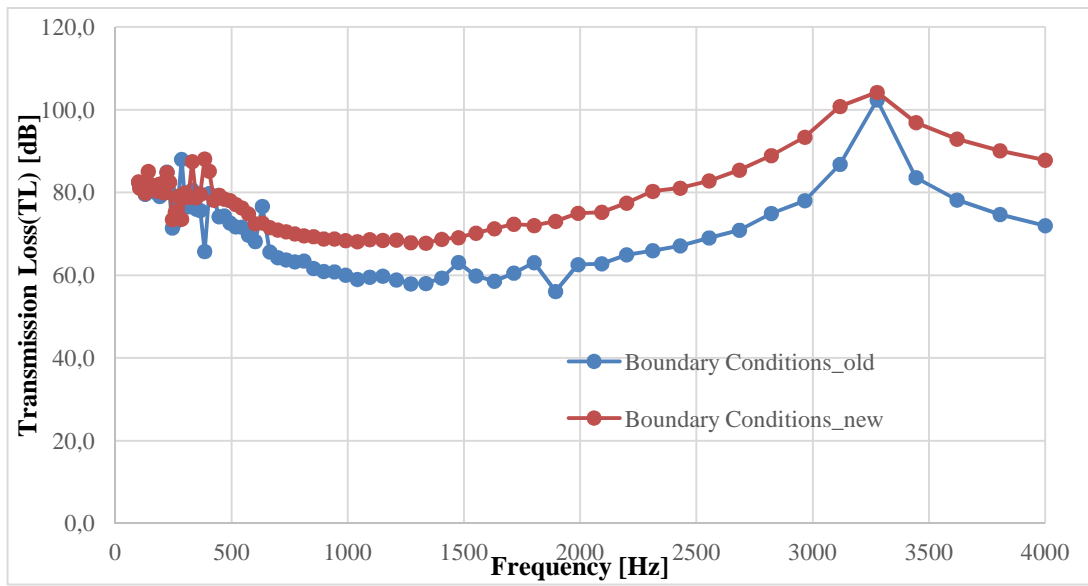


Figure 68. Effect of different boundary conditions, BilPlas, case1

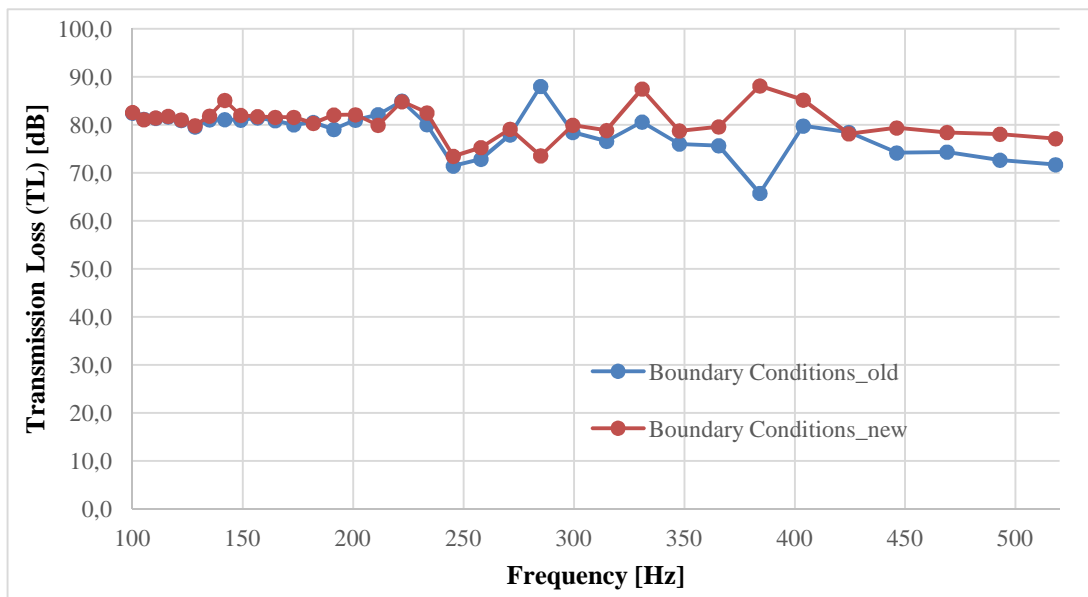


Figure 69. Effect of different boundary conditions, BilPlas, case1 (Close-up view at low frequencies)

CHAPTER 5

SUMMARY AND CONCLUSIONS

5.1. SUMMARY

In this study, sound transmission loss of elastomeric bulb seals is predicted by finite element modeling technique. Two main steps were identified for analyzing the sound transmission loss phenomena. First one is to determine the seal shape after compression. Second step is to determine the sound transmission loss of bulb seal in its compressed form.

Three different seal geometries sampled from industry are treated as cases. Both 2D and 3D models are constructed from the section of seal geometries. 2D analyses have a mating body, different from the 3D analyses, in order to show contact and deformation behavior. 3D models are used to determine the seal shape after compression, and deformed geometries were carried to the acoustic analyses.

Both static and harmonic analyses were performed using ANSYS Workbench. For the acoustic analyses, ACT_Acoustics extension was also used. Workbench is the user-friendly environment of ANSYS and improving day by day as it involves more commands and specialties from ANSYS APDL. ACT_Acoustics is an extension for solving 3D acoustic problems. Extensions are being developed currently by decreasing the need for APDL.

5.2. CONCLUSIONS

Elastomeric bulb seals are hyperelastic materials with nonlinear material behavior. Modeling and solving a nonlinear behavior in FEA requires different approaches. It was possible in ANSYS to characterize hyperelastic material behavior. Different hyperelastic material models were explained in this work and some of them were chosen to model hyperelastic material characteristics.

Ten different material constant sets are taken from the literature to observe their effect on deformation analyses. These material sets includes Neo-Hookean model, 2 and 5 term Mooney-Rivlin model, 3rd order Ogden model and Arruda-Boyce model.

Acoustic analyses were performed in 3D and required air parts were modeled as separately. As the deformed geometries were imported from the static structural analyses, air had to be modeled in deformation analyses. Specifically the air within the seal structure could cause problems during deformation analyses. Hence, air was modeled as a dummy material with zero Poisson's ratio and nearly zero Young's modulus in deformation analyses. In this way, it was possible to produce an air part in 3D models to be evaluated in acoustic analyses without any interference in static deformation analyses.

The effect of pre-stresses caused by the deformation analyses were not in the scope of this work. The total deformation of the seal geometry under compression was the only parameter to be considered. Therefore, only the total deformation values were presented both within the main body of the thesis and Appendix.

Evaluated values for the BilPlas geometry were the same for all ten cases. However, results show discrepancies for the Standart Profil geometry. This was because of the limitations arising from 3D models. BilPlas geometry has a flat top surface and it was possible to define a displacement boundary condition. However, since the top flat surfaces of the 3D Standart Profil model were only air parts, it was impossible to define directly displacement boundary conditions. Therefore, forcing was applied to the top surfaces of the sealant geometry with the internal air structure to get

deformation in defined time steps. In order to have a flat top surface for the acoustic analyses, similar deformation-time step information was applied to the top surfaces of the model. However, forcing creates problems in deformation definitions resulting difference in total deformation information. Figures 60 and 61 explain this situation.

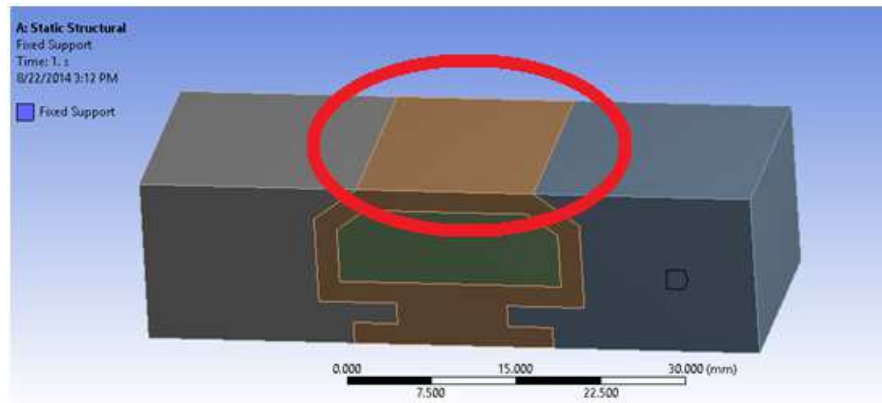


Figure 70. 3D model of BilPlas geometry. Note the upper flat surface to assign displacement

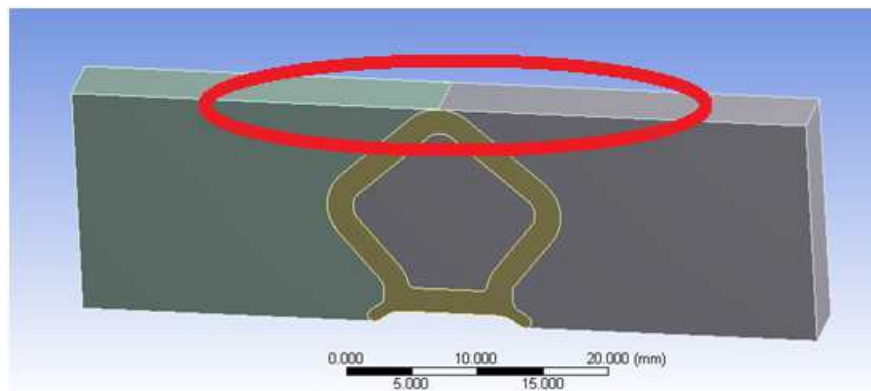


Figure 71. 3D model of Standart Profil geometry. Note that displacement cannot be assigned to upper surface

On the other hand, the same ten different cases were applied to the 2D geometries having mating bodies in contact. In these 2D analyses, 10 cases give exactly the same results for both BilPlas and Standart Profil geometries. In 2D analyses, contact information was defined between the sealant body and its mating body.

Another important point encountered in deformation analyses was the buckling problem. Buckling was investigated using 2D models, since 2D models involved contact between the seal and its mating geometry. Both BilPlas and Standart Profil geometries buckled under some compression ratio. However, Zero International geometry showed no buckling even under high compression ratios since it possessed an extra surface. This extra surface behaves like a one-end free surface and does not buckle under high compression ratios.

Validation of the acoustic analysis results are performed by simplified models of the sealant with known mathematical models. The first simple model consists of the two membranes separated from each other by a distance. The mathematical formulation and results are taken from the literature and the results obtained from FEA of simple two-membrane model are compared. Mathematical models by the transfer matrix method shows similar trend with the solutions obtained from the FEA. Second simplified model is the rectangular model. Rectangular model is rather complex than the two membrane model and gives closer results to the analyses performed with the exact shape of the seal. Similar trends are also obtained for mathematical model and FEA results of simplified rectangular model. In this validation process, similar boundary conditions and loading conditions are defined to the simple model with the full FE acoustic models. It has been assured that both results exhibit the same trends, and acoustical analyses are performed afterwards.

At the onset of acoustical analyses, six different cases are defined. For the first three different cases, Young modulus of the elastomer material is changed. These modulus values are taken from the literature with the similar bulb seal configuration. Minimum and maximum values of modulus values are treated in cases 1, 2 and 3 and their effects on transmission loss are studied. For the other three different cases (case4, 5 and 6), loss factor value dependency is considered. Again minimum and maximum values are obtained from literature and their effects on again transmission loss are evaluated.

Resolution in frequency range is an important parameter in this study. Increasing the resolution yields longer computational time and after some point it becomes impossible. Yet, different solutions with higher resolutions are obtained for BilPlas geometry in case 1. With higher resolution, some peak points can be observed especially in low frequency range. Thus far, solutions are acceptable in a broad frequency range, no big discrepancies occur by differing frequency resolution.

Different boundary conditions, for describing the radiation boundary condition at the end part of the model are considered. At first, only end section is assumed to have radiation boundary condition. In the second case, all of the outer surfaces are subjected to radiation boundary condition. Results show that, the more radiation boundary surfaces included, the higher transmission loss characteristics resulted, as expected.

Lastly, values obtained for the low frequency values are considerable. These values are too much to have in low frequencies. Normally, transmission loss is lower at low frequencies; however, that is not the case in this study. This result may be attributed to having a too narrow and small geometry with dimensions much smaller than the wavelengths corresponding to low frequencies. In order to consider the effect of model thickness, two different thickness values are compared and results are given in Figure 57. Both simulations yield exactly the same results, showing that the model thickness has no effect on low sound transmission loss outcome.

Results obtained for Standart Profil geometry shows fluctuating behavior. A convergence study may be performed on this geometry with finer mesh in future if the computational power is sufficient enough.

In two membrane model (simple model), FEA results show nearly zero sound transmission loss results near the zero frequency and at some definite frequency related to the mass-air-mass resonance of the structure and inner air part, as expected. However, full FE models show opposite behavior.

5.3. FUTURE WORK

As a future work and improvement, material samples may be considered having exactly the same compositions with the studied elastomers to carry out experiments with them. It was not possible for this work since the companies were not eager to give information about the composition of the sealants that they are producing and marketing. Composition of the elastomer is very important at this part since it affects the material's mechanical behavior. The results for deformation analyses can be improved by material testing.

Another reason for the discrepancies could be due to the effect of the channel (cavity in which the sealant is applied) which is not considered in this study. Different studies show that including the effect of channel may reduce the transmission loss of the system by around 10 dB. [27]

Lastly, a hybrid FE-SEA method may be applied as a future work, to overcome the computational burden. Inlet and outlet air structures can be modeled as SEA fluids while highly modal dense components can be described using SEA.

BIBLIOGRAPHY

- [1] Q. Li, "Licentiate Thesis," *Transmission Loss of Vehicle Seals*, 2008.
- [2] J Park, L. Mongeau, T Siegmund, "Sound Transmission Characteristics of Elastomeric Sealing System," *Sound Transmission Characteristics of Elastomeric Sealing Systems*, vol. 28, pp. 102-103, 2000.
- [3] V. Hongisto, *Sound Insulation of Doors - Part I: Prediction Models for Structural and Leak Transmission*, 1999.
- [4] Mark C. Boyce & Ellen M Arruda, *Constitutive Models of Rubber Elasticity: A Review*.
- [5] Ö. D. Okay, *Validation of Structural Analysis Model of a Layered Structure with Elastomeric Components*, September 2010.
- [6] ANSYS Learning Materials, "ANSYS Mechanical-Introduction to Structural Nonlinearities".
- [7] MSC_Software, *Nonlinear FEA of Elastomers - Technical Paper*.
- [8] S. Shah, "Product Manager, ANSYS Inc," *Stretching Your Elastomer Understanding*, vol. II, no. 3, 2008.
- [9] Stenti A.& Moens D. & Desmet W., *Dynamic Modelling of Car Door Weather Seals: A First Outline*, Proceedings of ISMA 2004.
- [10] Treloar, "The Elasticity of a Network of Long Chain Molecules - II,"

Transactions of the Faraday Society, pp. 241-246, 1943.

- [11] MSC_Software, "Nonlinear Finite Element Analysis of Elastomers - White Paper".
- [12] M. Mooney, "Theory of Large Elastic Deformations," *Journal of Applied Physics*, vol. 11, 1940.
- [13] R. S. Rivlin, *Large Elastic Deformations of Isotropic Materials I: Fundamental Concepts*, 1947.
- [14] E Dikmen, I Başdoğan, "Material Characteristics of a Vehicle Door Seal and Its Effect on Vehicle Vibrations," *Vehicle System Dynamics*, vol. 46, no. 11, pp. 975-990, 2008.
- [15] D J Charlton, J Yang, *A Review of Methods to Characterize Rubber Elastic Behaviour for Use In FEA*, Rubber Chemistry and Technology.
- [16] Kinsler L., Frey A., Coppens A., Sanders J. V., *Fundamentals of Acoustics*, John Wiley & Sons, Inc.
- [17] Gur Y., Morman K., "Sound Transmission Analysis of Vehicle Door Sealing System," *SAE Technical Paper Series*, 1999.
- [18] Andro B., Chaigne S., Diallo A., Mermet M., , "Prediction of Sound Transmission through Automotive Door Sealing Systems," in *Euronoise* , Paris, 2008.
- [19] Y. Gur and K. N. Morman, "Method and System for Designing Vehicle Door Seals Based on Predicted Sound Transmission Characteristics". US Patent 5,940,788, 17 August 1999.
- [20] V. Hongisto, "Airborne Sound Insulation of Wall Structures - Measurement and

Prediction Methods," *Helsinki University of Technology, Laboratory of Acoustics and Audio Signal Processing*, 2000.

- [21] V. Hongisto, "Sound Insulation of Doors - Part 2: Comparison between Measurement Results and Predictions," *Journal of Sound and Vibration*, vol. 230, no. 1, pp. 149-170, 2000.
- [22] Herrera J. M., Recuero M., "Influence of Seal Installation to Predict Sound Insulation of Double Panel Steel Doors," in *Building and Environment*, Spain, Elsevier, 2009.
- [23] Petniunas A., Otto N.C., Amman S., Simpson R., "Door System Design for Improved Closure Sound Quality," *SAE Technical Papers*, 1999.
- [24] Mahale P.S., Kalsule D. J., Muthukumar A., Raju S. , "Vehicle Interior Noise Source Identification and Analysis for Benchmarking," *SAE Technical Papers*, 2005.
- [25] A. Inc., *ANSYS 14.5 Theory Reference*.
- [26] COMSOL, "Software Technical Paper - Hyperelastic Seal".
- [27] Cardioli J, Rocha T, Calçada M, Cotoni V, Shorter P., "Application of the Hybrid FE-SEA Method to Predict Sound Transmission through Complex Sealing Systems," *SEA International*, 2011.

APPENDIX A

DEFORMATION RESULTS

CASE 1

BILPLAS

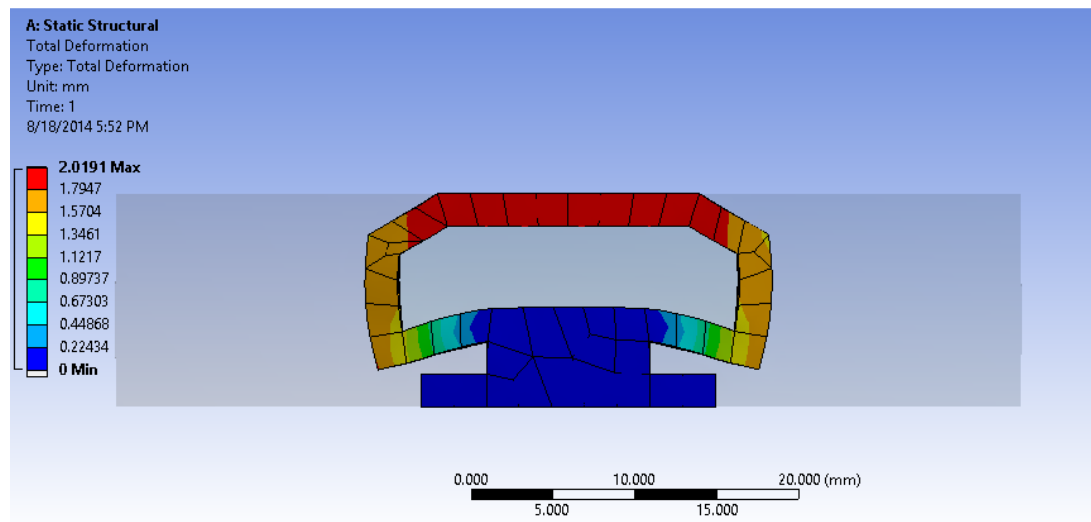


Figure 72. Total deformation of sealant, BilPlas, Case1

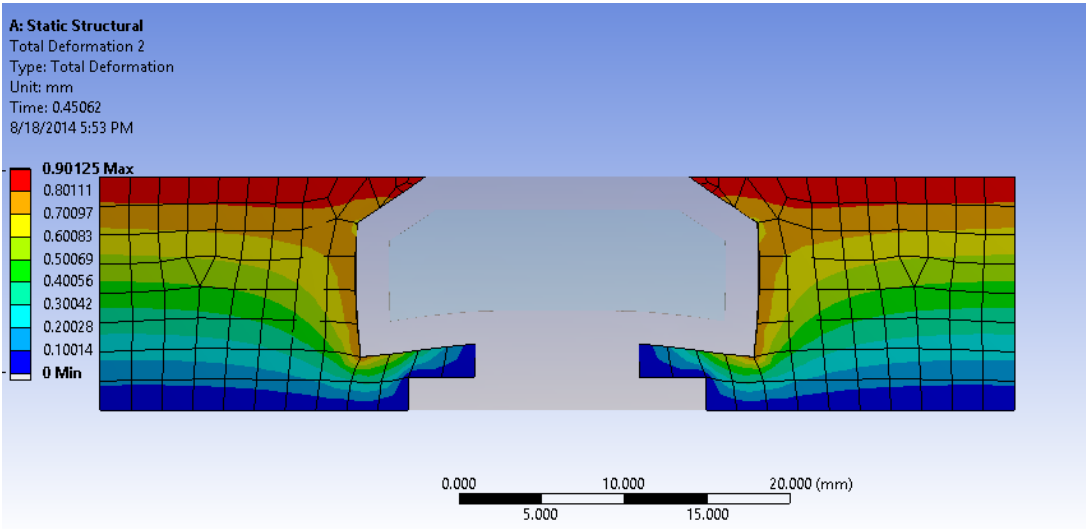


Figure 73. Total deformation of inlet and outlet air structure, BilPlas, Case1

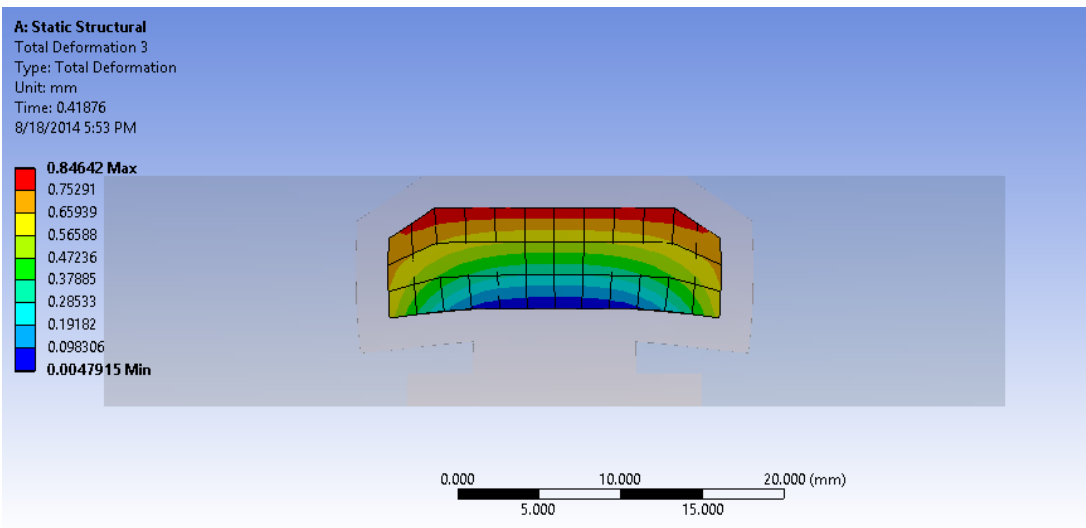


Figure 74. Total deformation of inside air, BilPlas, Case1

STANDART PROFIL

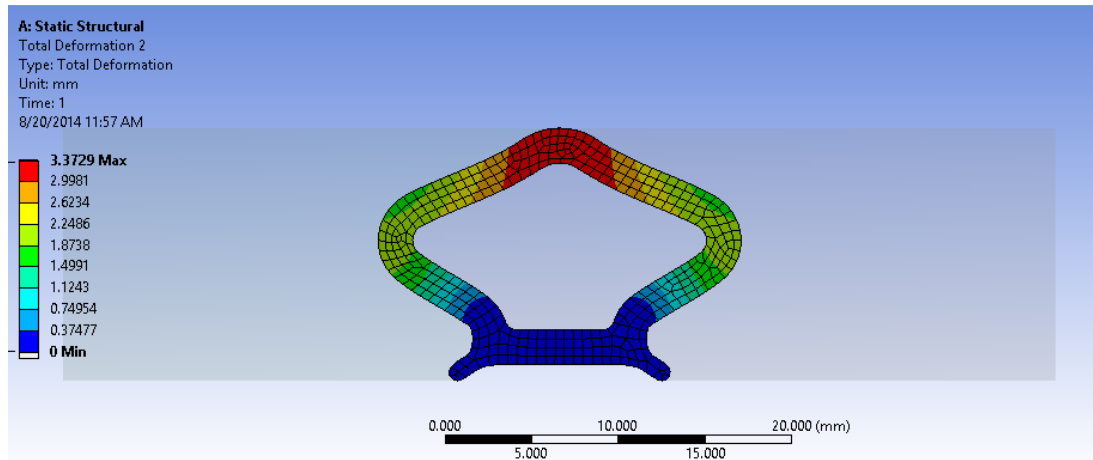


Figure 75. Total deformation of sealant, Standart Profil, Case1

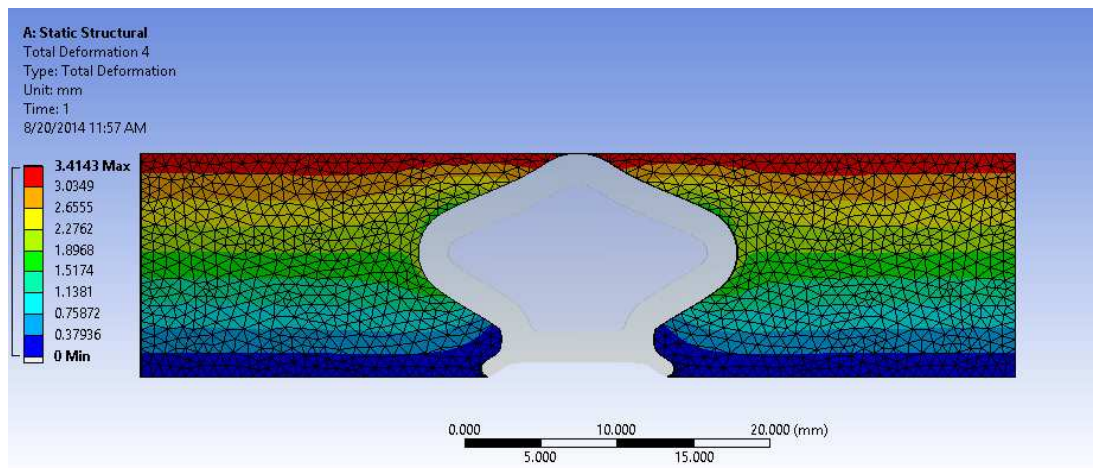


Figure 76. Total deformation of inlet and outlet air structure, Standart Profil, Case1

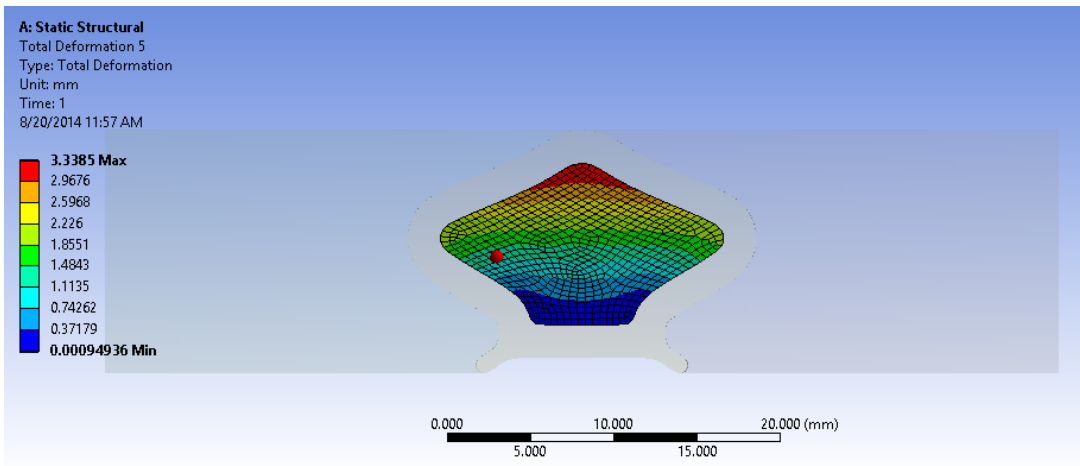


Figure 77. Total deformation of inside air, Standart Profil, Case1

CASE 2

BILPLAS

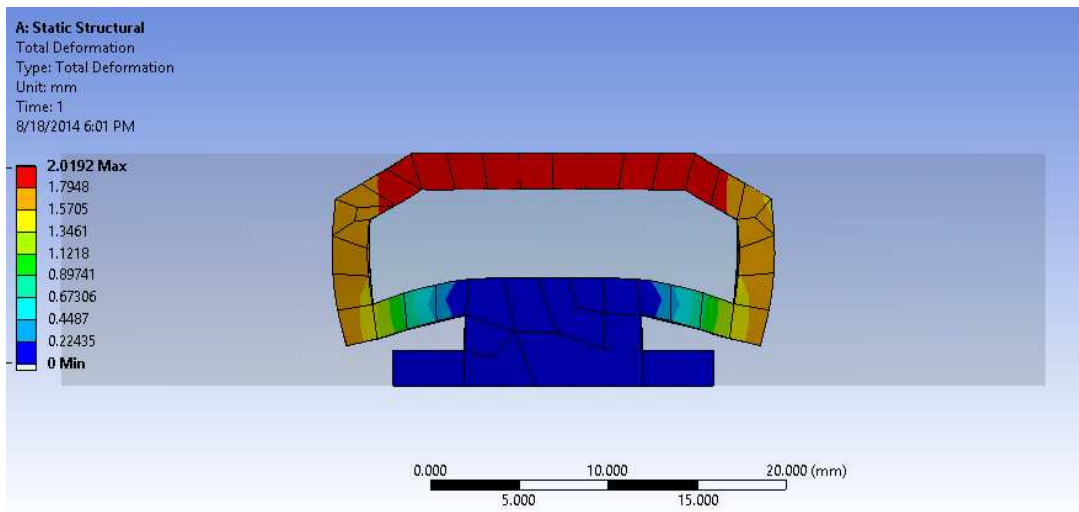


Figure 78. Total deformation of sealant, BilPlas, Case2

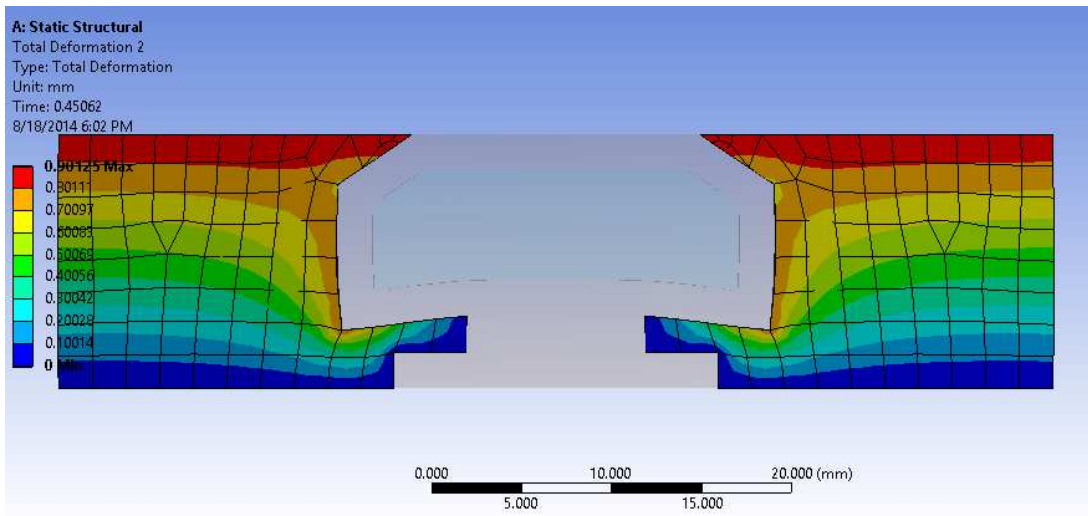


Figure 79. Total deformation of inlet and outlet air structure, BilPlas, Case2

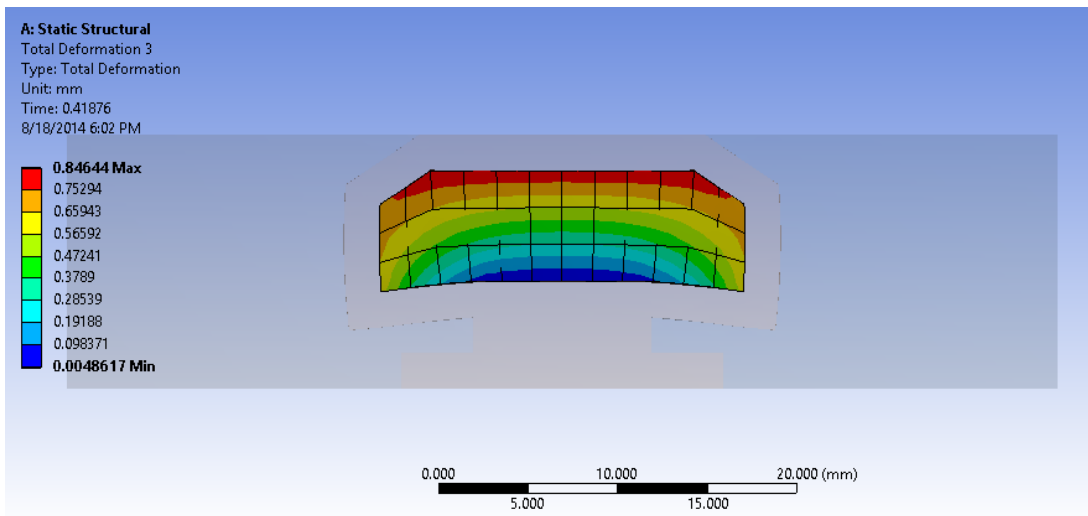


Figure 80. Total deformation of inside air, BilPlas, Case2

STANDART PROFIL

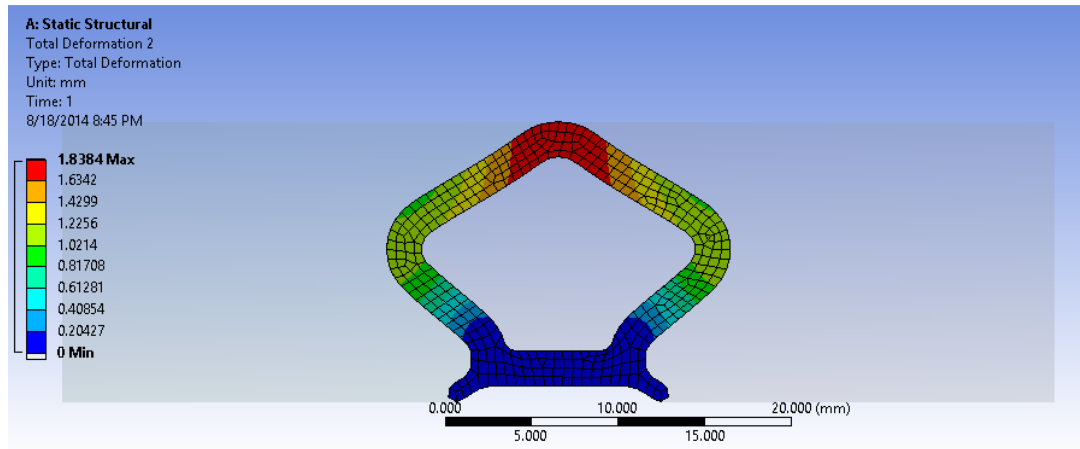


Figure 81. Total deformation of sealant, Standart Profil, Case2

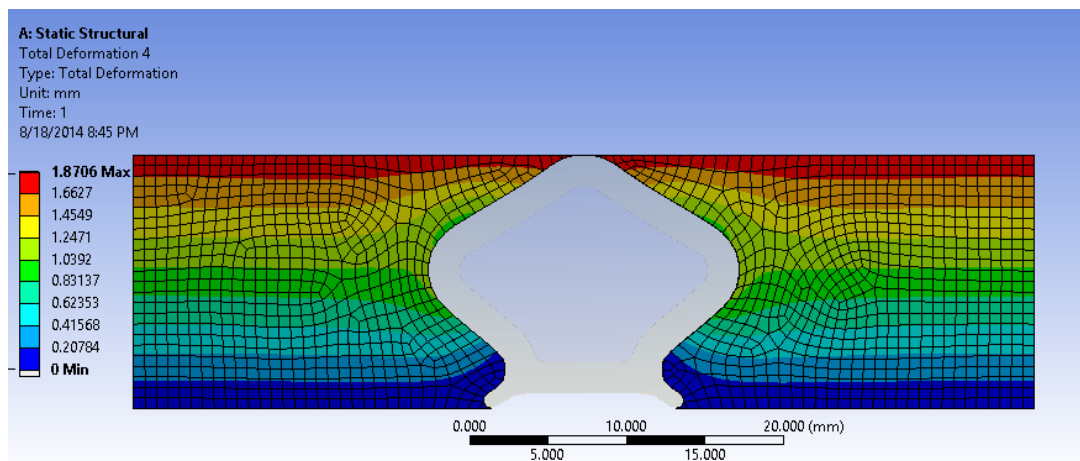


Figure 82. Total deformation of inlet and outlet air structure, Standart Profil, Case2

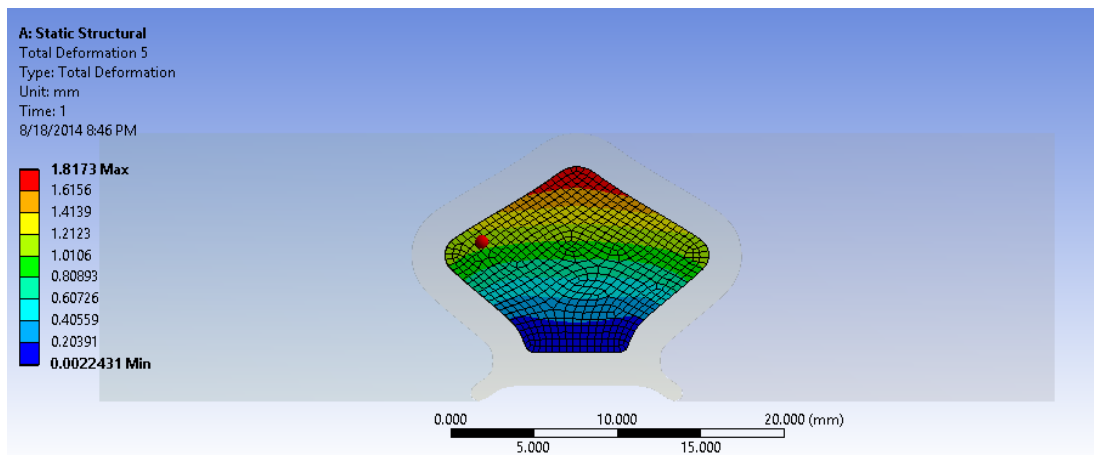


Figure 83. Total deformation of inside air, Standart Profil, Case2

CASE 3

BILPLAS

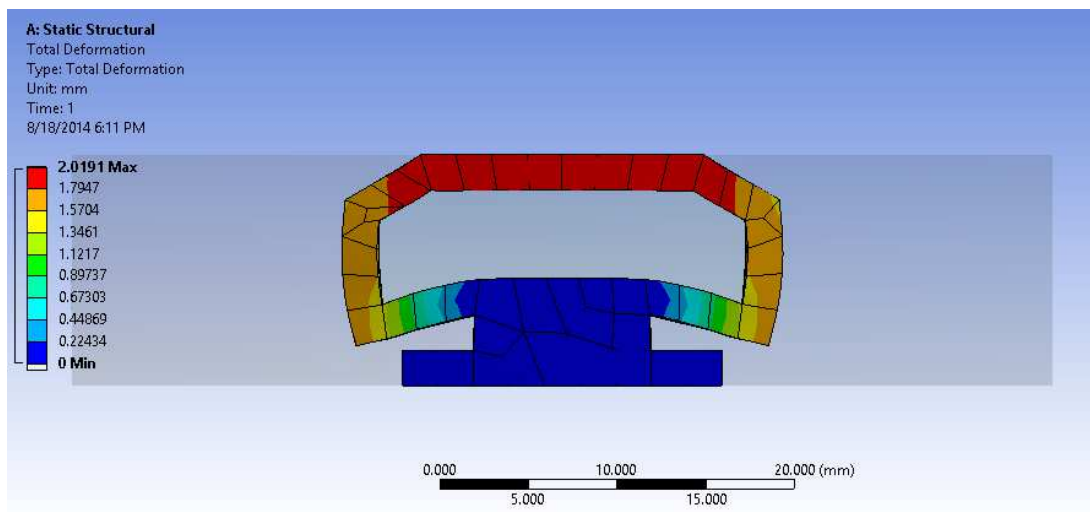


Figure 84. Total deformation of sealant, BilPlas, Case3

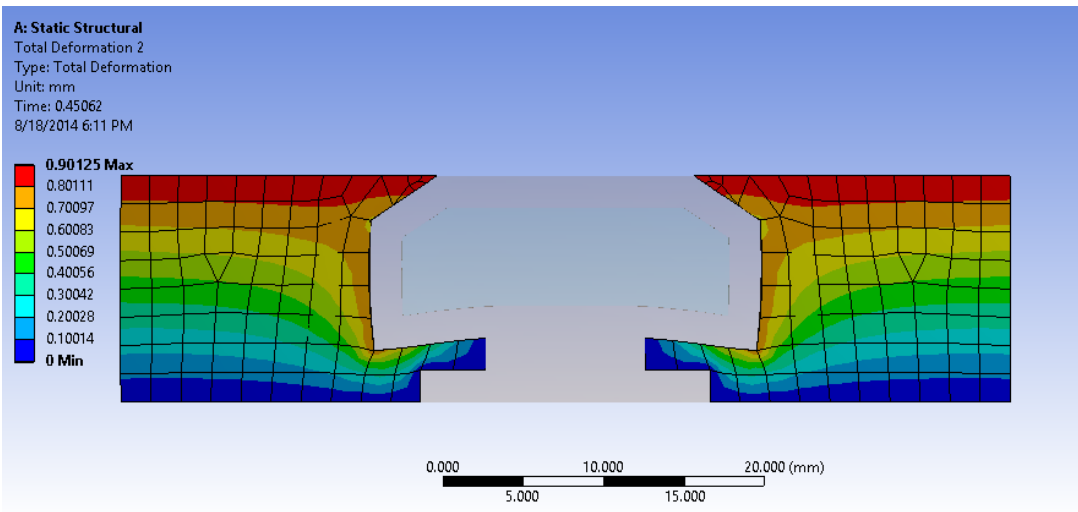


Figure 85. Total deformation of inlet and outlet air structure, BilPlas, Case3

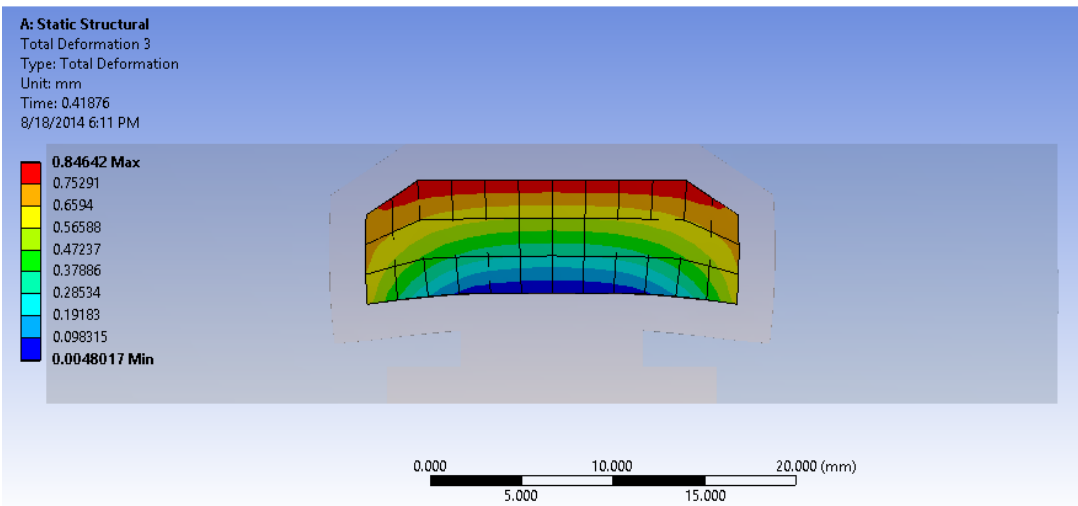


Figure 86. Total deformation of inside air, BilPlas, Case3

STANDART PROFIL

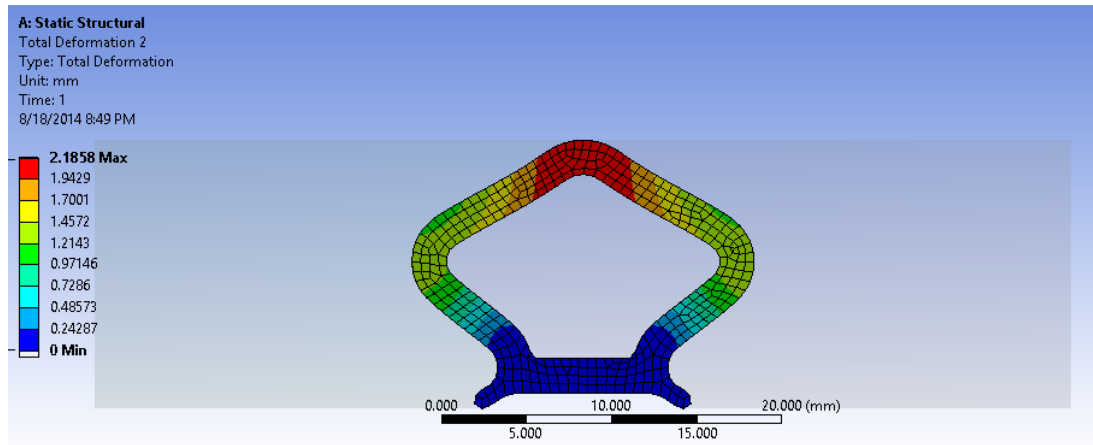


Figure 87. Total deformation of sealant, Standart Profil, Case3

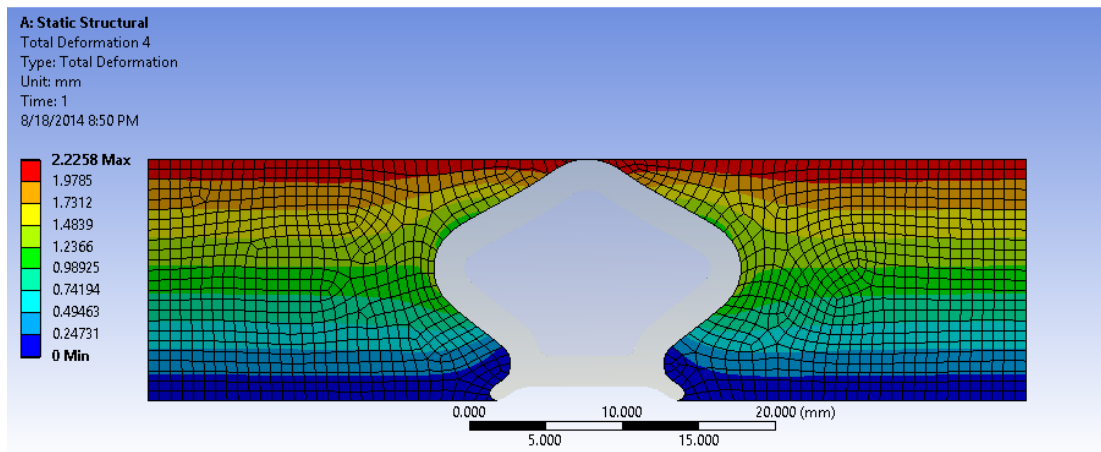


Figure 88. Total deformation of inlet and outlet air structure, Standart Profil, Case3

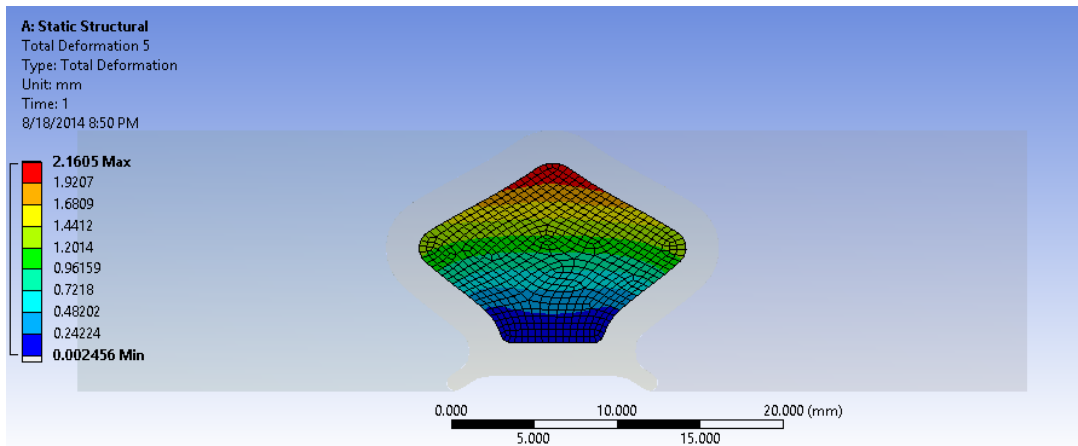


Figure 89. Total deformation of inside air, Standart Profil, Case3

CASE 4

BILPLAS

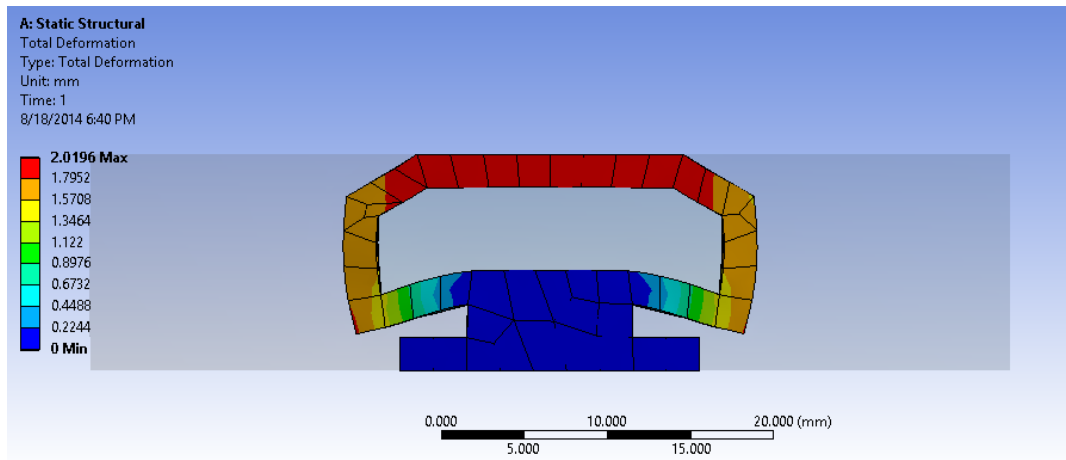


Figure 90. Total deformation of sealant, BilPlas, Case4

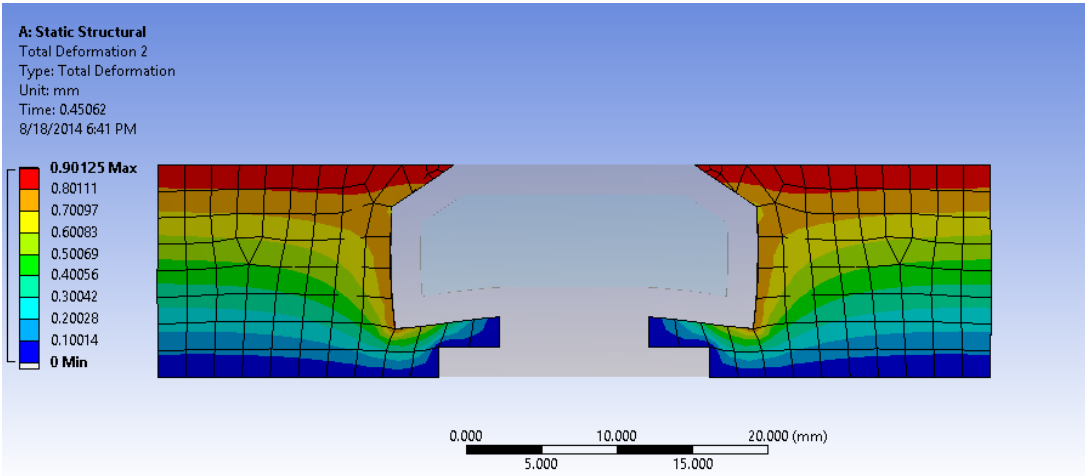


Figure 91. Total deformation of inlet and outlet air structure, BilPlas, Case4

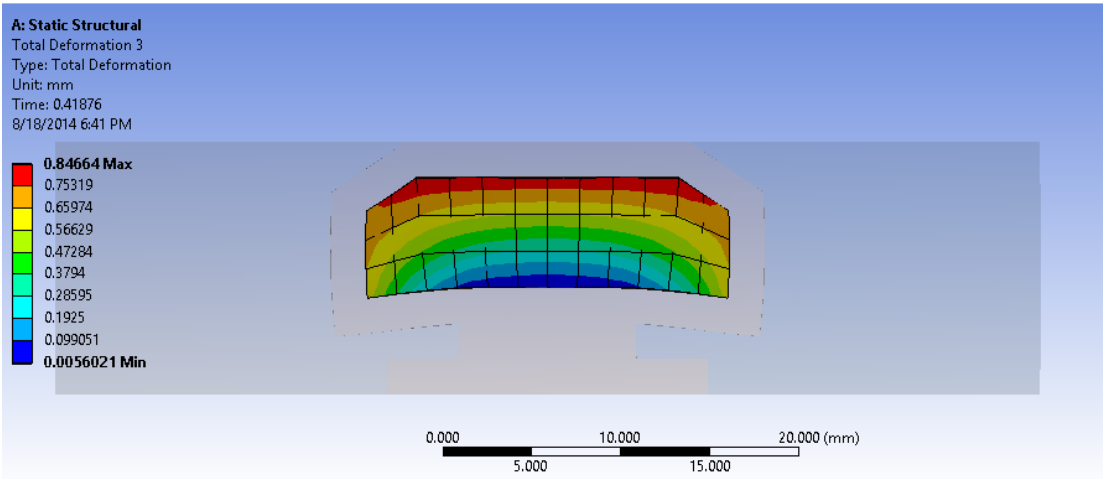


Figure 92. Total deformation of inside air, BilPlas, Case4

STANDART PROFIL

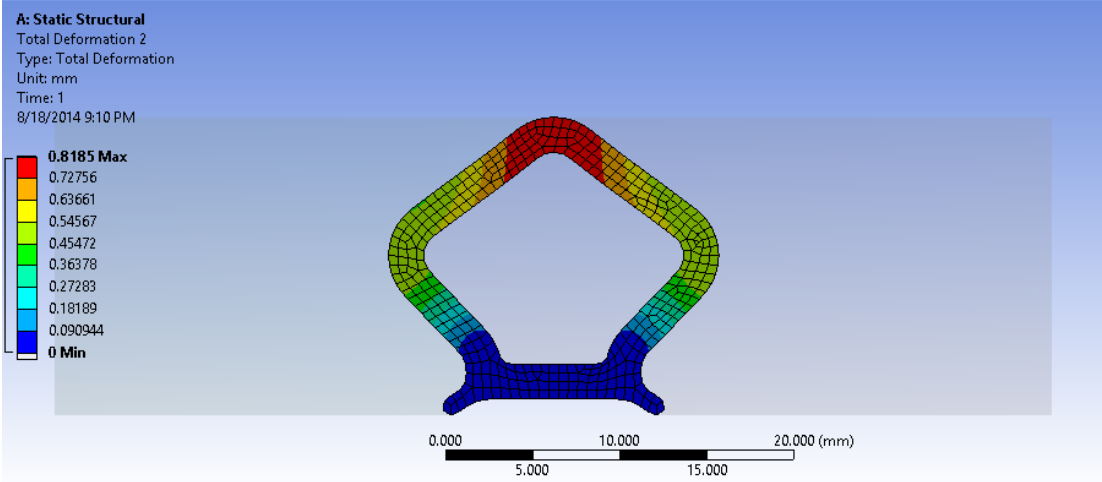


Figure 93. Total deformation of sealant, Standart Profil, Case4

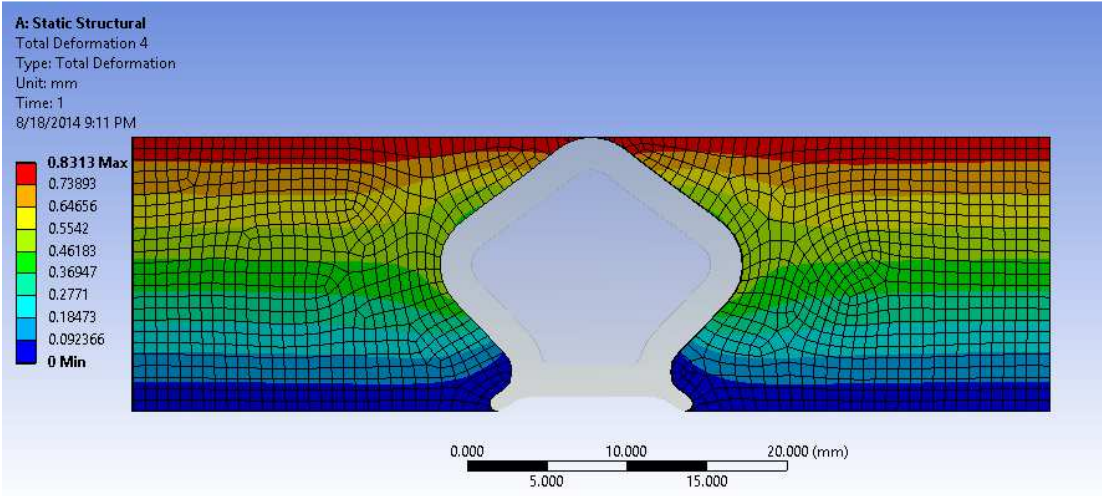


Figure 94. Total deformation of inlet and outlet air structure, Standart Profil, Case4

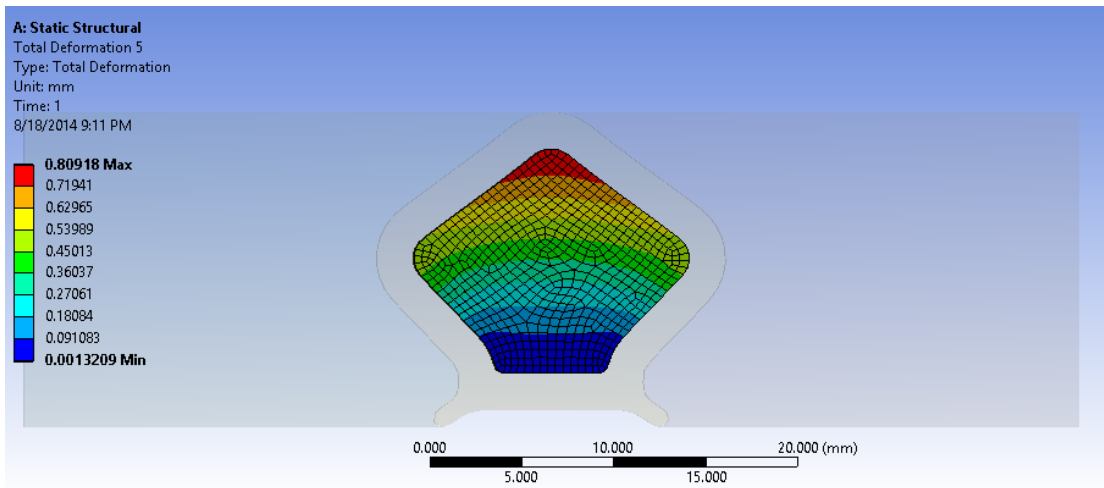


Figure 95. Total deformation of inside air, Standart Profil, Case4

CASE 5

BILPLAS

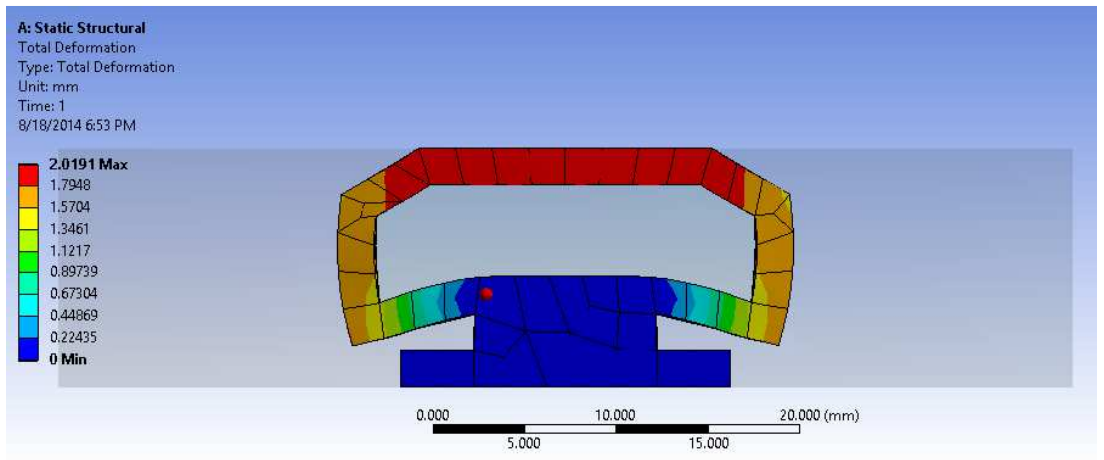


Figure 96. Total deformation of sealant, BilPlas, Case5

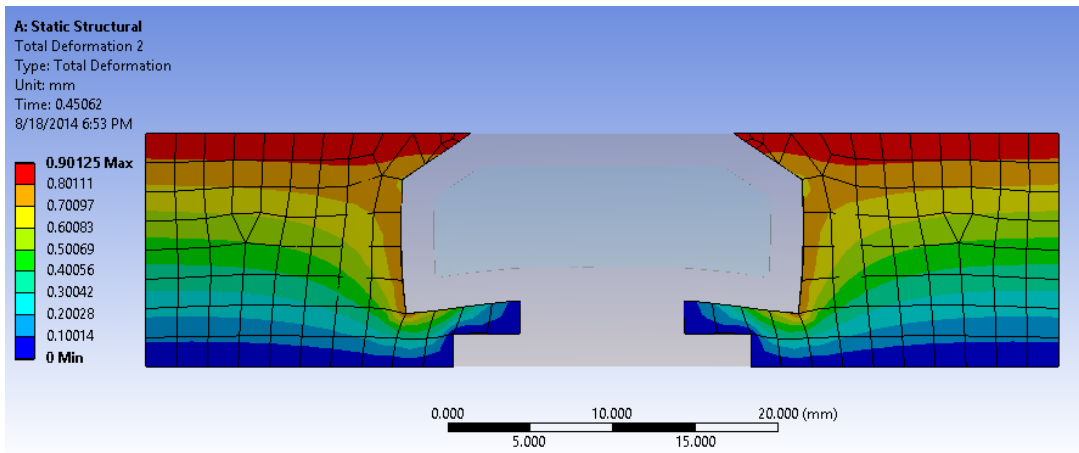


Figure 97. Total deformation of inlet and outlet air structure, BilPlas, Case5

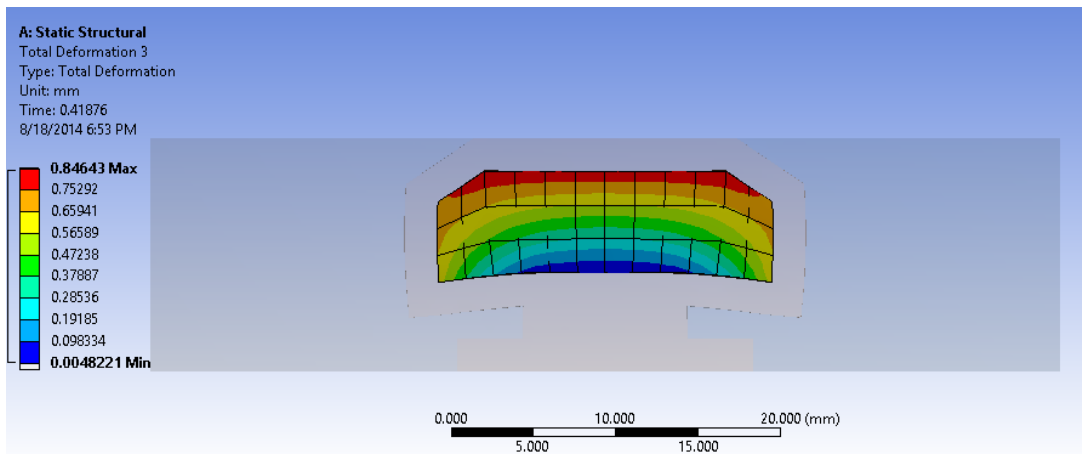


Figure 98. Total deformation of inside air, BilPlas, Case5

STANDART PROFIL

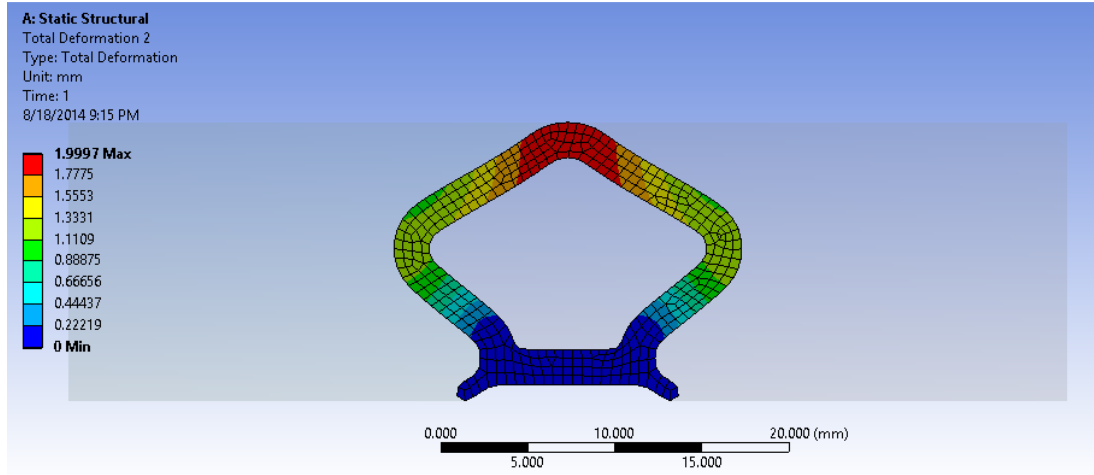


Figure 99. Total deformation of sealant, Standart Profil, Case5

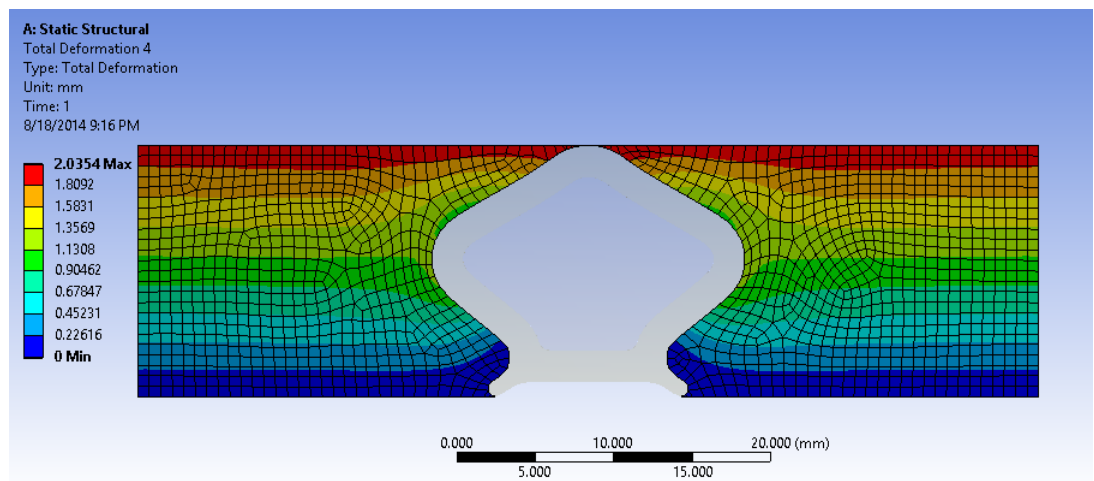


Figure 100. Total deformation of inlet and outlet air structure, Standart Profil, Case5

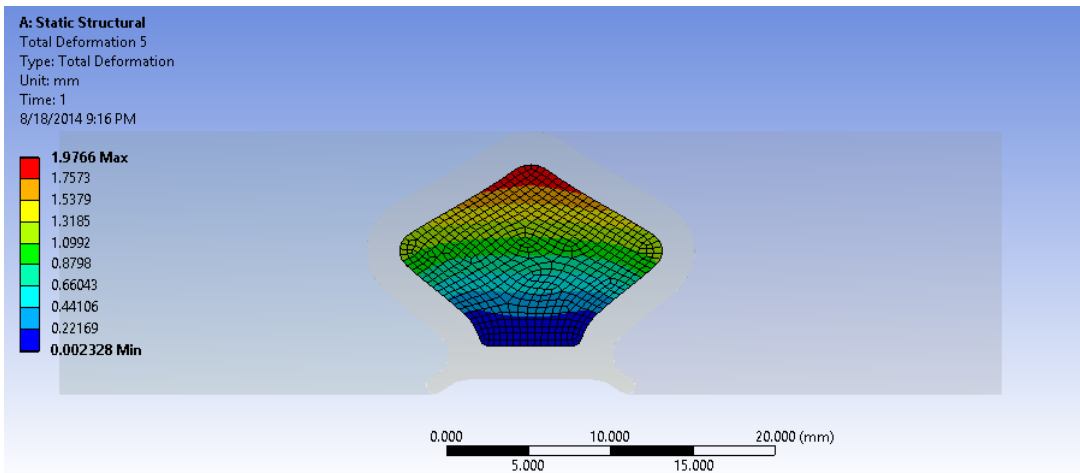


Figure 101. Total deformation of inside air, Standart Profil, Case5

CASE 6

BILPLAS

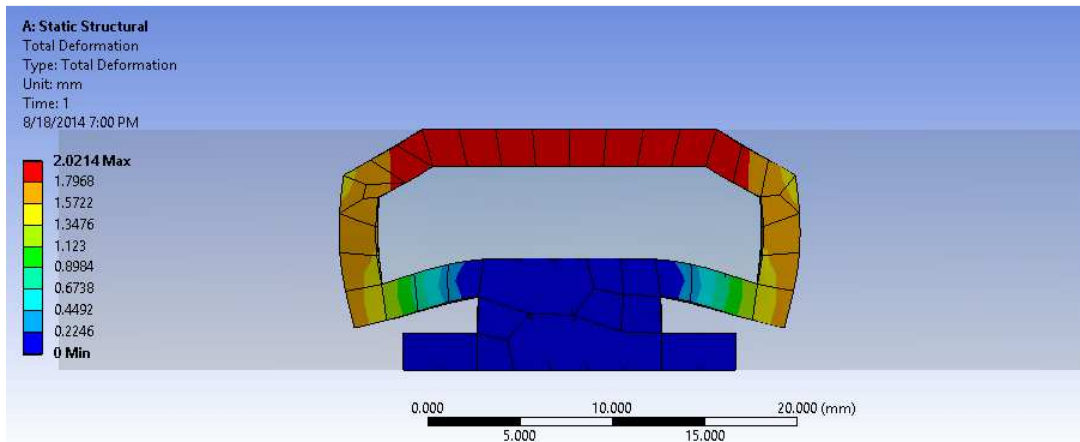


Figure 102. Total deformation of sealant, BilPlas, Case6

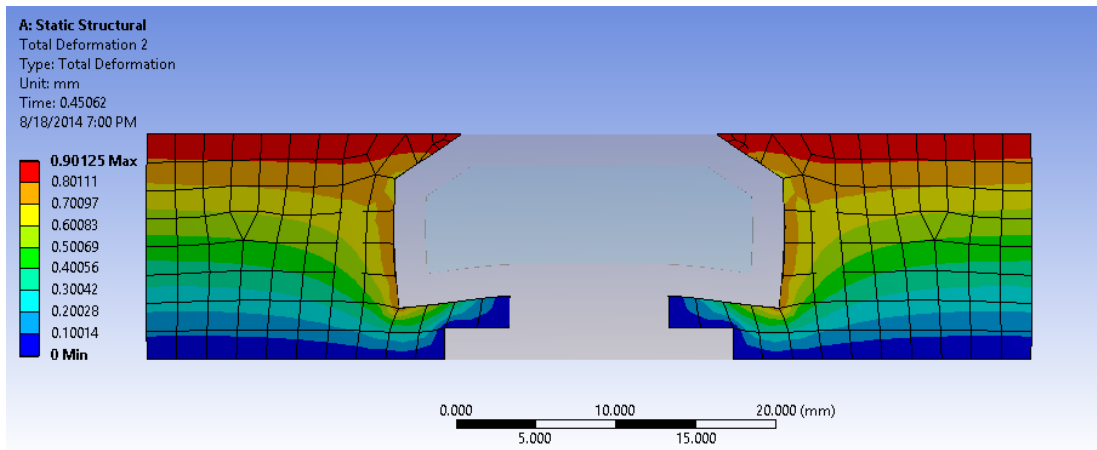


Figure 103. Total deformation of inlet and outlet air structure, BilPlas, Case6

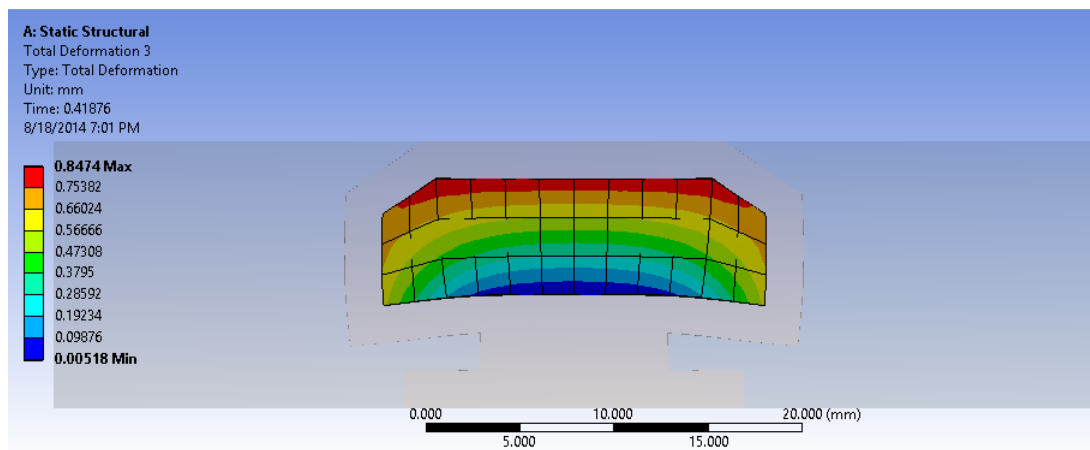


Figure 104. Total deformation of inside air, BilPlas, Case6

STANDART PROFIL

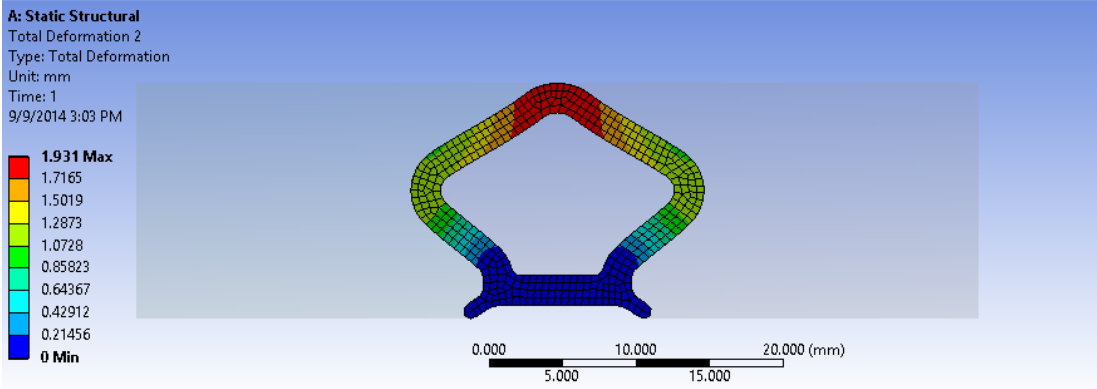


Figure 105. Total deformation of sealant, Standart Profil, Case6

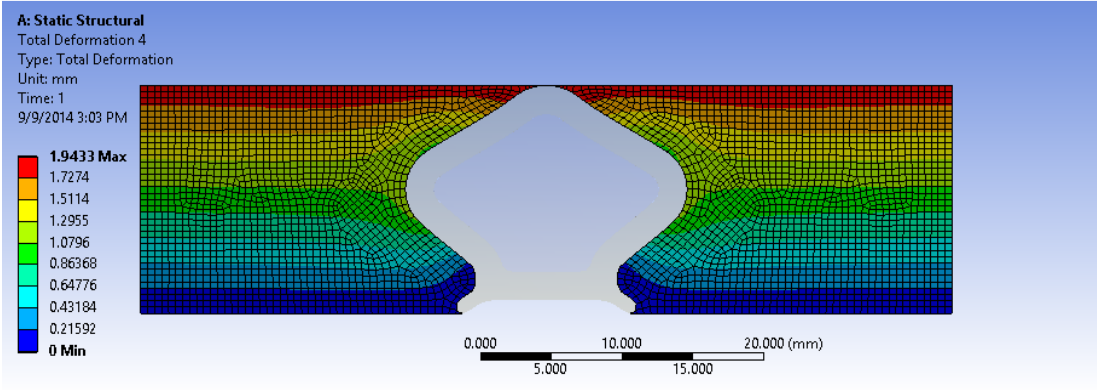


Figure 106. Total deformation of inlet and outlet air structure, Standart Profil, Case6

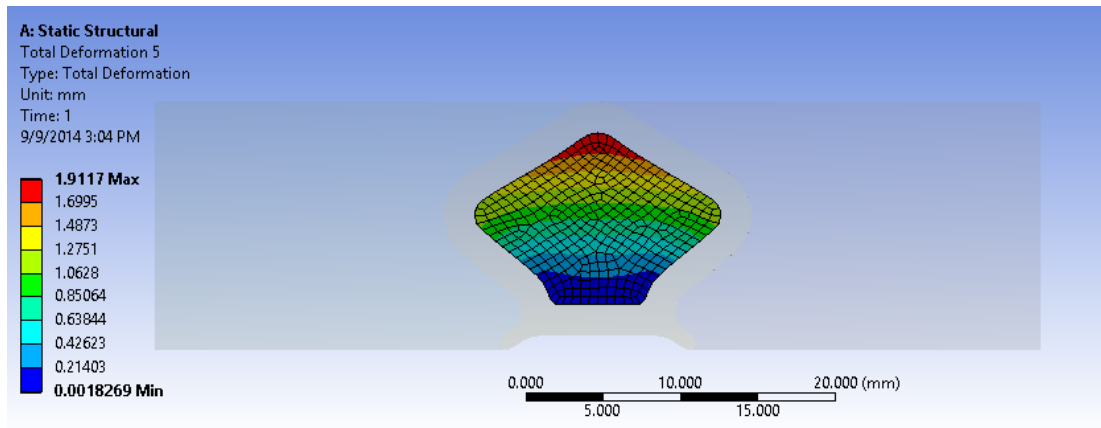


Figure 107. Total deformation of inside air, Standart Profil, Case6

CASE 7

BILPLAS

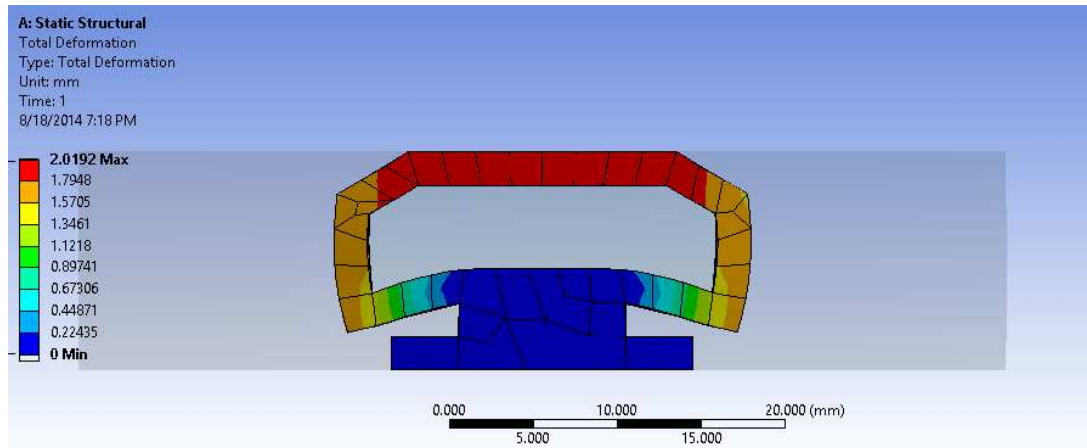


Figure 108. Total deformation of sealant, BilPlas, Case7

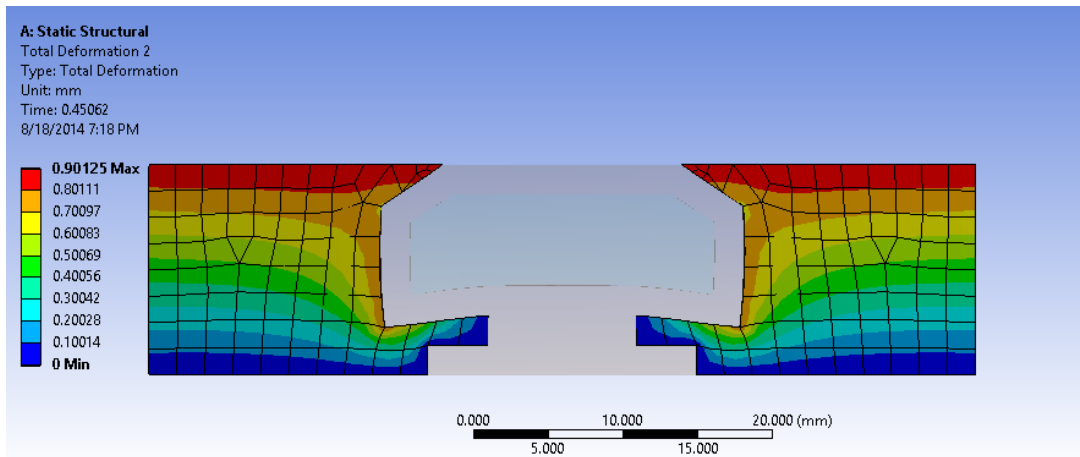


Figure 109. Total deformation of inlet and outlet air structure, BilPlas, Case7

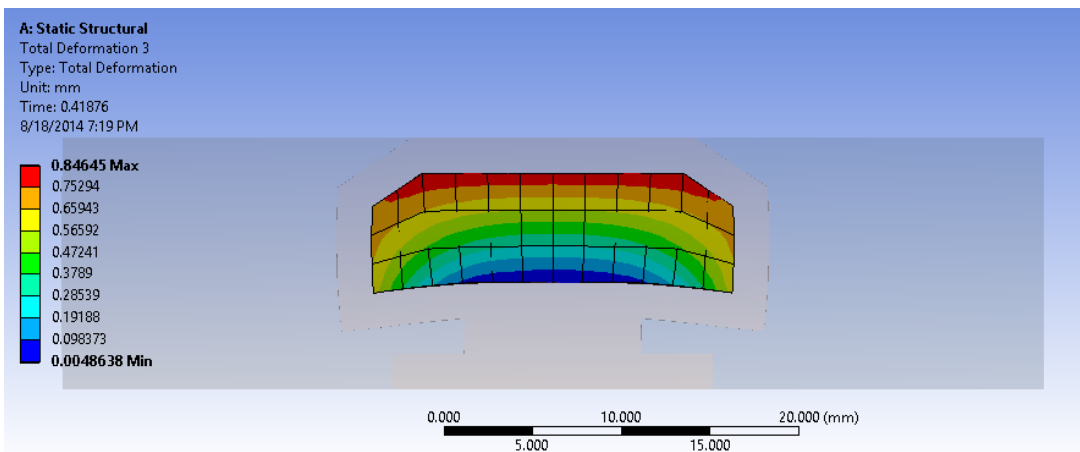


Figure 110. Total deformation of inside air, BilPlas, Case7

CASE 8

BILPLAS

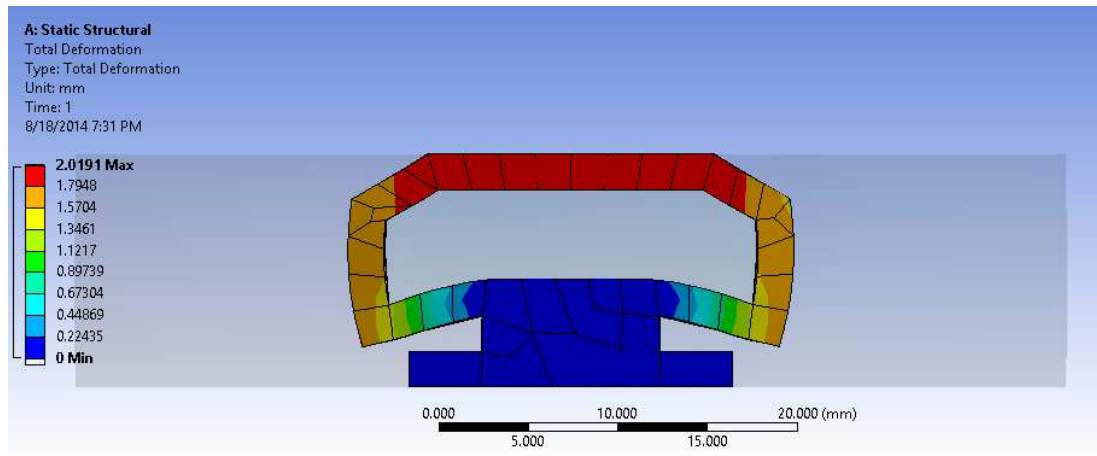


Figure 111. Total deformation of sealant, BilPlas, Case8

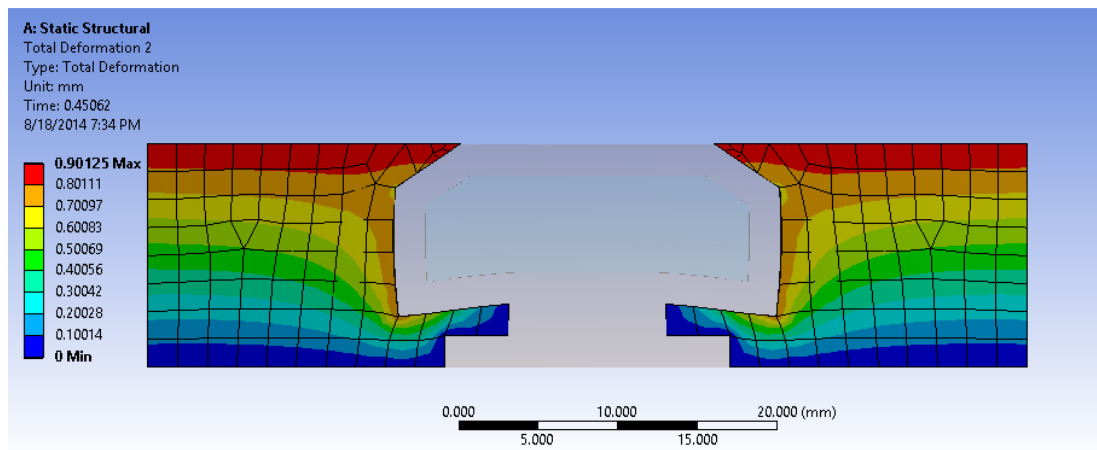


Figure 112. Total deformation of inlet and outlet air structure, BilPlas, Case8

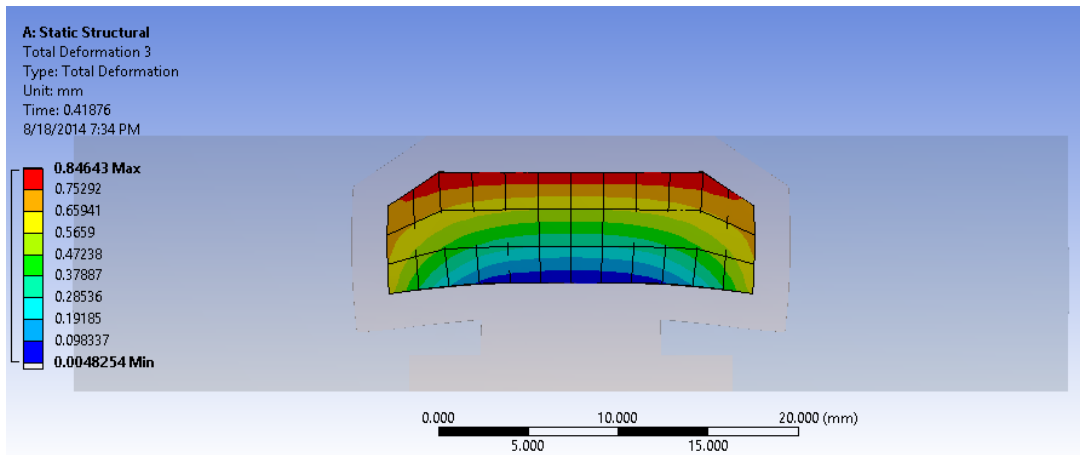


Figure 113. Total deformation of inside air, BilPlas, Case8

CASE 9

BILPLAS

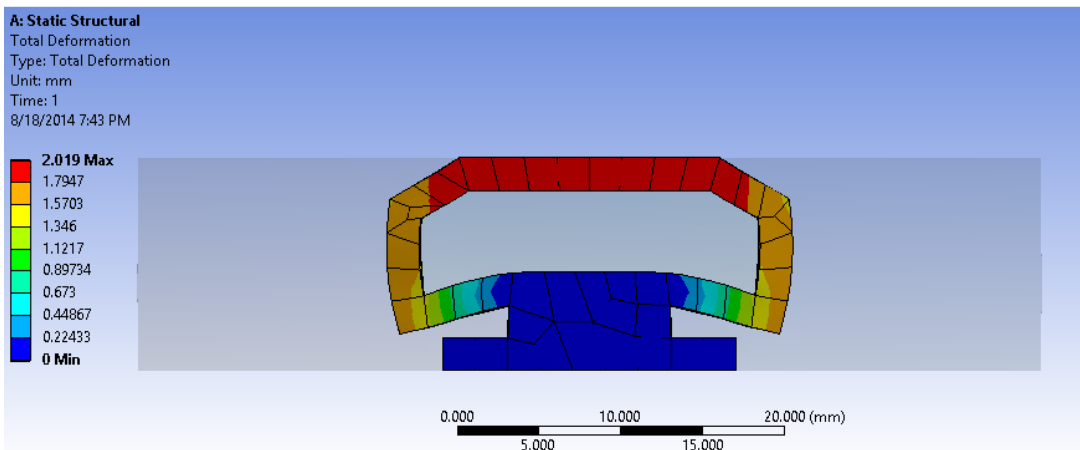


Figure 114. Total deformation of sealant, BilPlas, Case9

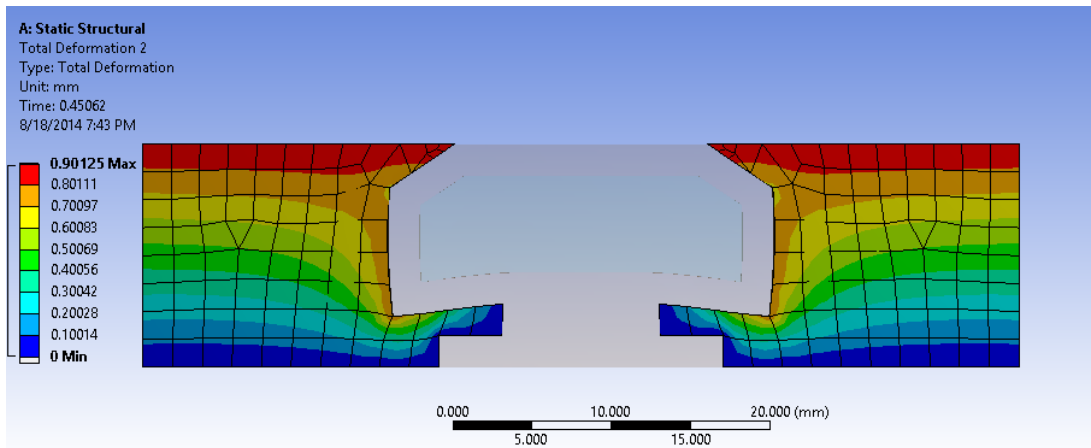


Figure 115. Total deformation of inlet and outlet air structure, BilPlas, Case9

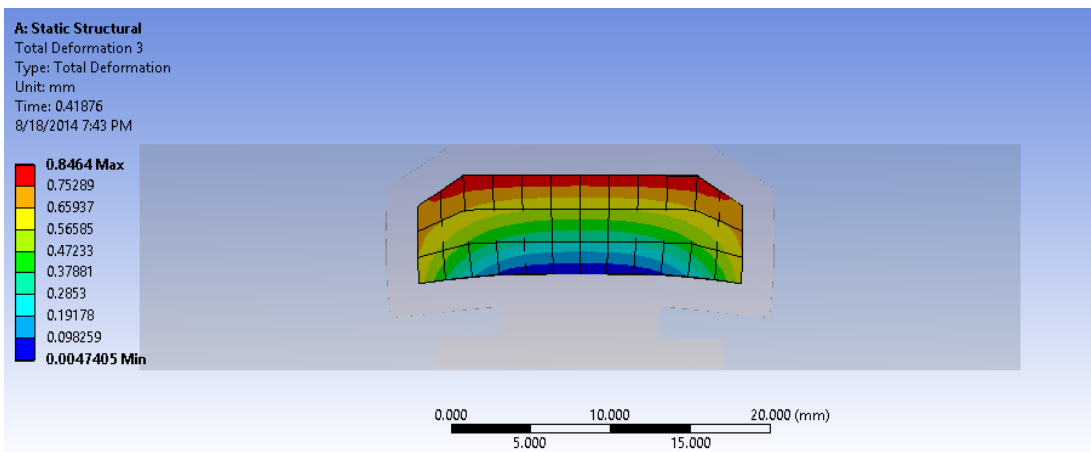


Figure 116. Total deformation of inside air, BilPlas, Case9

CASE 10

BILPLAS

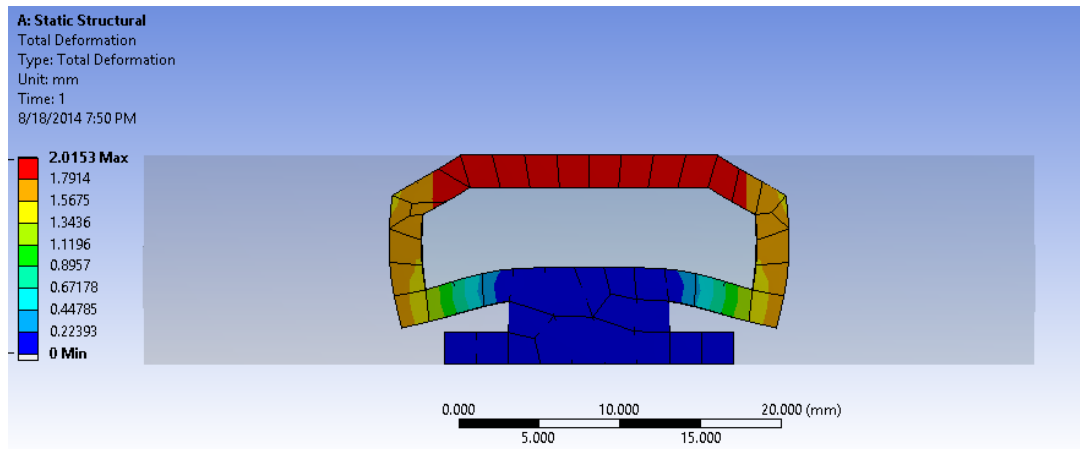


Figure 117. Total deformation of sealant, BilPlas, Case10

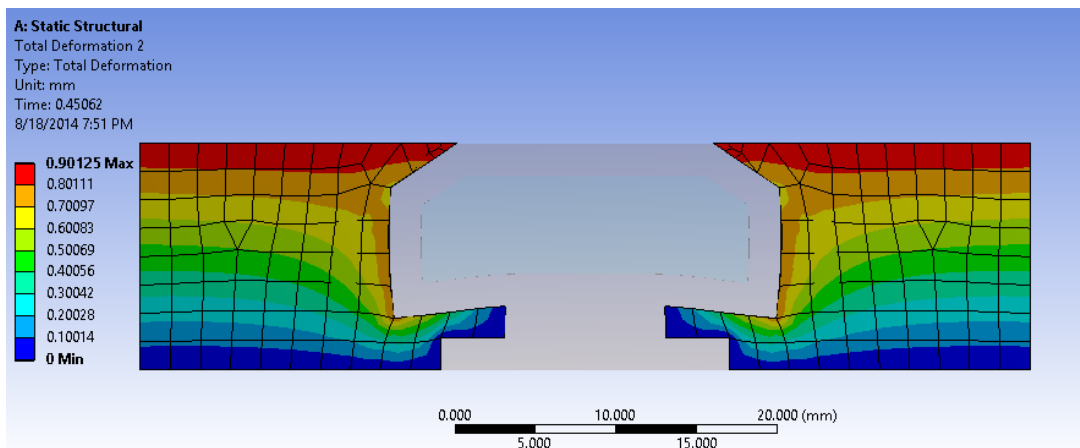


Figure 118. Total deformation of inlet and outlet air structure, BilPlas, Case10

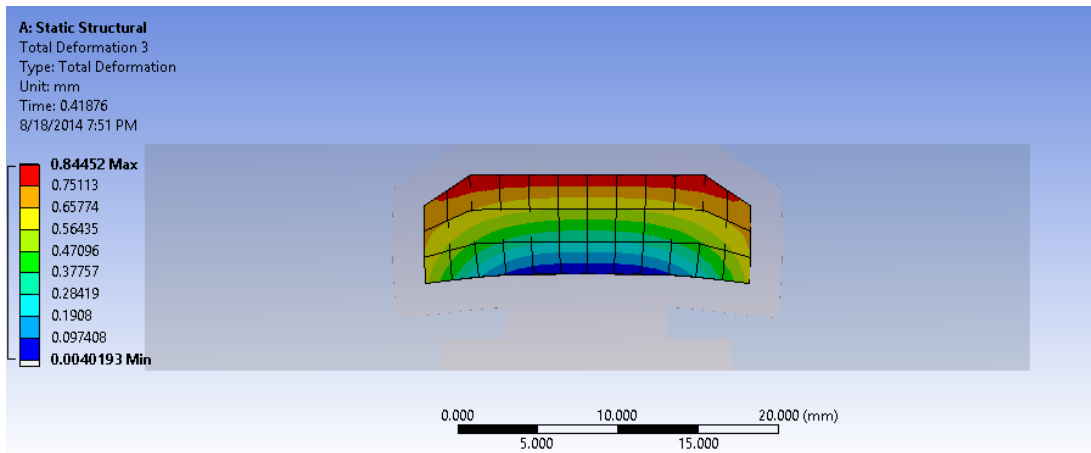


Figure 119. Total deformation of inside air, BilPlas, Case10